MODELING AND ANALYSIS OF INTERACTIONS BETWEEN A PULSATILE PNEUMATIC VENTRICULAR ASSIST DEVICE AND THE LEFT VENTRICLE

by

Andrew Zygmund Hunsberger

BS, Bucknell University, 2001

Submitted to the Graduate Faculty of

the School of Engineering in partial fulfillment

of the requirements for the degree of

Master of Science in Bioengineering

University of Pittsburgh

2004

UNIVERSITY OF PITTSBURGH

SCHOOL OF ENGINEERING

This thesis was presented

by

Andrew Zygmund Hunsberger

It was defended on

September 20th 2004

and approved by

Harvey S. Borovetz, Ph.D., Professor
Department of Bioengineering

James F. Antaki, Ph.D., Associate Professor
Department of Biomedical Engineering, Carnegie Mellon University
Department of Bioengineering, University of Pittsburgh

John Gorcsan III, M.D., Associate Professor of Medicine
Department of Medicine, University of Pittsburgh Medical Center

Thesis Advisor: Sanjeev G. Shroff, Ph.D., Professor
Department of Bioengineering

MODELING AND ANALYSIS OF SYNCHRONY BETWEEN A PULSATILE PNEUMATIC VENTRICULAR ASSIST DEVICE AND THE LEFT VENTRICLE

Andrew Zygmund Hunsberger, MS

University of Pittsburgh, 2004

The use of a ventricular assist device (VAD) is a promising option for the treatment of end-stage heart failure. In many cases VADs provide not only temporary support, but contribute to the recovery of the native ventricle. Many studies have reported incidences where the native ventricle has recovered function, leading to device explantation and eliminating the need for heart transplantation [1-9]. Despite strong interest in the subject for many years, the determinants of the recovery process are poorly understood and number of patients successfully weaned from chronic support remains low [10].

A mathematical model was developed to gain an understanding of the complex mechanical interactions between a pneumatic, pulsatile VAD and the left ventricle. The VAD model was verified in-vitro using a mock circulatory loop. Over a wide range of experimental conditions, it correctly described observed dynamic behaviors and was accurate in predicting both VAD stroke volume and fill-to-empty rate within 6% error. This validated VAD model was coupled to a simple, lumped parameter cardiovascular model. The coupled model qualitatively

reproduced the temporal patterns of various hemodynamic variables observed in clinical data. A concept of VAD characteristic frequency (f_c) was developed to facilitate the analysis of VAD-ventricle synchrony. Characteristic frequency, defined as VAD rate in the absence of ventricular contraction, was essentially independent of cardiovascular parameters. For a given set of VAD parameters, synchrony was found to occur over a range of native heart rates. While the lower bound was determined by f_c alone, the upper bound was a function of various cardiovascular parameters (e.g., left ventricular contractility, E_{MAX} and systemic vascular resistance, SVR). In the case of synchronous behavior, the VAD and native heart have matched rates and counter-pulse, resulting in reduced ventricular loading. A decrease in E_{MAX} or an increase in SVR increases asynchrony, resulting in frequent occurrences of co-pulsed beats (i.e., high ventricular loading).

In conclusion, we found that VAD-ventricle synchrony is determined by a complex interaction between VAD and cardiovascular parameters. Our model-based analysis of VAD-ventricle interaction may be useful for optimizing the VAD operation, characterizing native ventricular contractility, and better understanding of the recovery process.

TABLE OF CONTENTS

LIST OF TABLES

LIST OF FIGURES

ACKNOWLEDGEMENTS

I would like to thank my thesis committee members, Drs. Sanjeev Shroff, Harvey Borovetz, James Antaki, and John Gorcsan for their guidance and support. During my time at the University of Pittsburgh, I have learned a great deal from my teachers and colleagues; these experiences will serve me well in my future endeavors. I particularly wish to extend my sincere gratitude to Dr. Shroff for his dedication and commitment to his students.

I would also like to recognize several other individuals who have helped me along the way, particularly Martin Y. Tabaksblat for his time and efforts with this project, and the people at the University of Pittsburgh Artificial Heart Program. Most importantly, I wish to thank my wife and family for their support throughout my graduate career.

1.0 INTRODUCTION

In the 1960's, when ventricular assist devices began to show promise, researchers believed the problems associated with heart failure would be solved within 20 years.

- O.H. Frazier [11]

Heart disease still remains the leading cause of mortality in the United States [12]. Patients who meet the criterion of heart failure are a diverse group and have various reasons for elevated left ventricular (LV) filling pressure, low cardiac output, and pulmonary and peripheral congestion [13]. Cardiac failure affects an estimated 4.7 million Americans, with 550,000 new cases diagnosed annually and annual cost estimates for medical care ranging from $10 billion to $40 billion [12]. In most cases, the primary cause stems from the left ventricle's inability to fill and empty efficiently [14].

The use of a ventricular assist device (VAD) is a promising option for the treatment of end-stage heart failure. Many studies have been performed to examine the effects of assist devices on the overall performance, including effects on the circulatory system (heart, contractility, cardiac output, gene expression), compatibility (infection/bleeding, thromboemboli), and longevity [6, 15-19]. It can be concluded from these studies that in many cases VADs provide not only temporary support, but also contribute greatly to molecular remodeling and even change gene expression of the myocyte and calcium-metabolism associated genes. Many studies have reported incidences where the native ventricle has recovered function

leading to device explantation, altogether eliminating the need for heart transplantation [1-9]. VAD therapy is also significantly less expensive than replacement with a donor heart [20].

Despite the advantages of recovery therapy, the number of patients successfully weaned from mechanical support remains low [10]. One explanation is that the mechanisms of recovery are not fully understood. Total ventricular unloading has been presumed to provide the optimal environment for recovery [21]. However, long term, total unloading of the ventricle may be undesirable. It has been shown that prolonged unloading may lead to myocyte atrophy [22]. For this reason, partial unloading has been investigated [23]. The optimal degree of unloading is unknown. Another reason for the low occurrence of recovery is that native ventricular performance can be difficult to ascertain in the presence of mechanical assistance. Currently, "off-pump" recovery studies are the standard procedure for determining ventricular function of recovery candidates. However, an "off-pump" recovery study has the inherent risk of temporarily removing circulatory support. Therefore only a select few patients are subjected to recovery studies. The optimal solution would be to have a method wherein the recoverability of all VAD patients could be assessed non-invasively and continuously.

The phasic relationship between VAD and native left ventricle contractions determines the degree of ventricular unloading [24]: counter-pulsations and co-pulsations reduce and increase ventricular load, respectively. This phasic relationship can be monitored non-invasively during VAD support and may be useful in optimizing VAD operation. In addition, we hypothesize that information about native ventricular contractility is embedded in the temporal variations of this phasic relationship. However, better analytical tools are needed to extract this information from the clinical data recorded from VAD-assisted patients.

In the present study, a mathematical model of the VAD-ventricle system has been developed. The goal in developing this model is to gain a better understanding of the complex mechanical interactions between the VAD and the left ventricle. At the University of Pittsburgh Medical Center (UPMC), a large percentage of recovered VAD patients received the Thoratec® pneumatic VAD (Thoratec Labs, Pleasanton CA). For this reason we have chosen to focus our modeling efforts on this device. The following sections describe an electric analog of the Thoratec® VAD that was created and verified in-vitro with a mock circulatory loop. The VAD model was then coupled to a cardiovascular model. This coupled model was used to analyze the behavior of the VAD-native cardiovascular system.

2.0 BACKGROUND

2.1 VENTRICULAR PRESSURE-VOLUME RELATIONSHIP

A great deal of information can be gained about the heart by examining ventricular pressure-volume relationships. This approach was first applied to the heart by Frank Otto in 1898 [25]. Since that time, pressure-volume relationships have found many applications to aid in diagnosis of cardiac health.

Typical LV pressure and volume waveforms, as a function of time, are shown in Figure 1A. Ventricular pressure as a function of volume forms a loop over a complete cardiac cycle (Figure1B).

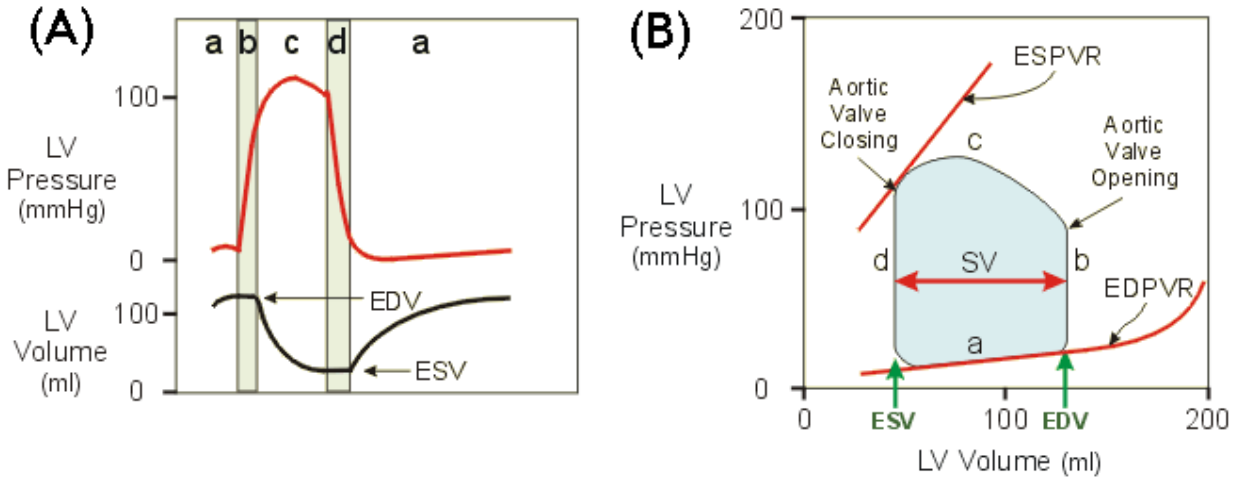

Figure 1: (A) Ventricular pressure and volume waveforms of a heart. (B) Corresponding PV Loop [26].

The four phases of the cardiac cycle are easily distinguished in a pressure-volume loop. Ventricular filling, or diastole (a), begins with the mitral valve opening, corresponding to the lower left hand corner of the diagram and ends in the lower right hand corner of the loop. At the end of diastole the mitral valve closes, however the pressure in the ventricle is not high enough to open the aortic valve. The volume of the ventricle at the end of segment (a) is known as the end-diastolic volume (EDV). The larger the EDV, the greater is the preload or stretch of myocardial fiber for that particular contraction. Segment (b) is the isovolumic contraction phase. The ventricular muscle begins to contract, building chamber pressure, marking the beginning of systole. Once the ventricular pressure exceeds aortic pressure, the aortic valve opens. Systole continues into segment (c), the ventricular ejection phase. When the ventricular pressure falls below aortic pressure, the aortic valve closes. The volume of the ventricle at this point is considered the end-systolic volume (ESV). The final phase (d) is isovolumetric relaxation. As the walls of the ventricle relax (start of diastole), pressure inside the ventricle decreases. When the pressure inside the ventricle falls below that of the left atrium, the mitral valve opens and the cycle repeats.

Suga and Sagawa made valuable contributions towards the analysis of the cardiac contraction and pressure-volume relationship [27]. They found that the end-systolic volume and pressure are linearly related, independent of preload or afterload conditions. This relationship is known as the end-systolic pressure-volume relationship (ESPVR). The slope of the ESPVR is referred to as end-systolic elastance (E_{ES}). E_{ES} is an index of the heart's strength of contraction, or contractility. (Figure 2)

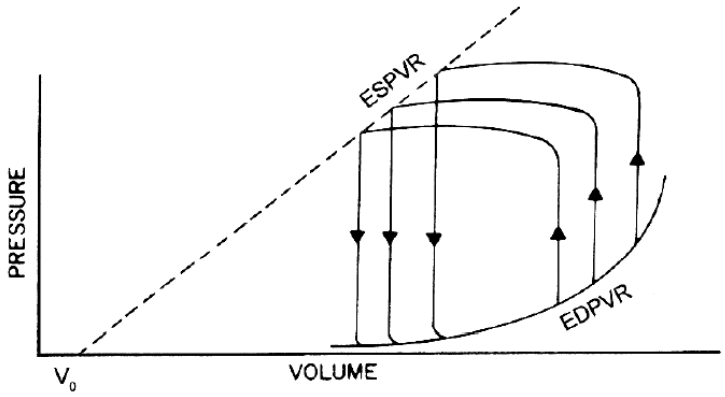

Figure 2: The ESPVR, obtained by changing the loading on the ventricle [5].

The end-diastolic pressure-volume relationship (EDPVR) is obtained by plotting the maximal volume during the cardiac cycle with the corresponding pressure. The EDPVR is best described as a curve rather than a straight line; however the slope of the linear segment yields important information regarding the passive ventricular status. A steeper EDPVR signifies that the ventricle, even in its relaxed state, is stiff and resistant to passive filling. Both the ESPVR and EDPVR are highly valuable in clinical diagnosis of cardiac illnesses.

2.2 HEART FAILURE & PHYSIOLOGIC COMPENSATION

Heart failure is a result of the ventricle's inability to meet the body's demand for blood flow [25]. This inability can arise suddenly from a heart attack or viral infection, which is referred to as acute heart failure. Heart failure may arise slowly over many years stemming from conditions such as hypertension, alcohol abuse, or hyperlipidemia. This condition is known as chronic heart failure. The heart responds to the decreased output with a variety of compensatory mechanisms. Rather than improving hemodynamic performance, these mechanisms can cause further progression of the disease.

Various types of heart failure and corresponding physiological compensations are illustrated using the pressure-volume construct in Figure 3 [25].

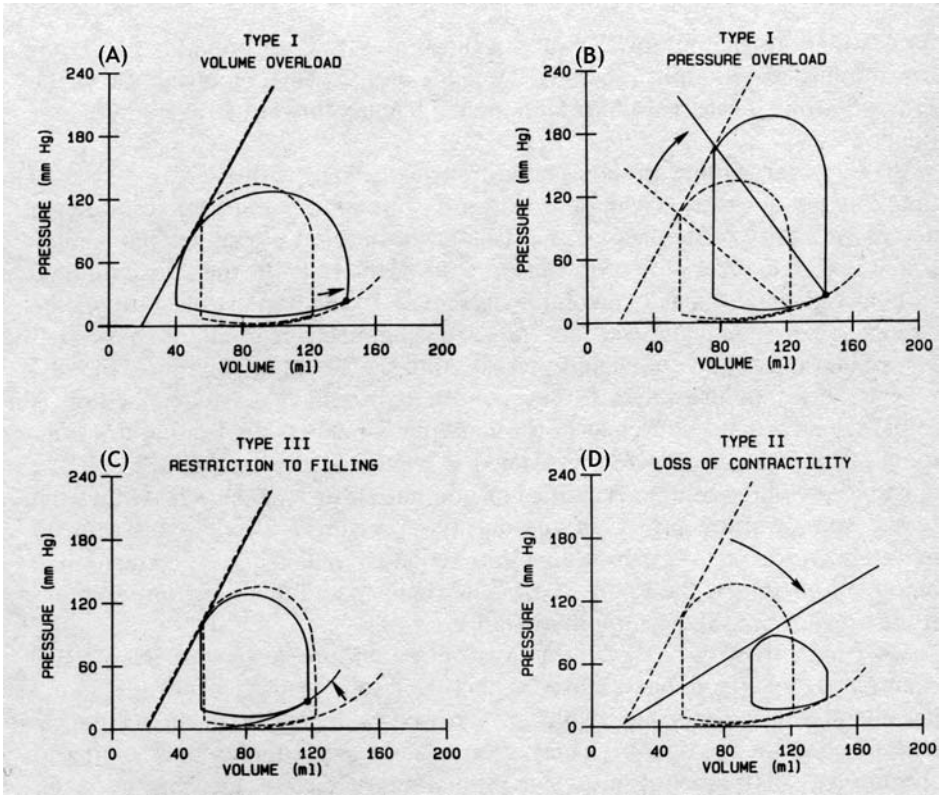

Figure 3: PV Loop representation of various types of heart failure [25]. (A) volume overload (B) pressure overload (C) restricted filling and (D) loss of contractility

In Type I heart failure, the end-systolic and end-diastolic pressure-volume relationships remain normal, however an abnormality such as valvular dysfunction or hypertension creates a greater demand on the heart. The increase in volume (A) or pressure load (B) on the heart can be seen in the pressure-volume loop from the normal case (broken lines) to the diseased case (solid lines). While the pumping capacity of the heart is not compromised, greater work is required to sustain flow.

Type II heart failure is characterized by a decrease in strength of contraction, relating to a decrease in slope of the ESPVR. In an attempt to maintain adequate blood flow, the circulation responds by increasing EDV, however with compromised contractility, the ventricle cannot generate adequate stroke volume.

Type III heart failure is characterized by a shifting of the EDPVR. Insufficient filling creates a leftward shift in the EDPVR and a lower EDV. Greater end-diastolic pressure is required to maintain normal stroke volume.

Some of the compensatory mechanisms described above can have damaging effects on the ventricle at the molecular level. Increased stress and load due to compensation causes overexpression of neurohormones that have toxic effects on the heart muscle and blood vessels[28-30]. These neurohormones have been linked to ventricular remodeling, a process which causes a deterioration in whole ventricular function as well as individual myocytes. The remodeled ventricle becomes larger, more spherical, and less capable of effective contraction [31].

2.2.1 Medical Therapy for Heart Failure

Heart failure therapy depends greatly on the temporal status of the disease. In early stages of chronic heart failure, patients are advised to undertake healthy lifestyle habits, exercise and diet. If symptoms worsen, a clinician will prescribe a variety of pharmaceutical therapies. Several types of pharmaceutical therapies exist which work to improve hemodynamic function [32].

1. Diuretics: which can decrease circulating blood volume or preload to reduce venous congestion.

2. Vasodilators: which can decrease afterload to improve cardiac pump function and tissue perfusion by dilating downstream vessels.

3. Inotropic agents: which can directly increase contractility to improve cardiac output.

Such drug therapies usually provide temporary deceleration or even suspension of the disease progression. If symptoms of heart failure progress despite the use of drug therapies, more aggressive (invasive) treatment becomes necessary.

2.2.2 Surgical Therapy for Heart Failure

Prior to the advent of cardiopulmonary bypass (CPB) in 1953, there were few options available to end stage chronic heart failure patients [33]. Prolonged bed rest was the primary treatment offered at the time. Since then, several surgical options have been developed, such as heart transplantation, which debuted in 1967 [34]. Today heart transplantation offers the best chance of survival and quality of life for patients with end-stage chronic heart failure [1]. However, the therapy is limited for a number of reasons: the need for donor organs greatly outnumbers the supply, complications with long-term immunosuppression and, debilitating effects of cardiac denervation [35].

By the early 1990's, the success of heart transplantation created a greater demand for donor hearts. Unfortunately, supply of donor hearts did not meet the demands. Because of the

discrepancy, waiting times for donor hearts grew in the early 90's [11]. Mechanical circulatory support has provided relief to the many heart failure patients awaiting heart transplants.

2.2.3 Mechanical Circulatory Support

Mechanical circulatory support has long been a challenge to engineers. In the 1960's researchers believed heart failure would be solved in 20 years [11]. The problem has since proved more complex. Undoubtedly, the most famous, or infamous, historical event in the field of mechanical circulatory support was the Jarvik-7 implantation in 1982 [36]. The device was implanted with the intent of serving as "destination" therapy. While the knowledge gained from the Jarvik-7 and other total artificial hearts was immeasurable to research, the clinical outcomes were less than desirable. The use of a total artificial heart (TAH) as destination therapy was halted. Currently, two TAH devices have been experiencing an increase in use: the CardioWest device (CardioWest Technologies Inc., Tucson AZ) and the AbioCor (Abiomed Inc., Danvers, MA). These devices are only approved for bridge-to-transplant therapy.

As a result of the clinical difficulties in total heart replacement, efforts shifted to assisting the heart, rather than replacing it. When originally implanted in 1963, VADs were intended to be used as short term support to aid patients who could not be immediately weaned from CPB. These devices were designed to unload the ventricle for a short period of time until normal function was regained. As VAD technology improved, the devices become more useful.

2.2.3.1 Bridge to Transplantation

In 1978 a VAD was used to support a patient with severe heart disease while awaiting transplantation [37]. This was the first application of a VAD used as a "bridge" to transplantation. Unfortunately, mortality rates on such devices were initially nearly 100% [11]. In the late seventies and early eighties, the National Heart, Lung, and Blood Institute issued funding to improve the poor performance of VAD technology. The goals were to develop a device for long term use (> 2 years) and to reduce the unacceptable mortality rates. The initiative produced two state-of-the-art devices: the Novacor Left Ventricular Assist System (Novacor, Ottawa, Ontario) and the HeartMate® Left Ventricular Assist System (TCI, Pleasanton, CA). Thoratec developed a second VAD, placed extracorporeally and capable or biventricular support. To date, the HeartMate® has been implanted in thousands of patients with 65% of recipients surviving to transplantation [11]. The Novacor LVAS has had similar success. Since their clinical introduction, these devices have increased a patient's likelihood of surviving until a donor heart is found for transplant.

2.2.3.2 Destination Therapy

Destination therapy is the permanent, mechanical support of end-stage heart failure patients, who are ineligible for cardiac transplantation. Recently, the HeartMate left ventricular assist system was approved for use as destination therapy [38]. A recent multi-center study lead by Rose *et al.* [39] concluded that improved quality of life can be achieved by implanting a VAD, even if no chance of transplant exists. These events have generated new interest in the VAD industry as destination therapy.

2.2.3.3 Bridge to Recovery

Studies have recently reported incidences where the ventricle has recovered function while receiving long-term VAD support. This has allowed device explantation of the VAD in select cases, altogether avoiding heart transplantation. Chronic VAD support has been linked to a reversal of many markers indicative of cardiac remodeling, and these observations have lead to the concept of "reverse remodeling" where the effects of heart failure appear to be undone as a result of unloading by VAD support [5, 8, 17, 40, 41]. These studies support the hypothesis that left ventricular assistance appears to be beneficial to LV function, and that recovery of LV function is possible. Ventricular device therapy for the purpose of recovery could have enormous benefits on the health care industry as well, reducing the number of heart transplants necessary.

Farrar *et al.* concluded that recovery of the native heart is the most desirable clinical outcome and should be actively sought, and transplantation used only after recovery of

ventricular function has been ruled out [42]. This opinion is widely accepted, however many aspects of the recovery process remain unknown, limiting its clinical success.

2.2.4 Recovery Studies

In 1995, Nakatani *et al.* were among the first to report on recovery of the native ventricle and subsequent removal of VADs in 4 of 6 heart failure patients supported for > 3 weeks [8]. However, two of the four patients died and detailed criteria for identifying LV recovery were not described in their report. Several other groups have made progress in standardizing a method to determine candidates for recovery [2, 43]. The Berlin Group used routine echocardiographic measures of LV ejection fraction and end-diastolic diameter taken with devices turned off for 4 minutes as a guide to LV functional recovery [7]. The Columbia Presbyterian group studied cardiac output and peak oxygen consumption using right heart catheterization during upright bicycle exercise [44]. Research at UPMC has also been focused on developing a systematic protocol for identifying patients who might be weaned from support. Such efforts have allowed clinicians to better identify ventricular recovery and have aided in lowering demand on heart transplantation.

Despite the efforts to standardize a protocol to identify recovery candidates, incidences of recovery remain relatively small [10]. There are several factors responsible for the limited success of ventricular recovery while on VAD support. One factor is that native ventricular function is difficult to ascertain in the presence of VAD support. Currently, "off-pump" recovery studies are the standard procedure for determining ventricular function of recovery candidates. However, an "off-pump" recovery study is limited to those patients already displaying signs of recovery due to the inherent risk of temporarily removing circulatory support.

Secondly, there is no standard control algorithm used which is known to optimize hemodynamic conditions in order to promote recovery. If better understood, clinicians may be able to use a particular VAD control algorithm to train a failing ventricle towards recovery. By training ventricles towards recovery, the number of potentially weanable cases can be increased, while better indices of recovery would improve identification of the new, larger candidate pool.

Efforts have been made at UPMC to develop non-invasive indices of recovery [3]. Non-invasive indices inherently pose less risk to the subject. By lowering risk, the pool of recovery candidates can be increased. UPMC has recently reported 33% (6 of 18 patients) success rate for ventricular recovery of patients with VADs [3]. All six of the recovered patients were implanted with a Thoratec® extracorporeal pneumatic VAD.

2.2.5 Thoratec® Pneumatic VAD

The Thoratec® VAD system (Thoratec Corp, Pleasanton CA.) is a pneumatically driven, pulsatile, extracorporeal blood pump, consisting of three major elements: blood chamber, cannulae and pneumatic driver. The blood chamber consists of a hard semi-transparent casing and a Thorlon ® polymer blood bladder [45]. Pneumatic drive pressure is created from the Dual Drive Console (DDC) (Figure 4A). The DDC is capable of providing either univentricular or biventricular support.

(A)  (B) 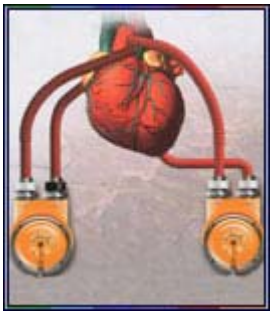

Figure 4: (A) Thoratec® pneumatic drive console and (B) Thoratec VAD with bi-ventricular support [12].

There are two control modes possible for this device, which can create very different hemodynamics. In fixed mode control, pressure is supplied to the VAD at a specific frequency. For long-term bridge-to-transplant therapy, the most effective and reliable mode has been thought to be fill-to-empty control [46],wherein, the VAD ejects when full, regardless of ventricular state. It maximizes blood flow; however VAD-ventricle synchrony may vary from beat to beat. The VAD and ventricle are in synchrony when they contract at the same frequency. The significance of VAD-ventricle synchrony and its effects on LV loading and myocardial recovery are unknown [24],however partial loading during different periods of VAD support may be advantageous for myocardial recovery [23].

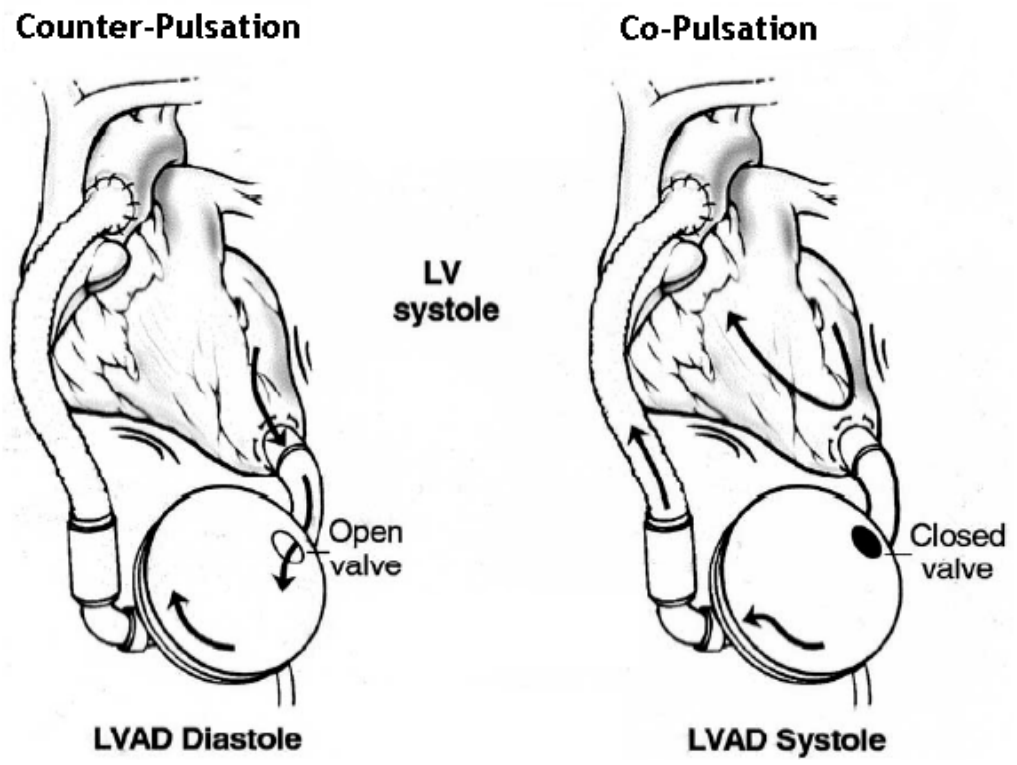

Figure 5: The VAD-ventricle system can exist in either a counter-pulsation or co-pulsation states. When counter-pulsing, ventricular loading is minimal; when co-pulsing, ventricular loading is maximized [35].

In the VAD fill-to-empty mode, the VAD-ventricle system can exist in a state of either co-pulsation or counter-pulsation. Ventricular ejection coincides with VAD filling during counter-pulsations, minimizing ventricular loading. In co-pulsation, ventricular and VAD ejection (systole) coincide; increasing ventricular loading. Maybaum *et al*. suggest that, if better understood, VAD-ventricle synchrony could be manipulated to promote myocardial recovery. In fill-to-empty control, VAD-ventricle asynchronous beats may occur regularly, randomly, or not at all. The benefits of various control modes on promoting recovery are virtually unknown. Loading conditions on the ventricle are highly dependent on the control mode used during VAD support; however no standard mode exists which is known to be beneficial to recovery

conditions. A mathematical model of the coupled VAD-cardiovascular system is likely to improve our understanding of VAD-ventricle interactions, including synchrony.

2.2.6 Clinical Data

Data from two heart failure patients treated at UPMC with ventricular assist device (Thoratec® VAD) are shown in Figure 6. Measurements of ventricular area were recorded using non-invasive echocardiographic border detection [47]. In addition, peripheral arterial pressure, EKG, and pneumatic VAD pressure were simultaneously recorded.

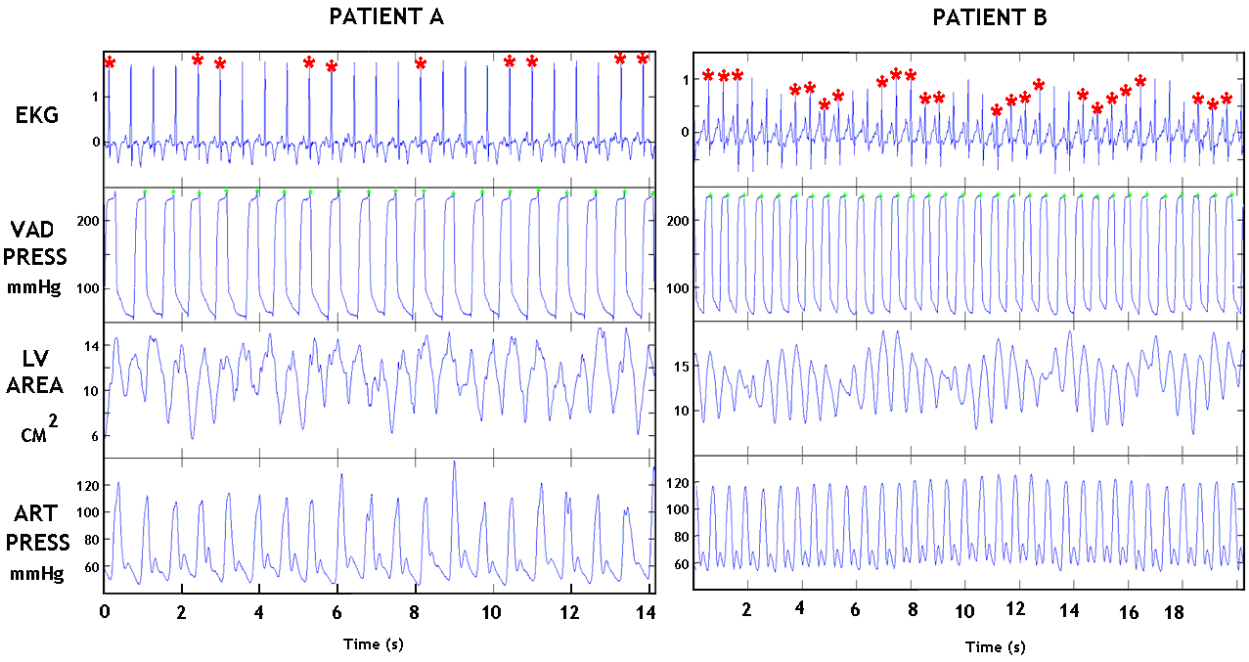

Figure 6: Examples of clinical data collected at UPMC – Thoratec® VAD patients with fill-to-empty mode. (* indicate co-pulsations)

Patient A was a successful recovery case. Patient B did not recover native ventricular function. The asterisks (*) on the EKG data in Figure 6 indicate co-pulsation of the VAD and LV. In this example, it is observed that Patient A exhibits a lower frequency of co-pulsating

beats than seen with Patient B. Also, the ventricular area data for both patients shows a periodic dampening, possibly related to co-pulsating beats. These phenomenons may be related to the underlying ventricular contractile performance. A better understanding of the system could lead to indices of recovery in the presence of VAD support. However, finding conclusive evidence would be difficult because of the variability in clinical data. A mathematical model of the system would be useful to reconcile the variability of clinical data.

2.3 CARDIOVASCULAR MODELING

Electric analogs are a common means of mathematically reproducing the bulk behavior of a fluid system, such as the cardiovascular system (CVS). By modeling the properties of a fluid system representing resistance, compliance, and inertance as electric elements, accurate representations of cardiovascular waveforms can be simulated using electric circuit theory.

2.3.1 Electric Analog Elements

Resistance occurs as a result of the frictional forces that act on a fluid traveling through a vessel. These forces are represented as hydraulic resistance and are defined as the pressure drop through of vessel divided by the flow. Hydraulic resistance is often a function of flow as well. However flow through blood vessels produce near constant resistance within physiological flow limits [48]. Accordingly, when modeling the CVS, linear resistors are often chosen and are characterized by the following constitutive relationship:

$$\Delta P(t) = R \times Q(t) \tag{2-1}$$

where P(t) and Q(t) are instantaneous pressure and flow, respectively and R is the hydraulic resistance, typically with units of mmHg×s/ml. The simplest formulation of the resistance is given by the Poiseuille formula [49]:

$$R = \frac{8 \times \eta \times \ell}{\pi \times r^4} \tag{2-2}$$

where η is the fluid viscosity, ℓ and r are the vessel length and radius, respectively. Inertance is used to model inertial forces arising from the motion of the mass of blood. Inertance is characterized by the following constitutive relationship:

$$\Delta P(t) = L \times \dot{Q}(t) \tag{2-3}$$

where $\dot{Q}(t)$ is the rate of change of flow, and L represents the inertance, typically with units of mmHg×s^2/ml. Based on the Newton's First Law of motion, one can derive the following simplified expression for inertance for a cylindrical tube:

$$L = \frac{\rho \ell}{\pi r^2} \tag{2-4}$$

where ρ is the fluid density. Due to the elastic nature of blood vessel walls, hydraulic compliance is a vital component to cardiovascular models. Compliance is analogous to

capacitance in the electric model. Compliance is defined by the following constitutive relationship:

$$P(t) = \frac{1}{C} \times V(t)\Delta \tag{2-5}$$

where V(t) represents instantaneous volume of the vessel and C represents the hydraulic compliance of the vessel, typically with units of ml/mmHg. The compliance of a cylindrical vessel with Young's bulk modulus of elasticity E, and vessel wall thickness h, can be estimated from the following equation [50]:

$$C = \frac{3\pi r^3 \ell}{2Eh} \tag{2-6}$$

2.3.2 Systemic Circulation Modeling

The modeling of the systemic circulation has been in existence since Frank in the late 19th century [51]. Since that time, a variety of approaches have been presented to model the human circulation. These techniques range from reduced models with a minimal number of parameters, to distributed models that attempt to capture every anatomical aspect of the circulation with many parameters.

2.3.2.1 Highly Reduced Lumped Parameter Models

The Windkessel model was first used by Frank [51] to describe the circulation as a single resistance and compliance in parallel. Frank's classic Windkessel model is depicted in Figure 7A. A three-element modified Windkessel model was proposed by Westerhof in 1968 [52]. The modified Windkessel [53] is a significant improvement over the classical Windkessel in that it better approximates the observed aortic input impedance spectrum ($Z_{IN}(\omega)$) of the systemic arterial circulation.

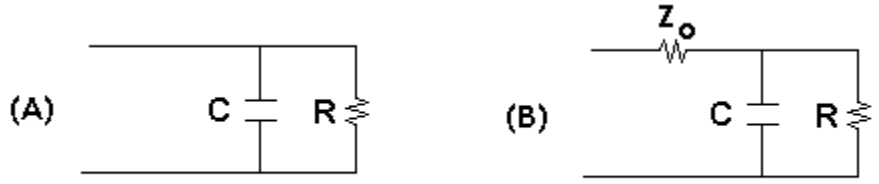

Figure 7: (A) Classical windkessel model, R is total systemic resistance and C is arterial compliance. (B) Modified windkessel, Z_o is characteristic impedance.

Highly reduced models, such as the modified Windkessel, provide simple and reasonably accurate representation of the hydraulic impedance imposed on the left ventricle. However, these models ignore the distributed nature of the system arising from the anatomical features. As a consequence, wave propagation and reflection phenomena are not considered in these models. Moreover, it is often difficult to assign calculated pressures and flows to specific anatomical sites; a more detailed distributed model would be required for this purpose.

2.3.2.2 Detailed Lumped Parameter Models

Distributed models do not lump system parameters. Individual elements or segments of the circulation are separately modeled and assembled in an anatomically correct manner. The benefits of this approach include a better representation of $Z_{IN}(\omega)$ and availability of hemodynamic data at various sites in the circulation. However, the parameter space increases rapidly as the model gets more complex, which adversely affects model identifiability from experimental data. Figure 8 shows a diagram of a distributed human circulation model by Rideout [48].

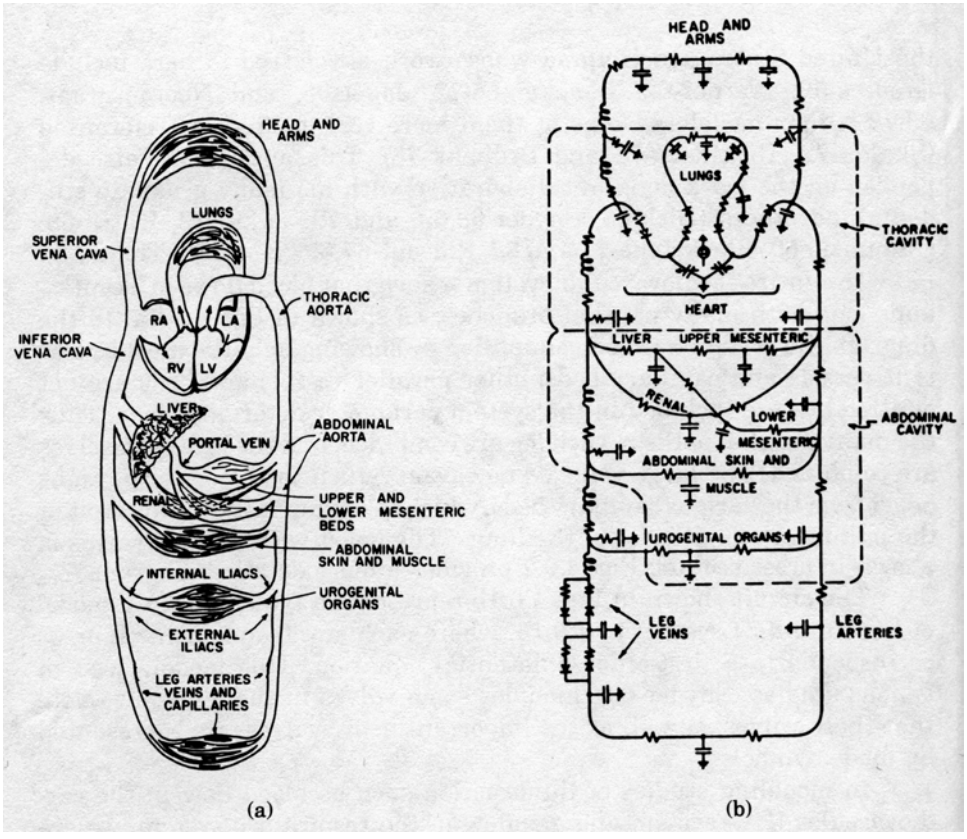

Figure 8: (A) Diagram of the human CVS. (B) Corresponding distributed model of circulation [48].

It can be seen that an accurate anatomical representation of the circulations is created by a distributed model. Other well-known distributed models have been developed by Avolio *et al*. [54] and Noordergraaf *et al.* [49].

2.3.2.3 Intermediate Hybrid Models

The reduced model approach remains popular because of its simplicity. However, several limitations of the reduced models have been identified [55]. Detailed lumped parameter models, while highly accurate, are limited in the practical applications because of their large number of parameters. For these reasons, intermediate models, which are both identifiable and accurate, have been developed. One such intermediate modeling technique is based on the use of tube-like elements to simulate the distributed nature of the system and consequently, the arterial wave propagation and reflection phenomena [56-59]. Specifically, a single and T-tube models with complex terminal loads (e.g., a 3-element Windkessel) have been developed [55, 60-62]. The term hybrid is a reflection of the fact that these types of models share properties of both distributed and reduced models, such as the Windkessel. In addition to being mode accurate than the highly reduced models, these intermediate hybrid models have a potential for providing physiological relevant information about the arterial circulation. For example, Shroff *et al*. [55] have shown that the T-tube model with complex terminal loads correctly distinguishes between proximal and distal arterial properties, especially the arterial compliance. Such a distinction is relevant because regional changes in vascular properties can affect cardiovascular function in a differential manner.

2.3.3 Ventricular Models

2.3.3.1 Mean Value Models

Early approaches to ventricular modeling related observable input(s) and output(s) of the ventricle [63, 64]. For example, Starling related the EDV of the ventricle (input) to cardiac output [63]. Guyton related mean right atrial pressure (input) to cardiac output to characterize the entire heart [65], while Herndon & Sagawa [66] related mean left atrial pressure and mean aortic pressure (inputs) to cardiac output to characterize the left ventricle in a 3-dimensional space. Sarnoff introduced ventricular stroke work as the output variable and described the contractile state of the ventricle in terms of ventricular function curves [64, 67] by plotting mean atrial pressure (input) against stroke work. Glower *et al*.[68] modified Sarnoff's approach by replacing atrial pressure by ventricular EDV and proposed the relationship between ventricular EDV (input) and stroke work. Elzinga and Westerhof related mean left ventricular pressure (input) to mean left ventricular outflow [69]. Mean value methods have been very useful in characterizing ventricular contractile function. However, by definition, they do not provide any information about ventricular dynamics or pulsatile behavior.

2.3.3.2 Ventricular Time Varying Elastance

The method of time-varying elastance is a widely accepted means of modeling ventricular dynamics. Elastance is the reciprocal of capacitance. As the name implies, a time-varying elastance is a periodic function with respect to time. For the time-varying elastance model, the relationship between instantaneous ventricular volume, V(t), and instantaneous ventricular pressure, P(t), is given by [25]:

$$P(t)=E(t)\times\left[V(t)-V_D\right] \tag{2-7}$$

where E(t) is the time-varying elastance function and V_D is unstressed volume of the ventricle. The elastance function, which rises and falls throughout the cardiac cycle, is an active element that is responsible for the energy of contraction in the CVS model.

2.3.3.3 Ventricular Internal Resistance

Since the introduction of the time-varying elastance concept, studies have provided evidence that the ventricular pressure-volume relationship is not absolutely load independent [70-73]. These findings have led to the development of a ventricular model where the time-varying elastance is in series with a pressure-dependent ventricular resistance. This resistance was described by Shroff *et al.* [71, 74] as:

$$R_{LV}=K\times E(t)\left[V_{LV}(t)-V_D\right] \tag{2-8}$$

where K is a proportionality constant (s/ml), and E(t) and V_D are the same as in Equation 2-7. For the elastance-resistance model, the expression for P(t) is given by:

$$P(t) = E(t)\times\left[V(t)-V_D\right] - R_{LV}Q(t) = \left\{E(t)\times\left[V(t)-V_D\right]\right\}\left\{1-KQ(t)\right\} \tag{2-8}$$

where Q(t) is instantaneous ventricular outflow.

2.3.4 Electrical Analog Models of Coupled Vascular-Ventricular System

Early coupled ventricle-vascular models were developed in the late sixties and early seventies by Beneken [75], Dick [76], Rideout [48], and McLeod [77]. McLeod's Physiological Simulation Benchmark Experiment (PHYSBE) was an early electrical analog of the entire cardiovascular system, combining the heart and circulatory system. McLeod made several assumptions when he simulated the CVS with an electrical analog: lumped parameters represent distributed properties of the CVS, and resistance and compliance of blood flow in vessels are linear. McLeod also assumed that heart valves operate ideally, and atrial contraction and blood mass were negligible. The model produces reasonable human pressure waveforms and is still currently used. Others have improved upon McLeod's model and have successfully produced more accurate physiological waveforms, usually accompanied by increasing complexity. In fact, complex models are available that accurately describe all aspects of the CVS, including baroreflex, coronary blood flow and right/left ventricle interactions [78-81].

2.4 VAD MODELING

The interaction of a VAD with the native cardiovascular system has also been studied with the help of electric analogs [48, 78-86]. In this regard, the studies by Platt [79-81], Ferrari [80], and Jin [83], are of particular interest. Each of these studies describes a model of a pulsatile, pneumatic VAD similar to the Thoratec® VAD.

The model developed by Platt assumed linear elements (compliance, resistance) to represent the VAD and a distributed CVS model including central nervous system (CNS) control. Results focused on the optimal insertion site for VAD inlet cannulae and VAD control with respect to cardiac output and oxygen consumption. The VAD model was controlled in both fixed rate and EKG triggered control modes, but not the fill-to-empty mode. The study does not supply any validation information regarding the accuracy of the VAD model.

Ferrari *et al.* developed a model of the circulation system coupled with a pneumatic, pulsatile VAD. The VAD was modeled as a compliant chamber, having a flat pressure volume relationship at intermediate volumes and steep pressure volume relationship when nearly full or nearly empty. The pressure developed by the pneumatic driver was modeled using ideal gas laws. This model was later used by De Lazarri [87] to investigate the effects of VAD control (fill-to-empty, fixed, and EKG triggered) on cardiovascular energetic variables (external work, pressure volume area, cardiac mechanic efficiency). The model has since been copyrighted under the name CARDIOSIM®.

The Jin model uses a constant compliance bladder [83]. The focus of this particular study was to validate a method of valve modeling with time-vary resistors. Rather than operating ideally, valves required some finite time to open and close. The use of non-ideal valves was

shown to be considerable improvement for accurately matching experimental data. A schematic of the electric analog with a systemic load is shown in Figure 9.

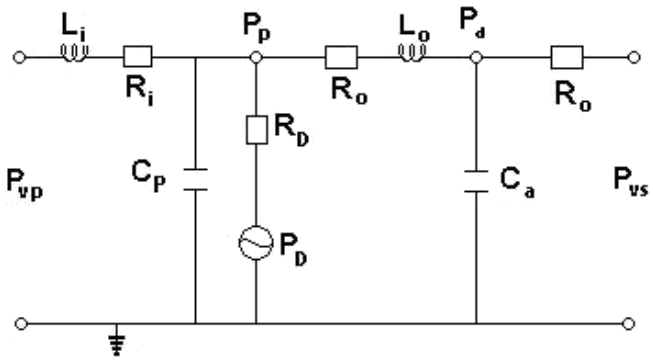

Figure 9: Electric analog developed by Jin *et al.* Pulsatile pneumatic VAD with systemic loading [83].

Inlet and outlet cannulae were modeled with inductors (L_I & L_O) and resistors (R_I & R_O) in series. The compliance of the bladder was represented with the capacitor C_P. The pneumatic drive pressure was modeled as a pressure source (P_D) and resistor (R_D) in series. P_D was a step function, which instantaneously switches between ejection pressure and filling pressure.

2.5 BACKGROUND SUMMARY

Applications of pressure-volume relationships, heart failure and its clinical management, the current state of mechanical circulatory support, and ventricular recovery have been discussed. Recovery, while not fully understood, has the potential to alleviate many of the limitations of heart transplantation. Several studies have been presented that propose methods for identifying possible recovery candidates and to monitor the recovery process. Frequently, "off-pump" studies are used to assess native ventricular function by temporarily removing VAD support,

which is likely to increase the risk to the patient. We believe that mathematical modeling-based analysis of the VAD-native cardiovascular system has a potential to provide valuable insights into the VAD-ventricle interaction and the recovery process. Electric analog modeling of the cardiovascular system was introduced. A better understanding of VAD-ventricle interactions could lead to improved methods for optimizing VAD operation and for assessing the native ventricular contractile function without the need for "off-pump" studies.

3.0 RESULTS AND DISCUSSION: MODEL DEVELOPMENT

The goal of the present study was to develop an accurate mathematical model of the Thoratec® pneumatic VAD in order to simulate its interactions with the left ventricle. We have elected to model this VAD because all cases of recovery in the UPMC recovery studies have involved this device. A model was proposed and experimentally tested in-vitro. Improvements to the model were made as a result of in-vitro studies. The final model was shown to accurately predict pressure and volume waveforms obtained experimentally. The VAD model was then coupled to a native cardiovascular model to investigate VAD-left ventricular interaction.

In a clinical setting, one can record several hemodynamic waveforms in the presence of the VAD. Although these waveforms contain a great deal of information, their interpretation is problematic because they depend on a number of unobservable factors: intrinsic properties of sub-systems (heart, circulation, VAD) and the interactions among these sub-systems. Mathematical models have potential to provide a better understating of the net function of interacting sub-systems and to extract intrinsic properties of each sub-system. We have also hypothesized that a better understanding of the waveforms obtained from the VAD-ventricle system may reveal possible markers of recovery.

3.1 VAD MODEL

A new model of the Thoratec® pneumatic VAD was developed. This model shares some of the characteristics of previous models described in section 2.4, but also contains several new elements. A series of experiments were performed to characterize the VAD. The first of which was a static pressure-volume study.

3.1.1 Static Study

3.1.1.1 Methods

A static pressure-volume study was performed to characterize the behavior of the VAD bladder. The slope of the pressure-volume relationship was used to estimate a value for the compliance of the bladder. Under steady state, static conditions, water was added in steps of 5 milliliters into the VAD bladder. Simultaneous measurements of the internal pressure were taken with a 6F micro-tip pressure transducer (Millar Instruments, Houston, Texas).

3.1.1.2 Static Pressure-Volume Behavior

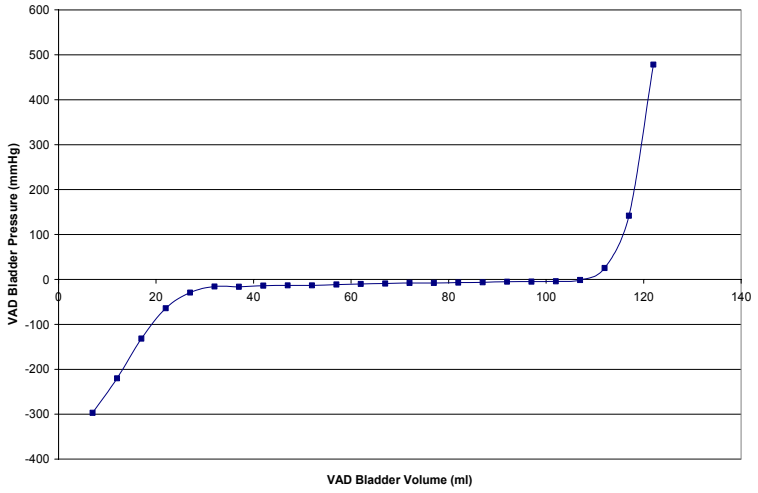

Figure 10: Static pressure-volume relationship in the Thoratec® pneumatic bladder.

It can be seen that for volumes between 32 and 107 milliliters, there is very little pressure change. The relationship of the VAD bladder pressure to volume is shown to be extremely linear in the volume this range (r^2 = 0.98). Volumes above ~107 ml cause much higher pressure increase per volume increase because of the stretching of the bladder and eventually because of the rigid outer case of the VAD. Volumes below ~32 ml deviate from linearity because of resistance to collapse by the bladder. The experimental data were approximated with piece-wise linear regions with five segments, as shown in Figure 11.

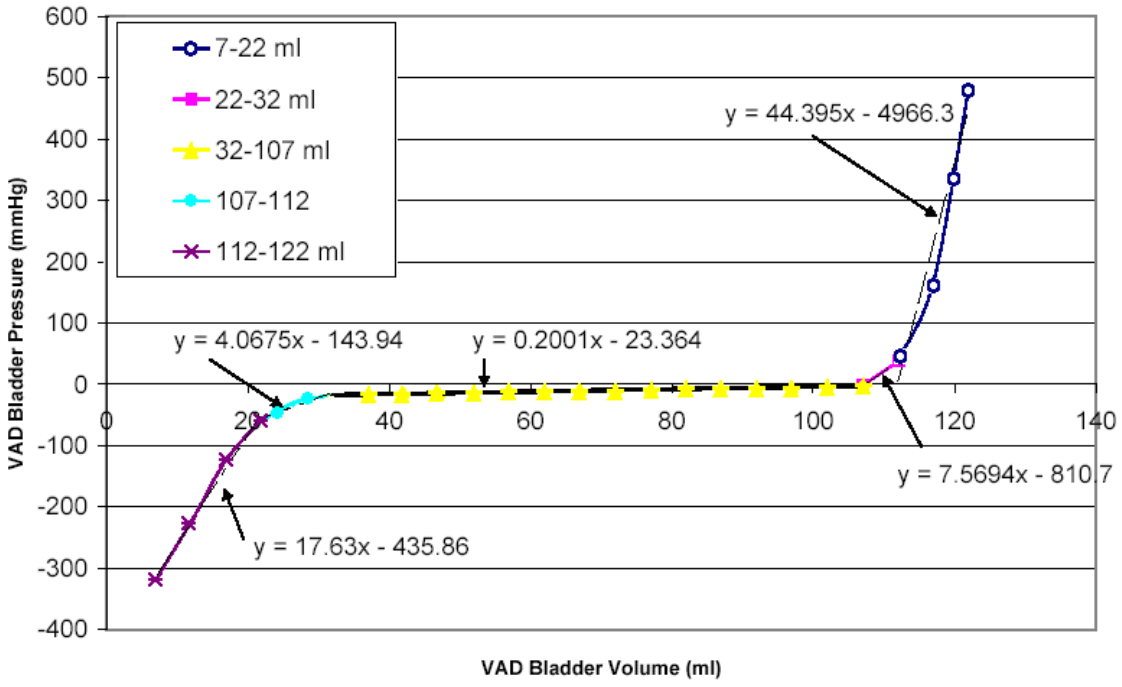

Figure 11: Linear piece-wise approximation of VAD bladder compliance.

Clearly, the compliance of the bladder is not constant; it changes with bladder volume and can be approximated as a piece-wise linear function. The piece-wise linear method will allow the state equation to remain with respect to volume. Depending upon the calculated volume of the bladder, as determined in the mathematical model, one of the five linear regions can be chosen to quantify the compliance value (= inverse of the slope).

It was also necessary to know the bladder's pressure-volume relationship with the presence of the external pneumatic pressure (P_d). This was accomplished by repeating the static experiments under a variety of pneumatic pressures. The findings from this experiment are shown in Figure 12.

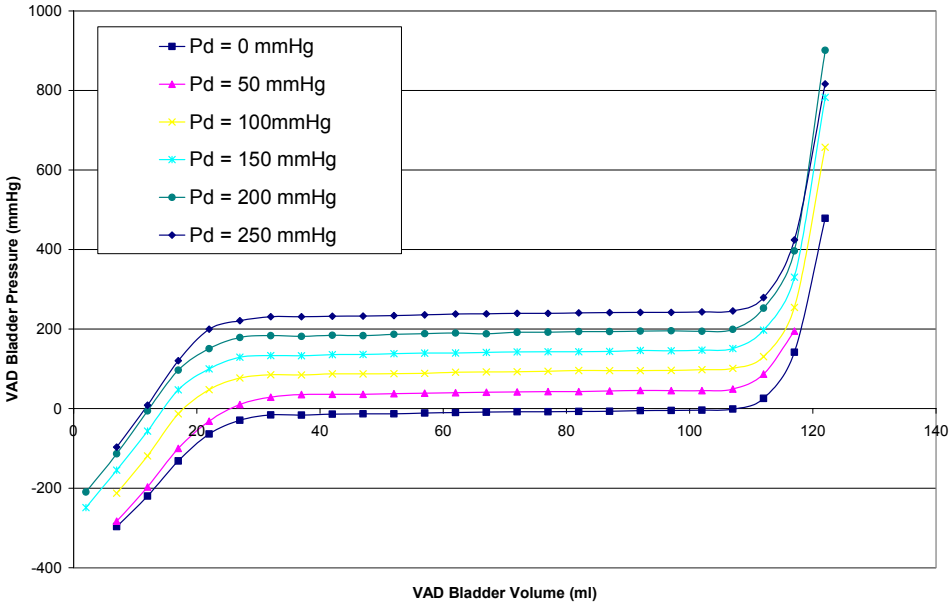

Figure 12: Effect of pneumatic drive pressure (P_d) on VAD pressure-volume relationship under static conditions.

This plot shows a similar relationship as in Figure 10, with only a vertical offset equivalent to the pneumatic pressure applied. From this experiment, it can be observed that under static conditions, instantaneous pressure in the bladder (Pp) can be estimated with the following equation:

$$C(V_V) = \frac{V_V - V_{D\text{-}VAD}}{P_P - P_d} \tag{3-1}$$

where V_V is the volume of the VAD bladder, $C(V_V)$ and $V_{D\text{-}VAD}$ are the slope^{-1} and volume intercept, respectively, of the static pressure-volume curve as shown in Figure 11. From these static data and an intuitive analogy of the physical system, the following electric analog model for the VAD is proposed (Figure 13).

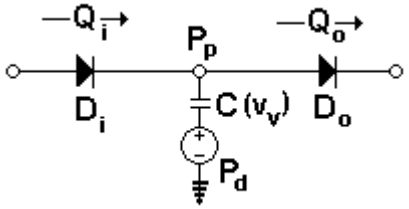

Figure 13: Initial electric analog model of the VAD

The VAD bladder is a volume dependent capacitor with a value of $C(V_V)$. $C(V_V)$ can be calculated using the piece-wise linear relationship in Figure 11. The external pneumatic drive pressure, P_d, is a pressure source, and is added to the instantaneous bladder pressure Pp. The two diodes represent the inlet and outlet valves.

3.1.2 Dynamic Study

3.1.2.1 Methods

To further investigate the behavior of the VAD, experiments were performed under dynamic conditions. An in-vitro fluid circuit was used for this purpose, depicted in Figure 14.

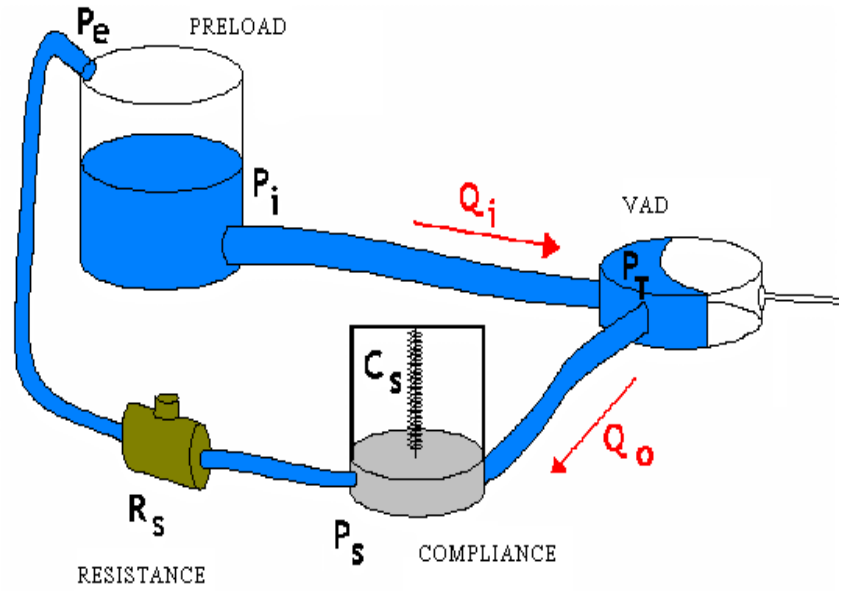

Figure 14: In-vitro setup of VAD with constant preload and variable afterload.

Inlet pressure P_i was created by a constant water level in a resevior. Flow in and out of the Thoratec® bladder, Q_i and Q_o respectively, were measured with ultrasonic flow probes. (5/8'' ID, Transonic Systems, Ithaca, New York). The entire system was filled with water at ambient temperature. The VAD ejected against an external hydraulic load consisting of a compliance (C_S) and a resistance (R_S). The custom-made compliance chamber was a steel cylinder with a rubber, diaphragm lid pushing against a spring. A needle valve (Deltrol Fluid Products, Bellwood, IL) served as the hydraulic resistor, R_S, which could be altered by adjusting the valve orifice opening. Characterization of the valve as a function of handle position can be found in Appendix D. Pressure (P_S) was recorded at the compliance chamber with a disposable pressure transducer (PX272, Edwards Lifesciences, Irvine CA) and an electronic monitor (870, Datascope Corp., Paramus NJ). The VAD was fitted with a custom port to enable pressure measurements inside the bladder (P_T) without interfering with the function of either the inlet or

outlet valves. A 6F micro-tip pressure transducer (Millar Instruments, Houston, Texas) was inserted into the custom port. Figure 15 shows the Thoratec® VAD fitted with the custom pressure port and flow probes.

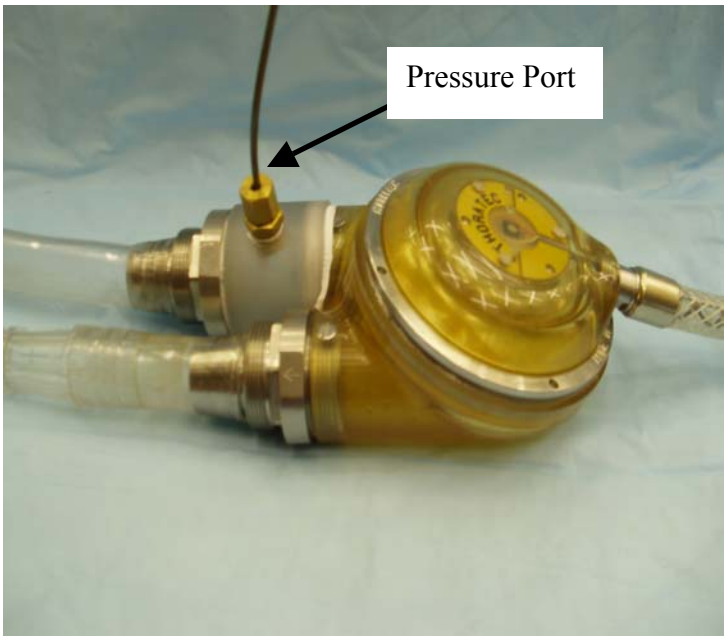

Figure 15: Thoratec® pneumatic VAD, retrofit with pressure port.

A PC-based data acquisition system was used to acquire data. Steady-state data were collected for a minimum of thirty seconds at a sampling rate of 200 Hz. Multiple runs were performed, and afterload to the ventricle was adjusted by moving the position of the needle valve opening. A series of experiments were performed under various resistances and different VAD control modes. Table 1 outlines the different experimental conditions.

Table 1: Experimental Summary

	Algorithm	Rate (bpm)	Resistance (mmHg*s/ml)
Run 1	fixed	60	0.2
Run 2	fixed	60	11.2
Run 3	fixed	60	12.0
Run 4	fixed	60	1.7
Run 5	fixed	60	0.3
Run 6	fixed	30	0.5
Run 7	fixed	30	0.4
Run 8	fill-to-empty	N/A	0.2
Run 9	fill-to-empty	N/A	12.8
Run 10	fill-to-empty	N/A	12.9
Run 11	fill-to-empty	N/A	14.4
Run 12	fill-to-empty	N/A	1.9
Run 13	fill-to-empty	N/A	0.3
Run 14	fill-to-empty	N/A	0.5
Run 15	fill-to-empty	N/A	1.6
Run 16	fill-to-empty	N/A	1.5
Run 17	fill-to-empty	N/A	2.1

The experimental data were then compared to numerical results obtained from an electric analog. Figure 16 shows the electric analog used to model the experimental system.

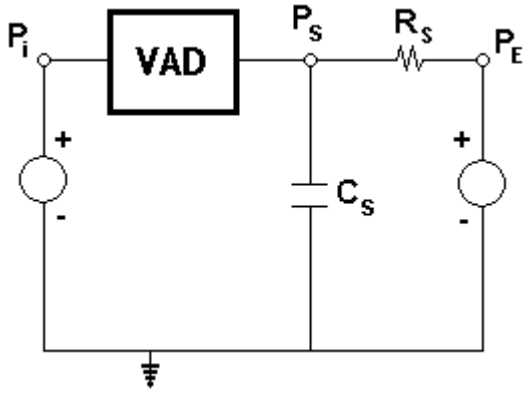

Figure 16: Schematic of the in-vitro set up.

3.1.2.2 Dynamic Pressure-Volume Behavior

Figure 17 shows the actual dynamic pressure-volume relationship inside the VAD bladder. Volume of the bladder was obtained by integrating the inlet flow waveform and subtracting the integral of the outlet flow waveform. Initial volume was estimated by aligning the dynamic data with the static curve.

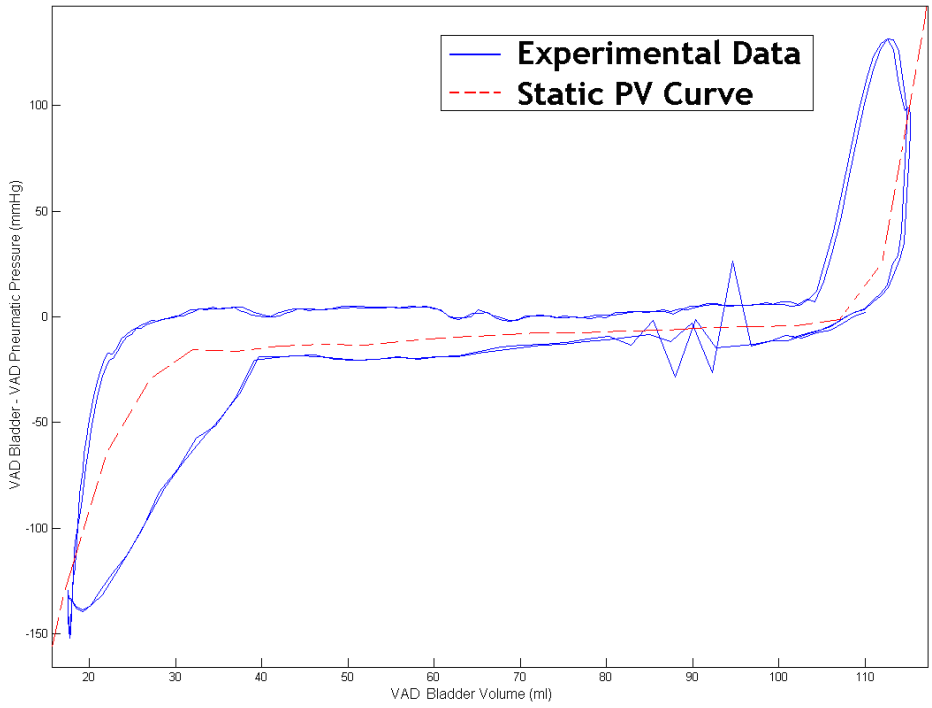

Figure 17: Dynamic pressure-volume behavior of VAD bladder.

The dynamic pressure-volume relationship did not directly follow the static curve derived earlier: measured pressure was greater and less than predicted static pressure during the filling phase and ejection phase, respectively. These deviations can be reconciled by the addition of resistive and inductive elements to the static model. The improved electric analog model of the VAD is shown in Figure 18.

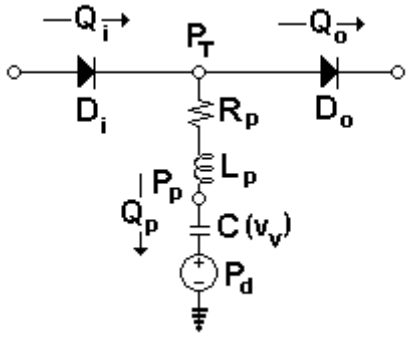

Figure 18: Updated electric analog model of the VAD to correct for dynamic observations.

The value of the series inductor L_P was calculated using Equation 2-4. The value of the resistor, R_P, was adjusted until simulated model data closely matched the dynamic pressure curve shown in Figure 17. Results of the revised VAD model are compared to the experimental dynamic pressure-volume relationship in Figure 19.

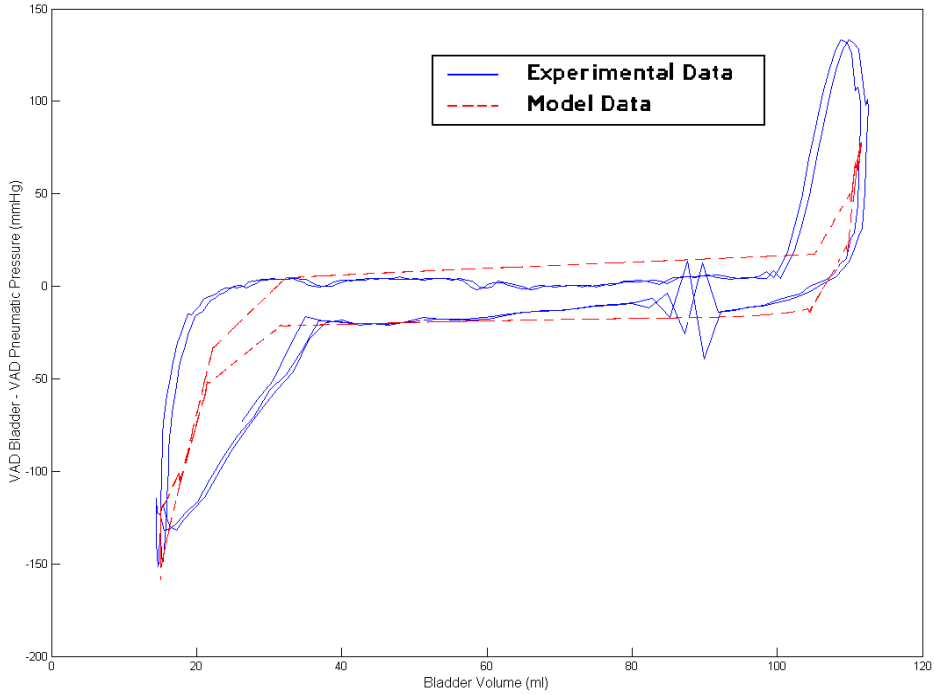

Figure 19: Data for revised model, including bladder resistance (Rp) and inductance (Lp).

Qualitatively, it is observed that the revised model characterizes the dynamic pressure-volume response of the VAD better than the static model. There is still noticeable error in the regions of maximum and minimum volume, possibly a result on system non-linearities.

3.1.2.3 Pneumatic Driver

Ejection and filling pressures for the driver can be set independently by the user. In the clinical setting, ejection (P_E) and filling (P_F) pressures are typically set to 220 and -35 mmHg, respectively. The Thoratec Dual Drive Console (DDC®) provides an analog signal corresponding to the pneumatic pressure, P_d (Figure 21). It appeared that the dynamics of this pneumatic drive pressure can be modeled as a simple RC circuit (Figure 20).

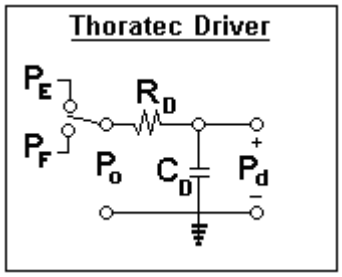

Figure 20: Electric analog model of the VAD pneumatic driver.

Values of VAD pneumatic driver parameters were estimated through least squares regression. The optimal values of C_D and R_D were 4.0 ml/mmHg and = 0.01 mmHg*s/ml, respectively. As illustrated in Figure 21, this simple model of the pneumatic driver can reproduce the experimental data quite well.

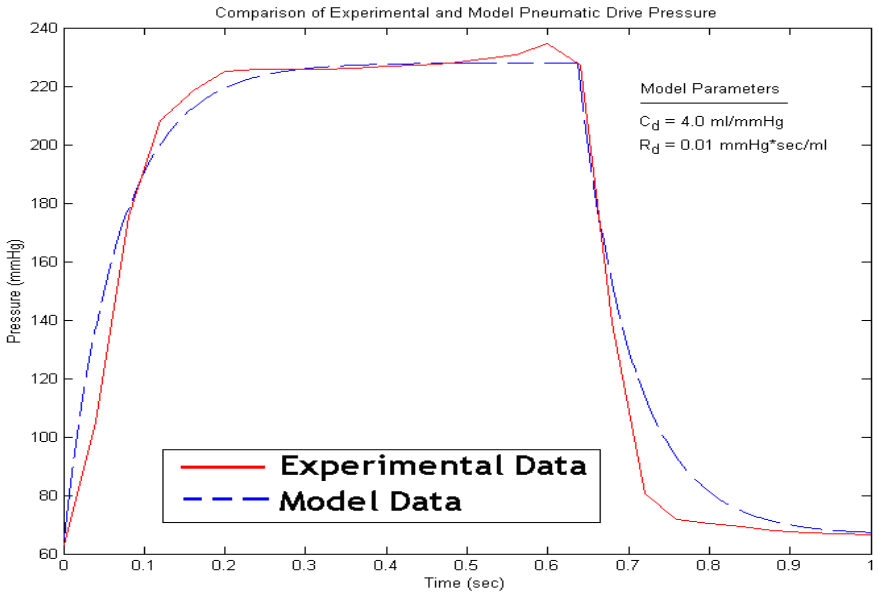

Figure 21: Comparison of modeled pneumatic pressure and experimental data.

In our experiments, pressure outside the VAD bladder (P_{ex}) was recorded directly and was found to be different from that reported by the DDC pneumatic pressure signal (P_d). This

difference depended on dynamic conditions. For example, when VAD volume decreased rapidly during ejection, P_{ex} was less than P_d, presumably due to a rapid expansion of the air in the pneumatic system. Ferrari et al. [87] modeled the properties of the pneumatic pressure with ideal gas laws. We chose a different approach to this modeling problem. It appeared that the ratio of P_{ex} and P_d was proportional to the rate of change of fluid volume in the chamber ($\dot{V}_V$). Thus, the following equation was used to relate P_{ex} to P_d:

$$P_{ex} = P_d \times \alpha \dot{V}_V \tag{3-2}$$

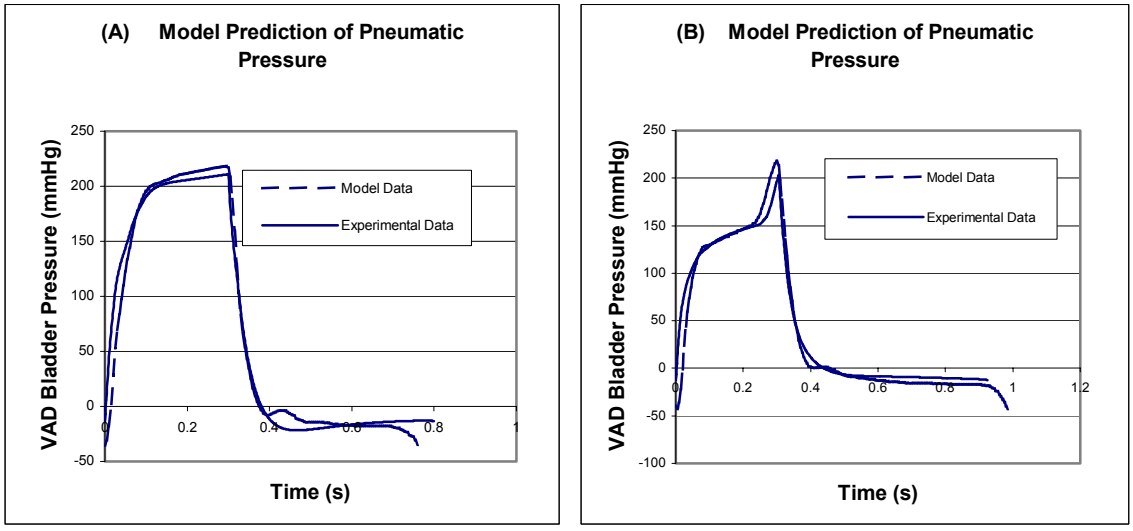

Figure 22: Measured pneumatic pressure in the VAD chamber under (A) high afterload, and (B) low afterload.

An empirical estimate of α was 0.15 (s/ml). Figures 22A and 22B show that the proposed modeling technique accurately describes measured P_{ex}. These illustrations correspond to two settings of VAD afterload. In Figure 22A, afterload was 12.8 mmHg*s/ml and the user defined

console ejection pressure was 234 mmHg. Because of the high afterload on the VAD, $\dot{V}_V$ was low and therefore, P_{ex} (Figure 22A) closely resembles P_d (Figure 21). In contrast, Figure 22B shows a low afterload case, where output resistance was 0.5 mmHg*s/ml and the user defined console ejection pressure was 211 mmHg. Due to high initial $\dot{V}_V$, there is a slower rise in P_{ex}. When ejection nears completion and $\dot{V}_V$ approaches zero, P_{ex} reaches the prescribed user-defined ejection pressure. The proposed model reproduces this phenomenon.

3.1.2.4 Cannula Modeling

Inlet and outlet cannula are modeled as an inductor and resistor in series. Initial values for the cannula inductors were estimated using Equation 2-4 and a correction factor [48]:

$$L=\frac{9}{4}\left(\frac{\rho\ell}{A}\right) \tag{3-3}$$

where ρ is the fluid density, ℓ is vessel length, and A is vessel cross sectional area. Although Equation 3-3 provided a good estimate of outlet cannula inductance (L_o), inlet cannula inductance (L_i) had to be increased by a factor of 1.75 to yield a good match between model-based predictions and experimentally measured data.

Experimentally measured inlet cannula resistance, R_i, (Appendix C) was found to be greater than that estimated by Equation 2-2. This may be due to turbulence, exit and enterance effects, and non-ideal inlet valve (i.e., finite resistance in the open position). The value for inlet resistance (R_i) listed in Table 2 matches the value found in literature [83]. While flows through

inlet and outlet cannulae were both turbulent (inlet N_{Re} = 8000; outlet N_{Re} = 24,000), the non-linearities were more prominent for the outlet cannula. Therefore, the outlet cannula resistance (R_o) was modeled as a flow-dependent resistor as described in Table 2.

3.1.2.5 Leaky Valve Model

The VAD inlet (D_i) and outlet (D_o) valves were originally assumed to be ideal. Experimentally, this assumption was found to be incorrect; both valves exhibited reverse flows. The following scheme was followed to model leaky valves. Consider the flow through the valve (D) in Figure 23.

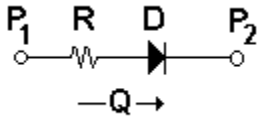

Figure 23: Schematic of flow through a vessel with a one-way valve

The expression for flow from P_1 to P_2 can be written as:

$$Q = \frac{D\left[P_1 - P_2\right]}{R} \tag{3-4}$$

A value of 1 is assigned to D when P_1 is greater than P_2; this is the open state of the valve wherein flow can occur in the forward direction (i.e., from P_1 to P_2; positive Q). A value of 0 is assigned to D when Q first becomes less than zero; this is the closed state of the valve wherein flow in the reverse direction is prohibited. Assigning a nonzero value to D when the valve is in

the closed state creates reverse flow or leakage through the valve. The values for D_i and D_o (Table 2) were empirically chosen to provide best fit of negative flows at the VAD inlet and outlet.

Table 2 lists the values of all model parameters used in the modeling of the Thoratec® VAD system.

Table 2: VAD model parameters

	Description	Value
C_D	compliance of pneumatic drive line	4.0 ml/mmHg
R_D	resistance of pneumatic drive line	0.0100 mmHg*s/ml
L_i	inertance of Thoratec® inlet cannula	0.0854 mmHg*s^2/ml
L_o	inertance of Thoratec® outlet cannula	0.0087 mmHg*s^2/ml
R_i	resistance of Thoratec® inlet cannula	0.15 mmHg*s/ml
R_o	resistance of Thoratec® outlet cannula	0.05 + 0.00015*|Qo|
R_P	resistance of Thoratec® Bladder	0.0500 mmHg*s/ml
L_P	inertance of Thoratec® Bladder	0.0033 mmHg*s^2/ml
D_i	one-way inlet valve to Thoratec® blood sac	0.08 (closed) or 1 (open)
D_o	one-way outlet valve to Thoratec® blood sac	0.03 (closed) or 1 (open)

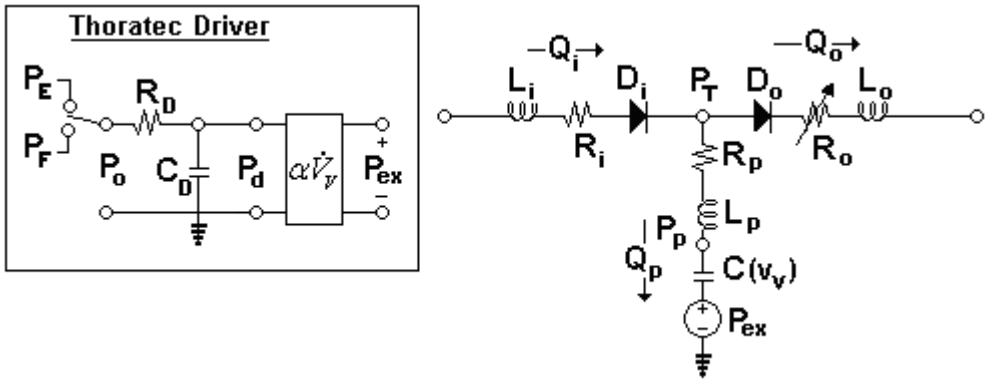

Figure 24: Final electric analog model of the VAD.

The schematic diagram for the final VAD electric analog model is shown in Figure 24. The final VAD model contains a volume-dependent capacitor, two linear resistors, a flow-dependent resistor, and three inductors. The DDC model is an RC circuit whose output, P_c, is multiplied by $\alpha\dot{V}_V$ to yield P_{ex}.

3.1.3 VAD Model Validation

VAD model parameters values were adjusted (diode leak parameters, inlet and outlet cannula resistances, and outlet cannula inductance) to fit a subset of experimental data (runs 1-4, Table 1). Figures 25-27 show the model performance with respect to fitting experimental data (run 4, Table 1). Here the VAD was controlled with a fixed rate of 60 per minute.

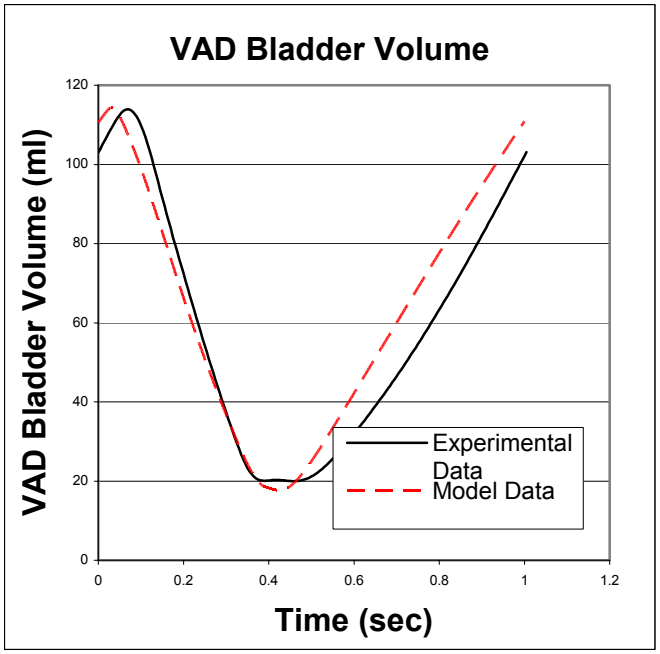

Figure 25: Comparison of experimental and model-based VAD volumes (run 4, Table 1).

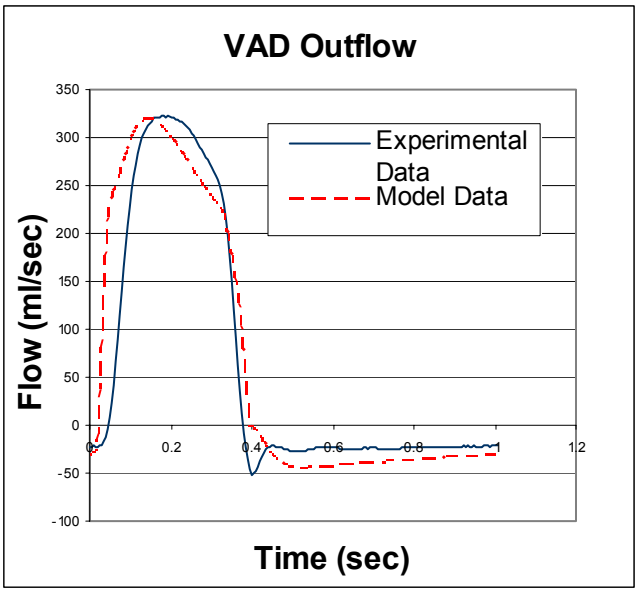

Figure 26: Comparison of experimental and model-based VAD outflows (run 4, Table 1).

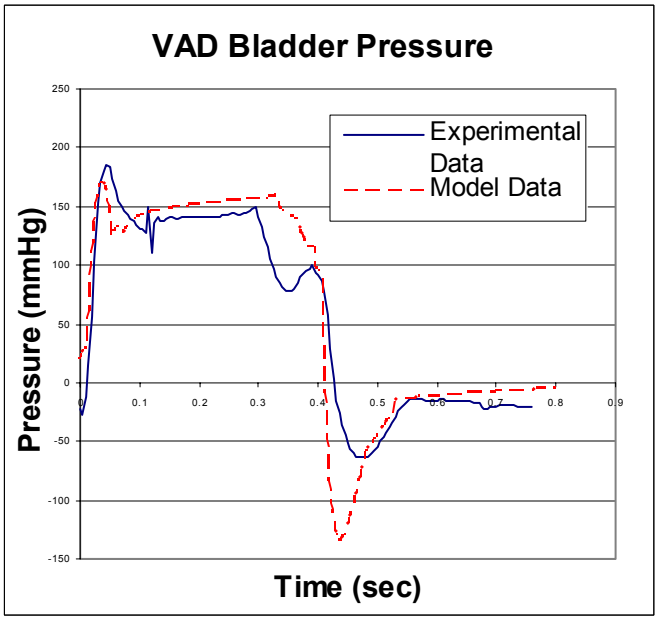

Figure 27: Comparison of experimental and model-based VAD bladder pressures (run 4, Table 1).

It can be seen that VAD pressure, flow, and volume are successfully modeled in the fixed rate mode. The optimized model was then used to predict experimental data for conditions other

than those used for parameter adjustments. Figures 28-29 show model-based predictions for one of the fill-to-empty mode experimental data (run 9, Table 1). In this mode, ejection begins when the VAD bladder is full. When full, the VAD triggers a magnetic hall switch, signaling the pneumatic drive to begin ejection [88].

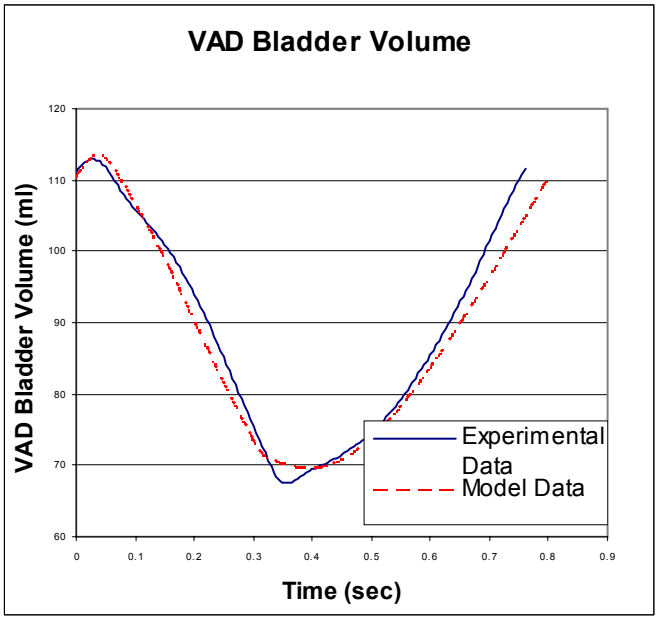

Figure 28: Comparison of experimental and model-based VAD bladder volumes (run 9, Table 1).

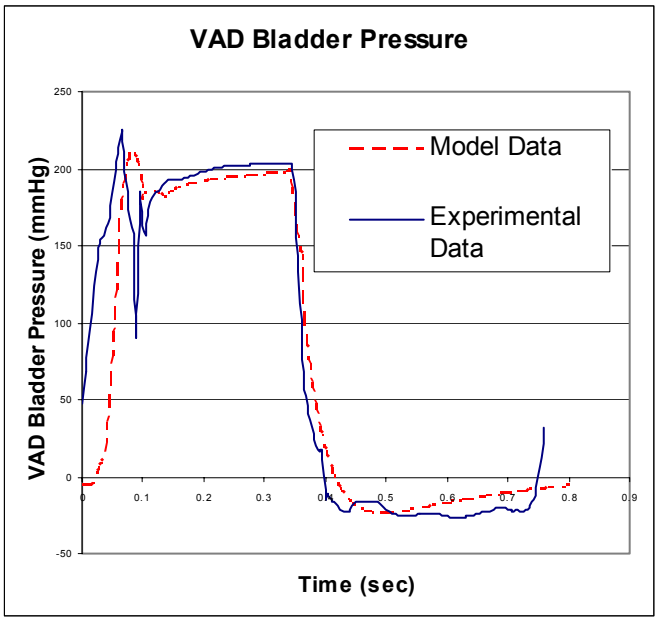

Figure 29: Comparison of experimental and model-based VAD bladder pressures (run 9, Table 1).

Similarly desirable predictability was noted with other experimental conditions. Figure 30 shows the model's ability to predict stroke volume and VAD rate in all experimental conditions wherein the fill-to-empty mode was used (n=10).

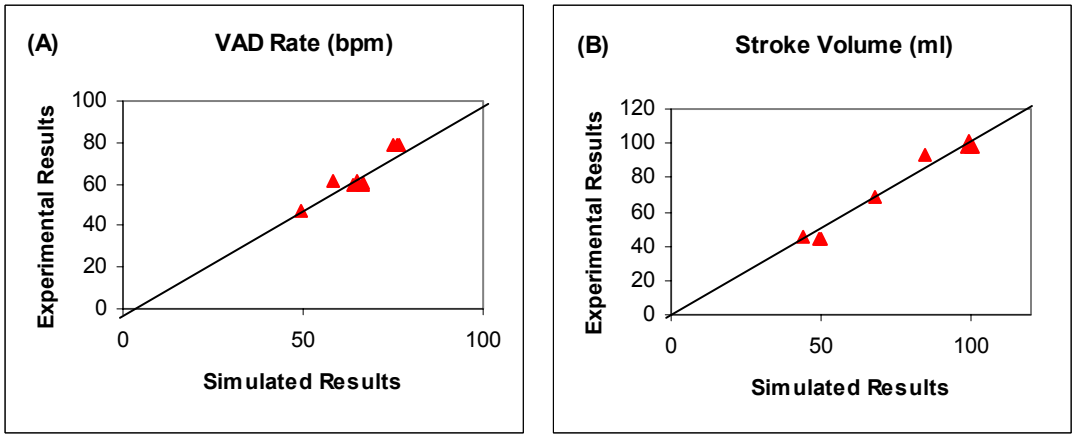

Figure 30: Comparison of experimental data (fill-to-empty mode) and model-based predictions: (A) VAD rate (B) and stroke volume (solid line: line of identity).

The percent error of each simulated point was measured against the respective experimental point. These individual errors were averaged to obtain an overall, average percent error for both stroke volume and VAD rate. The model accurately predicted stroke volume within 5.2±2.5% and VAD rate within 6.3±0.8%. In summary, the proposed VAD model was found to have both descriptive and predictive validity.

3.2 NATIVE CARDIOVASCULAR MODEL

A simple, lumped parameter electrical analog model (Figure 31) was chosen to represent the native cardiovascular system. This model has been used previously in other studies [82, 84, 89] and contains a left ventricle, systemic circulation, left atrium, and aortic and mitral valves. The left ventricle, systemic circulation, and left atrium are represented by a time-varying elastance (E(t)), a four-element Windkessel (R_C, L_S, C_S, R_S), and a passive compliance (C_R), respectively. The two valves are represented by ideal diodes in series with linear resistances.

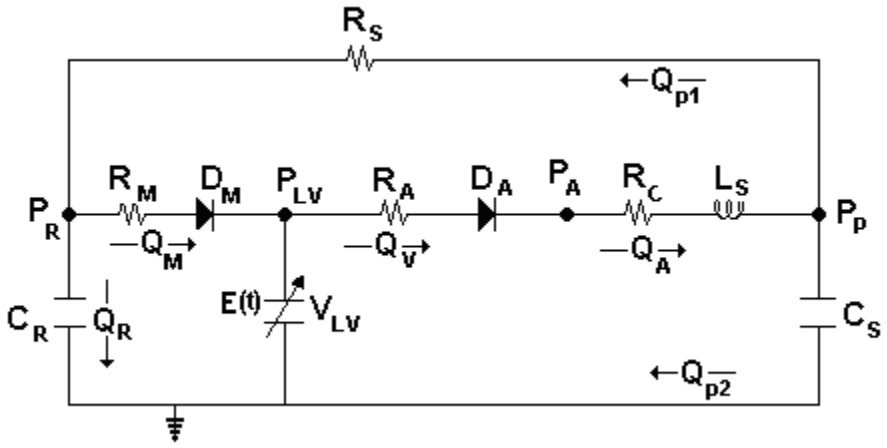

Figure 31: An electrical analog model of the native cardiovascular system.

Table 3: Native cardiovascular model variables

	Description
V_{LV}	left ventricular volume*
P_{LV}	pressure of the left ventricle
P_{AO}	aortic pressure
P_{Ao}	aortic pressure
P_A	peripheral arterial pressure*
P_R	left atrial pressure*
Q_V	flow exiting the ventricle (same as Q_A)
Q_A	aortic flow*
Q_M	flow through the mitral valve
Q_R	atrial flow

* denotes state variable

Table 4: Native cardiovascular model parameters

	Description	Normal Value
R_A	resistance of the aortic valve	0.01 mmHg*s/ml
D_A	aortic valve	0 or 1
D_M	mitral valve	0 or 1
R_C	characteristic resistance of the aorta	0.0398 mmHg*s/ml
L_S	inertance of blood in large arteries	0.001025 mmHg s^2/ml
Cs	systemic arterial compliance	2.896 ml/mmHg
R_S	systemic arterial resistance	0.8738 mmHg*s/ml
C_R	pulmonary and venous compliance	4.00 ml/mmHg
$E_n(t_n)$	left ventricular normalized time varying active elastance	See Equation 3-5
E_{max}	left ventricular maximum active elastance	3.0 mmHg/ml
T_{max}	Time to maximum left ventricular active elastance	See Equation 3-8
V_D	left ventricular systolic unstressed volume	5.0 ml
E_p	left ventricular passive elastance	0.06 mmHg/ml
V_0	left ventricular diastolic unstressed volume	15.0 ml
T_{CYCLE}	Cardiac cycle time	0.80 s

Parameter values for systemic circulation were taken from Yu [84]. The aortic (D_A) and mitral (D_M) valves are modeled as ideal diodes. Therefore, following the discussion in section

3.1.2.5, D_A and D_M take on values of either 1 (valve closed) or 0 (valve open). The software coding implemented for valve modeling can be seen in detail in Appendix A.

3.2.1 Left Ventricular Model

As described previously, the concept of time-varying elastance facilitates the modeling of ventricular active contraction (Equation 2-7). Analytical approximations are now available, such as the one shown in Equation 3-5, to provide a mathematical form for the experimentally observed active elastance ($E_a(t)$) waveforms [90].

$$E_n(t_n)=1.553174\left[\frac{\left(\frac{t_n}{0.7}\right)^{1.9}}{1+\left(\frac{t_n}{0.7}\right)^{1.9}}\right]\left[\frac{1}{1+\left(\frac{t_n}{1.173474}\right)^{21.9}}\right] \tag{3-5}$$

$E_n(t_n)$ is a normalized curve that begins with a value of zero, and reaches a peak value of one at $t_n = 1$, then returns to zero (Figure 32). $E_a(t)$ is given by:

$$E_a(t)=E_{MAX}*E_n(t_n) \tag{3-6}$$

$$t_n=\frac{t}{0.2+0.1555*T_{CYCLE}} \tag{3-7}$$

where E_{MAX}, T_{MAX}, and T_{CYCLE} are maximum elastance, time to maximum elastance, and cardiac cycle time, respectively. The expression in the denominator in Equation 3-8 is an empirically derived relationship between T_{MAX} and T_{CYCLE} (inverse of heart rate).

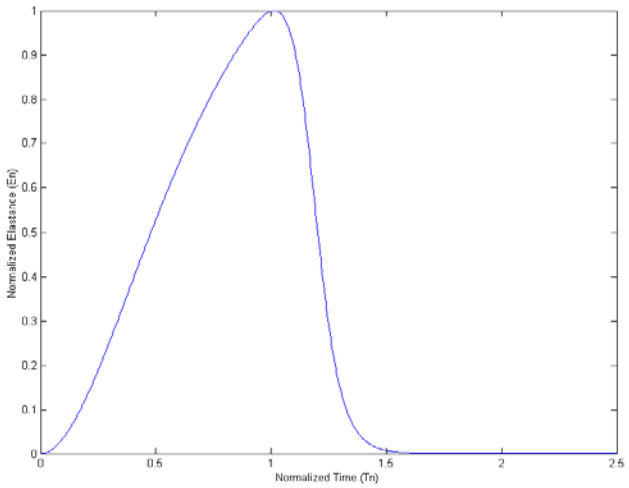

Figure 32: Normalized left ventricular elastance function.

$E_a(t)$ is a model of the active contraction of the heart. The heart also creates passive pressure as a result of the stretch of the ventricular muscle during diastole. This passive element can be approximated by a linear pressure-volume relationship (i.e., constant passive elastance). Equation 3-8 shows an elastance based model of ventricular contraction where the active and passive behaviors are given by:

$$P_{LV}(t)=E_a(t)\left[V_{LV}-V_D\right]+E_p\left[V_{LV}-V_0\right] \tag{3-8}$$

where $E_a(t)$ is the active elastance of the ventricle and E_p is the constant passive component of elastance. V_D and V_0 are the volume-axis intercepts of the ESPVR and EDPVR, respectively.

Equation 3-8 can be simplified to combine the V_{LV} term;

$$P_{LV}(t)=E(t)\left[V_{LV}-V_D\right]-E_p\Delta V \tag{3-9}$$

where $E(t) = E_a(t) + E_p$ and $\Delta V = V_0 - V_D$. This form of the equation is simplest to work with when using the state-space method for solving system differential equations (see section 3.2.2).

3.2.2 Governing System Differential Equations and Numerical Solution

The governing system differential equations for the native cardiovascular system (Figure 31) are as follows:

$$\dot{V}_{LV}=-D_A Q_A+\frac{D_M}{R_M}P_R-\frac{D_M}{R_M}\left[E(t)\left[V_{LV}-V_D\right]-E_p\Delta V\right] \tag{3-10}$$

$$\dot{Q}_A=\frac{-[D_A R_A+R_C]}{L_S}Q_A-\frac{D_A}{L_S}P_A+\frac{D_A}{L_S}\left[E(t)\left[V_{LV}-V_D\right]-E_p\Delta V\right] \tag{3-11}$$

$$\dot{P}_A=\frac{1}{C_S}Q_A-\frac{1}{R_S C_S}P_A+\frac{1}{R_S C_S}P_R \tag{3-12}$$

$$\dot{P}_R=\frac{1}{C_R R_S}P_A-\left[\frac{1}{C_R R_S}+\frac{D_M}{C_R R_M}\right]P_R+\frac{D_M}{C_R R_M}\left[E(t)\left[V_{LV}-V_D\right]-E_p\Delta V\right] \tag{3-13}$$

Each equation above expresses the first derivative of a state variable as a function of state variables and model parameters. Therefore, a solution for these four simultaneous differential equations can be obtained by numerical methods. Figure 33 shows model-based results for a normal, human cardiovascular system (model parameter values in Table 4).

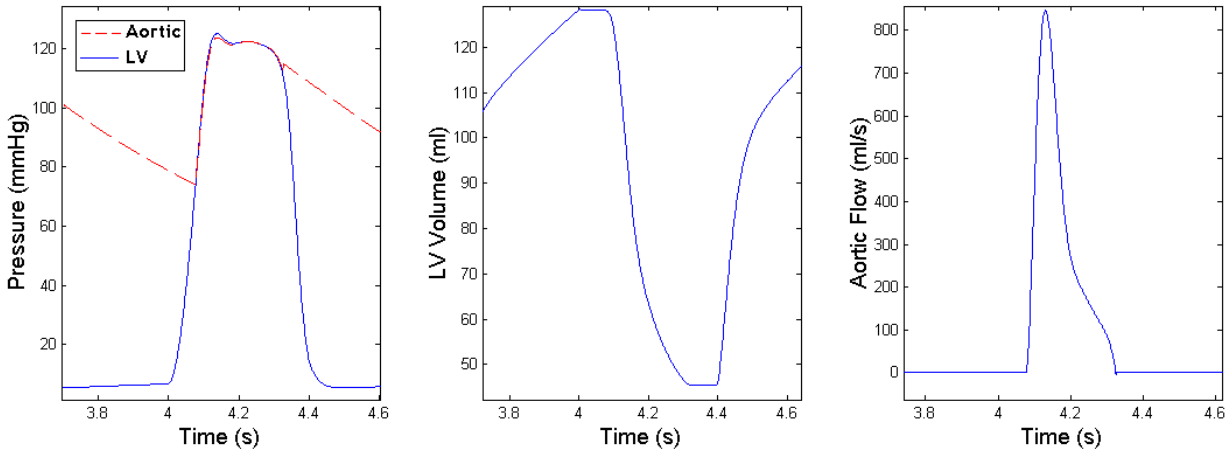

Figure 33: Hemodynamic results obtained using the native cardiovascular model with normal parameter values.

Results show aortic pressures of 123/73/100 mmHg (systolic/diastolic/mean), LV volumes of 128/46 ml (EDV/ESV), and cardiac output of 6.2 L/min. These values are typical for normal human physiology [91].

3.3 VAD-CARDIOVASCULAR MODEL

In this section, the VAD model is coupled to the model of the native cardiovascular system (CVS) to investigate VAD-ventricle dynamic interactions. Figure 34 shows the coupled VAD/CVS model. The inlet cannula of the Thoratec® is attached to the apex of the left ventricle at the node P_{LV}. Outlet flow from the Thoratec® returns to the CVS at the ascending aorta node, P_{Ao}.

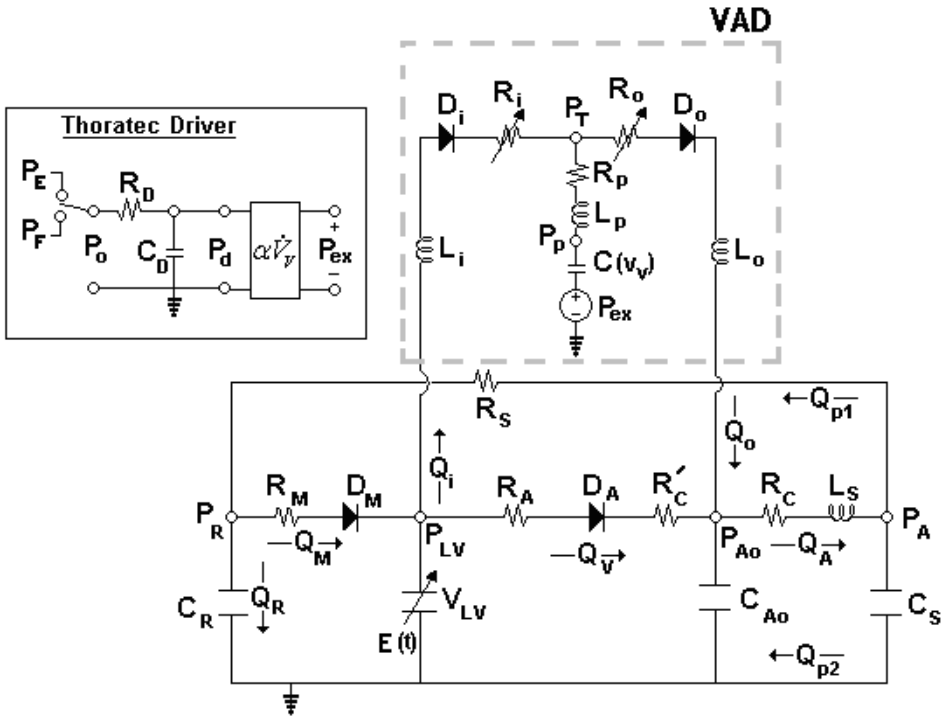

Figure 34: Electrical analog model of the coupled VAD and native cardiovascular system.

Two modifications were implemented in the coupled systems that were not present in the individual models. VAD filling pressures are often below zero and because of this, ventricular collapse must be considered. Otherwise the model would predict an impossible scenario of negative LV volume. Collapse was modeled by exponentially increasing R_i as V_{LV} approaches zero. In the VAD/CVS system, R_i was not constant, but a function of V_{LV} as described by the following expression:

$$R_i = R_i + \exp(-k*V_{LV}) \tag{3-14}$$

A value of 0.25 was chosen for k. This value allows the effect of collapse to be minimal at volumes above 15 ml, and rapidly reduces flow into the VAD as V_{LV} falls below 15 ml, ensuring

that volume in the LV is never zero. A plot of inlet resistance as a function of LV volume is shown in Figure 35.

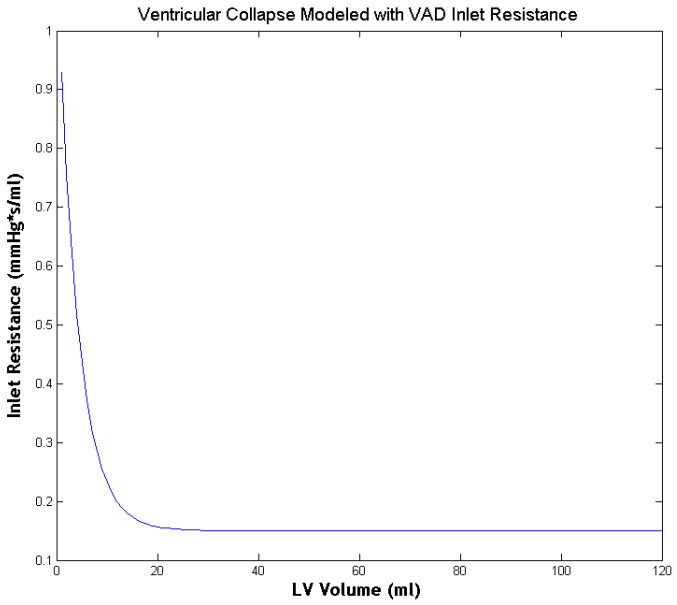

Figure 35: Ventricular collapse model; inlet VAD resistance as function of ventricular volume

A second modification was made to the native CVS model described earlier. An additional compliance element (C_{Ao}) was added at the aortic node and aortic characteristic resistance (R_C) was divided into R'_C, placed before C_{Ao}, and R_C, placed after C_{Ao} (Figure 34). The benefit of this modification is that the pressure (P_{Ao}) in the aorta becomes a state variable, which greatly reduces the complexity of writing the governing system differential equations. It should be noted that this modification does not significantly alter the hydraulic input impedance (human heart rate frequency ranges) seen by the left ventricle (Figure 36) and therefore, has little effect on hemodynamic outcomes.

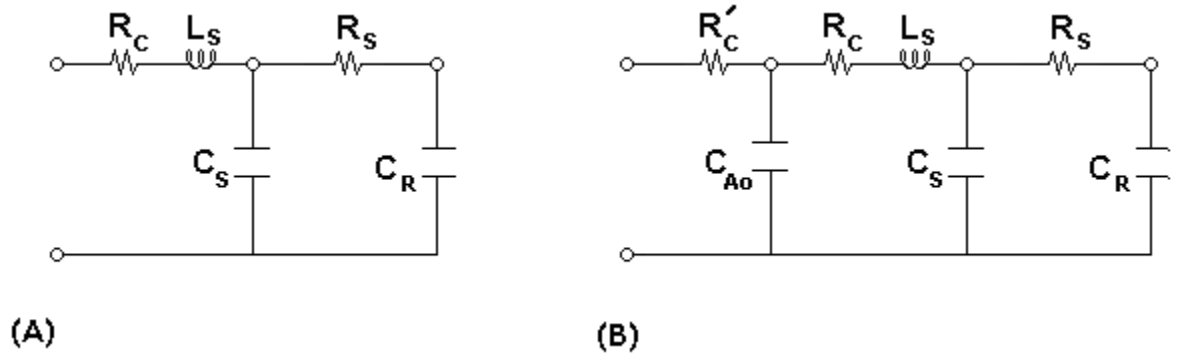

Figure 36: Original (A) and modified (B) cardiovascular models, with only the LV load elements shown.

The input impedances of the original (Z_0, Figure 36A) and modified (Z_M, Figure 36B) are given by:

$$Z_0 = R_C + j\omega L_S + \frac{1}{j\omega C_S} \| \left(R_S + \frac{1}{j\omega C_R} \right) \tag{3-15}$$

$$Z_M = R'_C + \left(\frac{1}{j\omega C_{Ao}} \right) \| \left[R_C + j\omega L_S + \frac{1}{j\omega C_S} \| \left(R_S + \frac{1}{j\omega C_R} \right) \right] \tag{3-16}$$

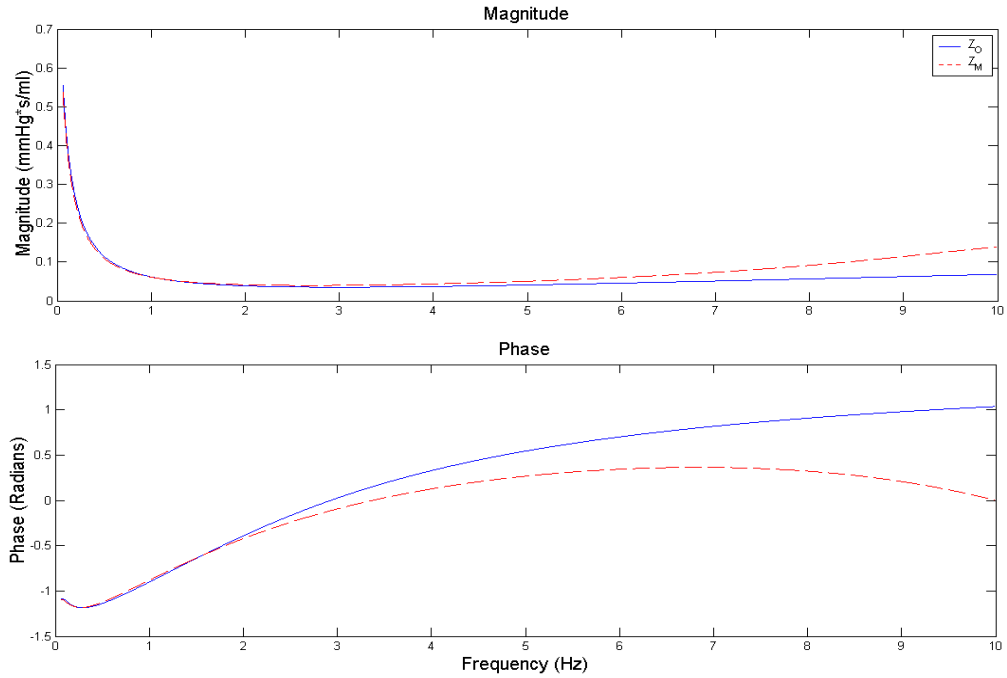

Figure 37: Input impedance spectra of the original and modified models.

The original cardiovascular model has previously been shown to compare well with human impedance spectra [82].

3.3.1 Governing System Differential Equations

The coupled VAD/CVS has nine state variables (Table 5) and four valves.

Table 5: VAD-CVS State Variables

	Description
$\mathbf{V_V}$	Thoratec® pump sac volume
$\mathbf{Q_i}$	Thoratec® cannula inlet blood flow
$\mathbf{Q_o}$	Thoratec® cannula outlet blood flow
$\mathbf{V_{LV}}$	left ventricular volume
$\mathbf{P_{Ao}}$	aortic pressure
$\mathbf{P_A}$	peripheral arterial pressure
$\mathbf{P_R}$	left atrial pressure
$\mathbf{Q_A}$	aortic flow
$\mathbf{P_d}$	pneumatic drive pressure from DDC

The governing system differential equations are as follows:

$$\dot{P}_d = \left(\frac{1}{C_D R_D} P_o - \frac{1}{C_D R_D} P_d \right) \tag{3-17}$$

$$\dot{P}_A = \frac{1}{C_s} Q_A - \frac{1}{C_s R_S} P_A + \frac{1}{C_s R_S} P_R \tag{3-18}$$

$$\dot{P}_{Ao} = \frac{D_A E(t)}{C_{Ao} R_A} \left[V_{LV} - V_O \right] - \frac{D_A E_p}{C_{Ao} R_A} [V_O - V_D] - \frac{D_A}{C_{Ao} R_A} P_{Ao} + \frac{1}{C_{Ao}} Q_o - \frac{1}{C_{Ao}} Q_A \tag{3-19}$$

$$\dot{P}_R = \frac{1}{C_R R_S} P_A - \frac{D_M E(t)}{C_R R_M} \left[V_{LV} - V_O \right] + \frac{D_M E_p}{C_R R_M} [V_O - V_D] + \left[\frac{D_M}{C_R R_M} - \frac{1}{C_R R_S} \right] P_R \tag{3-20}$$

$$\dot{V}_{LV} = \frac{D_M}{R_M} P_R - Q_i - \left[\frac{D_A}{R_A} + \frac{D_M}{R_M} \right] E(t) \left[V_{LV} - V_O \right] + \left[\frac{D_A}{R_A} + \frac{D_M}{R_M} \right] E_p [V_O - V_D] + \frac{D_A}{R_A} P_{Ao} \tag{3-21}$$

$$\dot{V}_V = Q_i - Q_o \tag{3-22}$$

$$\dot{Q}_A = \frac{1}{L_S} P_{Ao} - \frac{R_C}{L_S} Q_A - \frac{1}{L_S} P_A \tag{3-23}$$

$$\dot{Q}_i\left[1-\left(\frac{D_oL_P}{L_P+L_o}\right)\left(\frac{D_iL_P}{L_P+L_i}\right)\right]=\left(\frac{D_iE(t)}{L_P+L_i}\right)[V_{LV}-V_O]-\left(\frac{D_iE_p}{L_P+L_i}\right)[V_O-V_D]$$
$$-\left(\frac{D_o}{L_P+L_o}\right)\left(\frac{D_iL_P}{L_P+L_i}\right)P_{Ao}+\left(\left(\frac{D_iL_P}{L_P+L_i}\right)\frac{D_oR_P}{L_P+L_o}-\left(\frac{D_oR_P+R_i}{D_oL_P+L_i}\right)\right)Q_i$$
$$+\left(\left(\frac{D_iL_P}{L_P+L_i}\right)\left(\frac{D_o}{L_P+L_o}\right)-\frac{D_i}{L_P+L_i}\right)\left(\frac{V_V-V_{D\text{-}VAD}}{C_P}+\alpha\dot{V}_VP_d\right) \quad (3\text{-}24)$$
$$-\left(\left(\frac{D_iL_P}{L_P+L_i}\right)\left(\frac{D_iR_P+R_o}{D_iL_P+L_o}\right)-\left(\frac{D_iR_P}{L_P+L_i}\right)\right)Q_o$$

$$\dot{Q}_o\left[1-\left(\frac{D_oL_P}{L_P+L_o}\right)\left(\frac{D_iL_P}{L_P+L_i}\right)\right]=\left(\frac{D_o}{L_P+L_o}-\left(\frac{D_oL_P}{L_P+L_o}\right)\left(\frac{D_i}{L_P+L_i}\right)\right)\left[\frac{V_V-V_{D\text{-}VAD}}{C_P}+\alpha\dot{V}_VP_d\right]$$
$$\left(\frac{D_oL_P}{L_P+L_o}\right)\left(\frac{D_iE(t)}{L_P+L_i}\right)[V_{LV}-V_O]-\left(\frac{D_oL_P}{L_P+L_o}\right)\left(\frac{D_iE_p}{L_P+L_i}\right)[V_O-V_D]$$
$$-\left(\frac{D_o}{L_P+L_o}\right)P_{Ao}+\left(\frac{D_oR_P}{L_P+L_o}-\left(\frac{D_oL_P}{L_P+L_o}\right)\left(\frac{D_oR_P+R_i}{D_oL_P+L_i}\right)\right)Q_i \quad (3\text{-}25)$$
$$+\left(\left(\frac{D_oL_P}{L_P+L_o}\right)\left(\frac{D_iR_P}{L_P+L_i}\right)-\left(\frac{D_iR_P+R_o}{D_iL_P+L_o}\right)\right)Q_o$$

Details on the derivation of these equations are contained in Appendix B. As before, this system of coupled differential equations was solved using numerical methods in the Matlab® environment.

3.4 MODEL DEVELOPMENT SUMMARY

In this chapter, a model of a pulsatile pneumatic VAD was developed using ideas described in previous studies and new experimental measurements. Parameter values for the VAD model were estimated first from physical principles and subsequently modified as needed based on experimental measurements. The final VAD model was shown to be valid from both

descriptive and predictive perspectives. For example, it predicted fill-to-empty VAD rate and stroke volume within 6% error. The VAD model was then coupled to a model of native cardiovascular system. In the following chapter, this coupled VAD/CVS model is used to investigate VAD-ventricular interaction.

4.0 RESULTS AND DISCUSSION: MODEL-BASED ANALYSIS

The validity of individual VAD and CVS models has been established in the previous chapter and in other sources[82, 84, 89]. Now we can combine these two models to examine the coupled VAD-CVS behavior, especially in the setting of heart failure.

4.1 MODEL BASED RESULTS VS. CLINICAL DATA: A QUALITATIVE COMPARISON

As a starting point, model-based results were qualitatively compared to clinical data obtained from a study performed by Dr. John Gorcsan at UPMC. Left ventricular chamber area (short-axis), peripheral arterial pressure (at the fingers), EKG, and VAD signals were recorded in the clinical study. To facilitate comparisons, left ventricular volume (V_{LV}) in the model-based studies was converted to chamber area using a spherical geometric model. Peripheral arterial pressure (P_A) is the closest model variable available to compare to clinical arterial pressure. Model-based results and clinical data from an individual patient are illustrated in Figure 38. For model-based calculations, all cardiovascular parameters were the same as in Table 4, except for heart rate (equated to the observed heart rate) and left ventricular contractility (reduced to represent the failing left ventricle, E_{MAX} = 1.0 mmHg/ml). The VAD was operated in the modeling study according to the clinical settings, i.e., fill-to-empty mode with P_E = 220 mmHg and P_F = -35 mmHg.

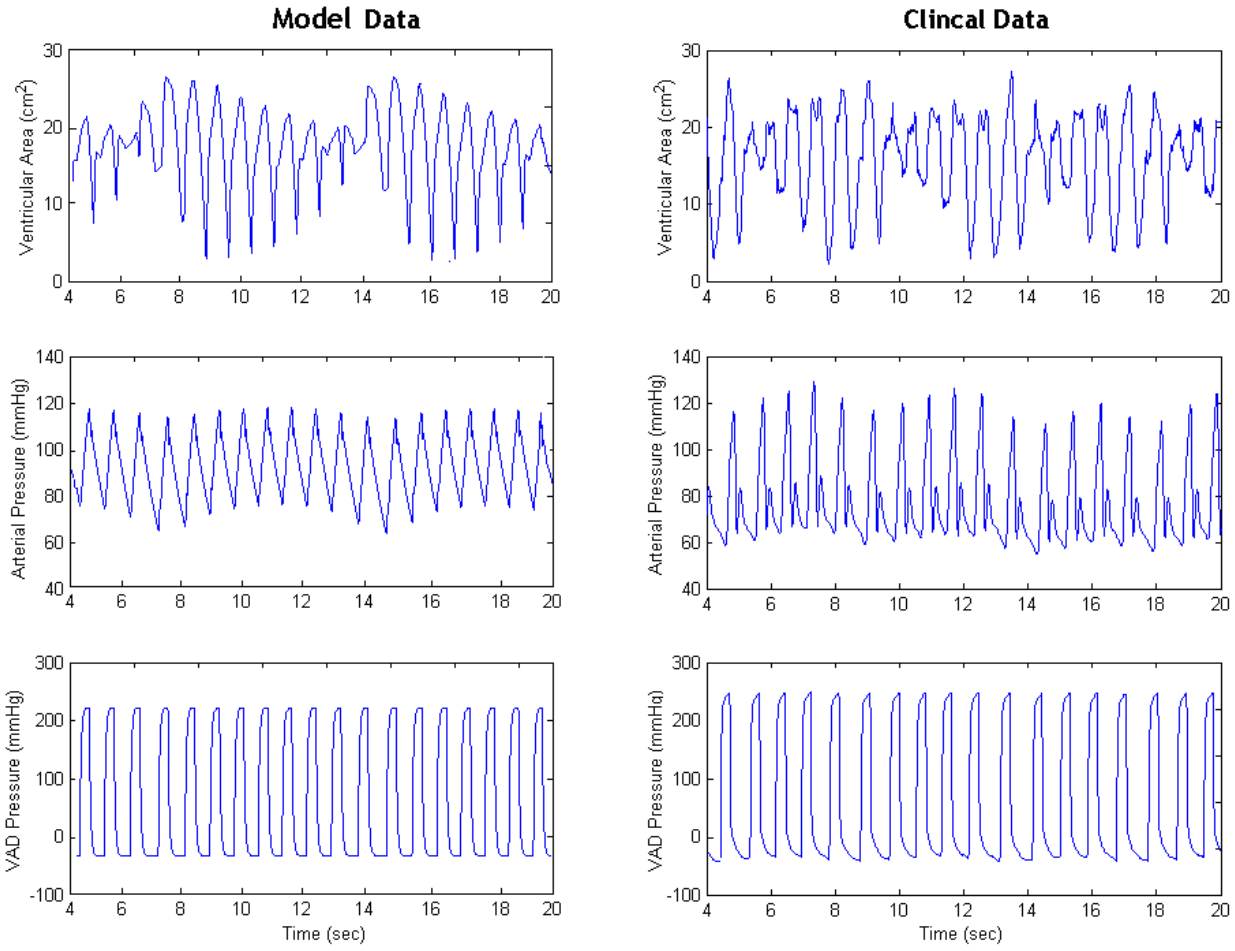

Figure 38: Qualitative comparison of model-based results and clinical data. Both sets of data are from a Thoratec® assisted LV.

Qualitatively, the patterns of hemodynamic responses are remarkably similar between the model-based results and clinical data. Similar VAD rates (model: 71 bpm, clinical data: 66 bpm) and left ventricular area and arterial pressure ranges were observed. The periodic dampening of the area curve is apparent in both the model-based results and clinical data, which is a result of the interaction between two independently running pumps: VAD and the native left ventricle. The contractions with smallest area changes correspond to co-pulsation (in phase contractions of VAD and native LV) and the largest area changes to counter-pulsations (out of phase contractions of VAD and native LV). This phasic relationship between contractions of the two

pumps (often termed the analysis of synchrony) will be shown, through model-based analysis, to have a significant effect on left ventricular hydraulic load and mechanical work. A more quantitative investigation was performed by varying key parameters of the cardiovascular model and observing their effects on the behavior of the coupled system, with a special emphasis on the analysis of synchrony.

4.2 VAD CHARACTERISTIC FREQUENCY

In the fill-to-empty mode, the frequency of VAD contraction (i.e., VAD rate) is dependent on both VAD parameters (ejection and filling pressures, bladder and inlet and outlet cannula properties) and native cardiovascular parameters, including left ventricular contractility. We define VAD characteristic frequency (f_C) as the rate at which the VAD will operate in the absence of active LV contraction, a condition corresponding to only one pump in the system. As will be seen later, this concept of VAD characteristic frequency facilitates the interpretation of the coupled behavior. The mathematical model was used to examine the influence of key cardiovascular parameters on VAD characteristic frequency. Parameters were varied over a wide range of values around the normal human physiologic levels. Figure 39 shows the dependency of f_C on systemic vascular resistance (SVR), systemic compliance (C_S), and passive LV elastance (E_P). In all of these simulations, LV active contraction was suppressed (E_{MAX} = 0 mmHg/ml).

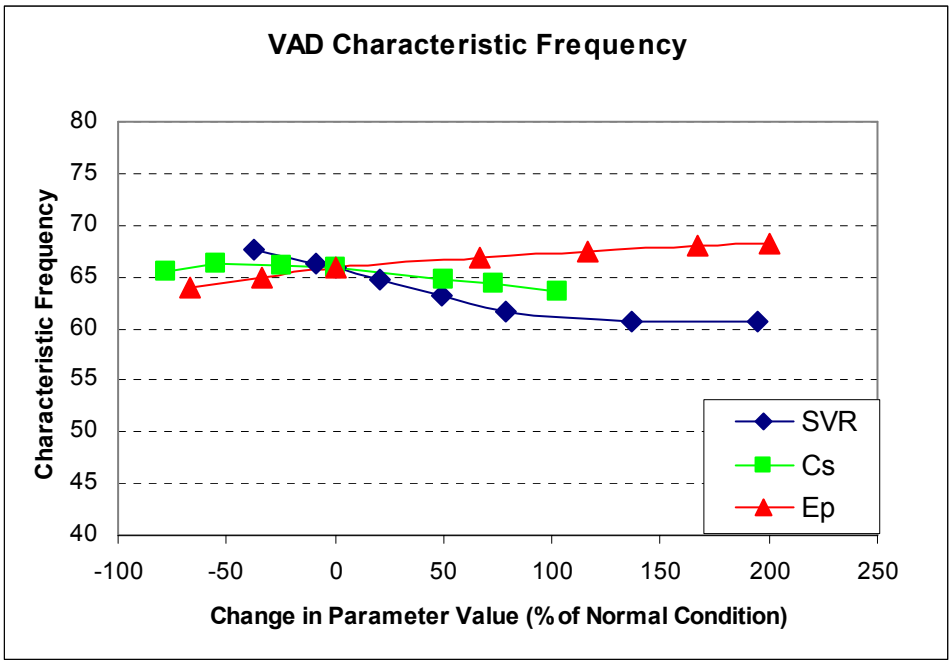

Figure 39: The effect cardiovascular parameters of the characteristic frequency

These results demonstrate that VAD characteristic frequency changes by only 10% over a large range of cardiovascular parameters. Thus, f_C can be considered as an intrinsic VAD property, independent of individual patient's cardiovascular characteristics.

4.3 ANALYSIS OF SYNCHRONY

4.3.1 Left Ventricular Contractility

Clearly, the VAD operating in the fill-to-empty mode will not function below f_C. This implies that the left ventricle must beat above f_C in order to be synchronized with the VAD. Synchrony can occur above the f_C if ventricular contraction significantly contributes to VAD filling (a condition of counter-pulsation). Consequently, a stronger left ventricle (i.e., greater E_{MAX}) has a greater potential to synchronize VAD rate to native heart rate and *vice versa*.

To vary left ventricular contractility in the model, the value of the maximum active elastance (E_{MAX}) was altered. The following plot shows the effect of E_{MAX} variations on VAD rate in the fill-to-empty mode.

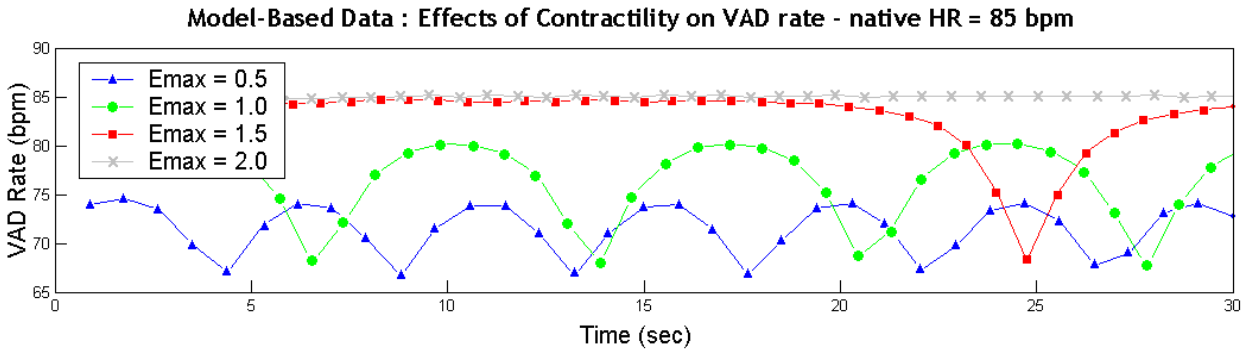

Figure 40: Model-based results: Effects of contractility on VAD rate.

The model results indicate that for a relatively strong heart (say, E_{MAX} = 2.0 mmHg/ml), the VAD rate completely synchronizes with the native heart rate of 85 bpm and there is no change over time. As contractility decreases, the VAD rate is unable to synchronize completely because the LV does not provide sufficient VAD filling within a single contraction. The VAD

rate in these circumstances is always lower than the native heart rate. Furthermore, as E_{MAX} decreases, the average VAD rate decreases and the frequency of cyclic VAD rate variations increases. The periodic minimum points of VAD rate correspond with VAD-ventricle co-pulsations (asynchronous behavior).

To further examine the effects of LV contractility on the behavior of the coupled system, we can take a closer look at model-based hemodyanmic data for a strong heart (E_{MAX} = 3.0 mmHg/ml) and a weak heart (E_{MAX} = 1.0 mmHg/ml) (Figure 41).

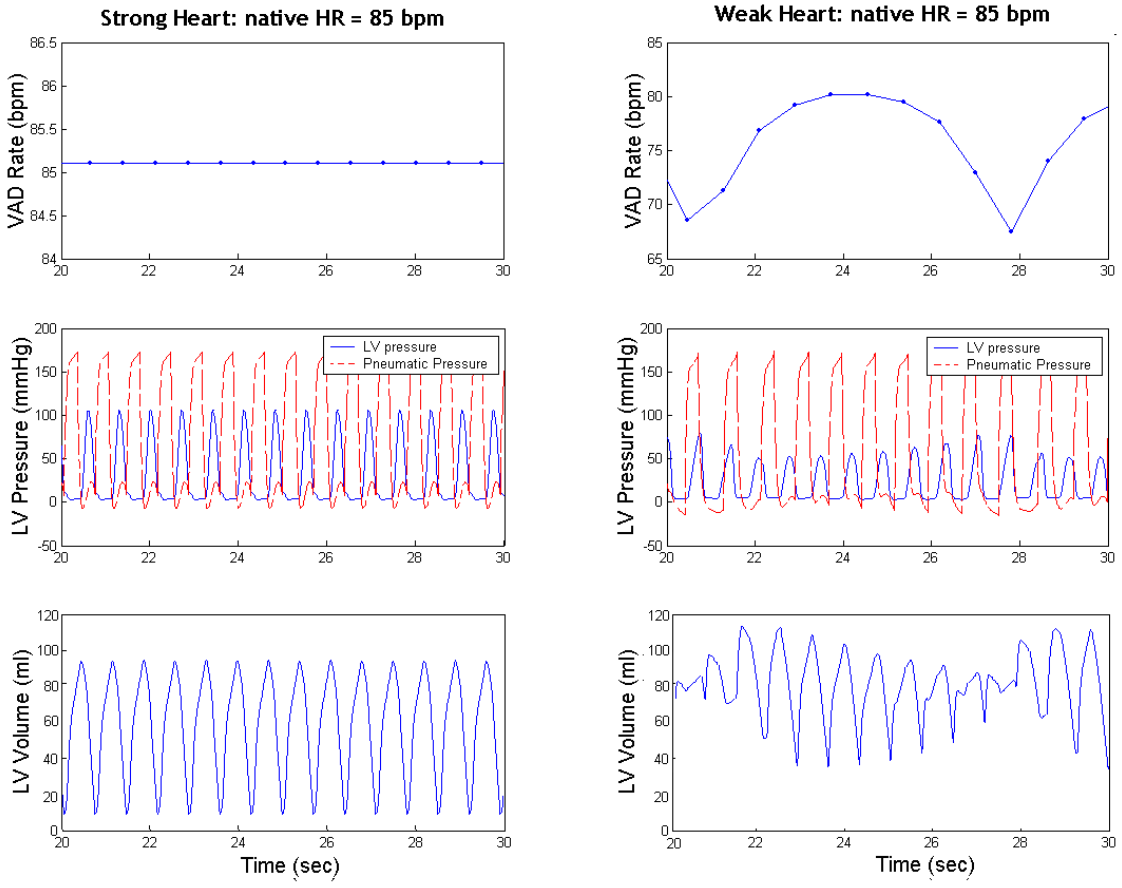

Figure 41: Model-based results (steady state data): strong heart vs. weak heart.

In the case of the strong heart (Figure 41, left panels), LV contraction is sufficiently powerful to totally fill the VAD within a single beat and therefore, the VAD rate completely synchronizes with the native heart rate. Steady state LV and pneumatic pressure waveforms clearly indicate that the LV and VAD are operating in the counter-pulsation mode (i.e., completely synchronized). In contrast, a great deal of asynchrony is seen with the weak heart (Figure 41, right panels). Here the LV is unable to completely fill the VAD in a single contraction and therefore, VAD rate is always lower than the native heart rate. In addition, VAD rate oscillates over time depending on the relative degree of synchrony (or asynchrony): regions of co-pulsations (more asynchrony) have lower VAD rate and regions of counter-pulsations (more synchrony) have greater VAD rate. Significant beat-to-beat changes in LV volume and pressure data can also be observed: increased LV end-systolic volume and pressure in regions of co-pulsations and *vice versa*. Thus, LV hydraulic load is greater during co-pulsations as compared to that during counter-pulsation. This asynchronous behavior is more frequent as the heart becomes progressively weaker, resulting in a greater occurrence of co-pulsating beats with greater hydraulic load. At this point, one would be tempted to conclude that the asynchronous behavior (i.e., cyclic changes in VAD rate, LV volume or area) can be used as an index of native LV contractility. However, results presented below indicate that factors other than LV contractility contribute to the asynchronous behavior.

4.3.2 Native Heart Rate

The rate at which the native heart contracts also plays a significant role in determining the synchrony of the VAD-ventricle system. Figure 42 shows the effects of native heart rate on synchrony for a weak heart (E_{MAX} = 1.0 mmHg/ml). These data indicate that the coupled behavior can be synchronous at some native heart rate (75 bpm in Figure 42), and asynchrony ensues above and below this rate.

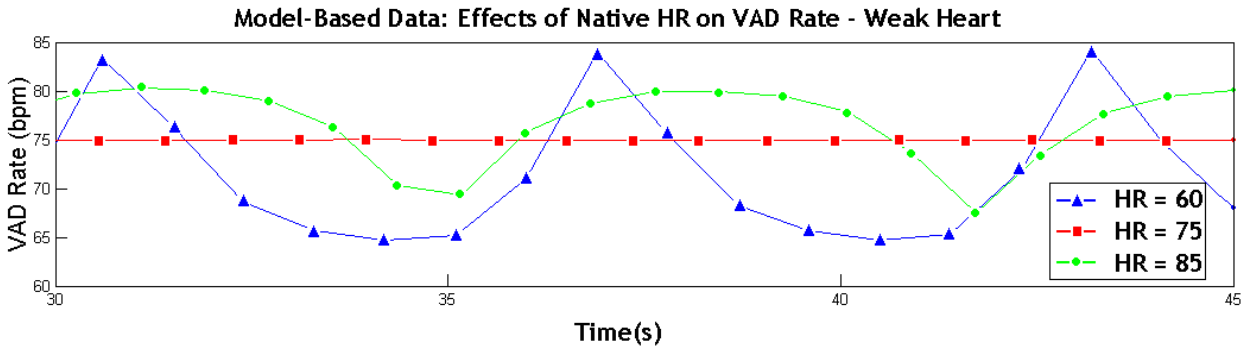

Figure 42: Effect of native heart rate on VAD-ventricle synchrony on a weak heart.

A similar pattern was observed for a strong heart (E_{MAX} = 3.0 mmHg/ml) (Figure 43). While the lower threshold for appearance of asynchrony was unchanged (60 bpm), the upper threshold increased (95 bpm for strong heart vs. 85 bpm for the weak heart).

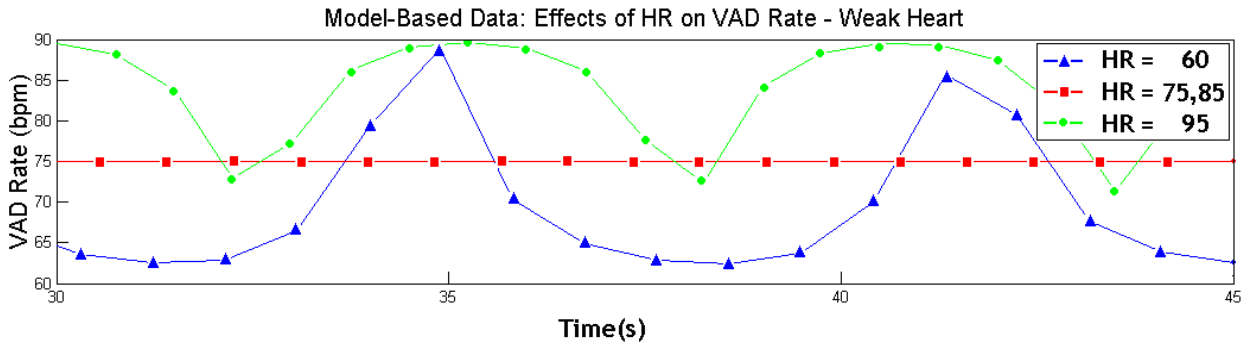

Figure 43: Effects of native heart rate on a strong heart.

The characteristic frequency (f_C) for this system was 65 bpm. The invariant lower threshold is related to f_C. If the native heart rate is below f_C, the minimum VAD rate is equal to f_C, periodically going above due to contributions by the native LV contraction to its filling. This assertion is supported by data in Figures 42-43 wherein the minimal VAD rate is always close to f_C.

The VAD-CVS model predicts that asynchronous behavior does not uniquely imply a weaker LV; native heart rate is also an independent determinant. Synchronous behavior is observed over a range of native heart rates. The lower limit of this range is governed by the characteristic frequency and the upper limit is dependent on the LV contractility: higher E_{MAX} yields higher upper limit and *vice versa*.

4.3.3 Systemic Vascular Resistance

The effects of systemic vascular resistance (SVR) on VAD-ventricle synchrony were also investigated. Figure 44 shows two examples, low SVR (0.53 mmHg*s/ml) and normal SVR (0.87 mmHg*s/ml), both with native heart rate of 85 bpm and E_{MAX} = 1.0 mmHg/ml (weak heart).

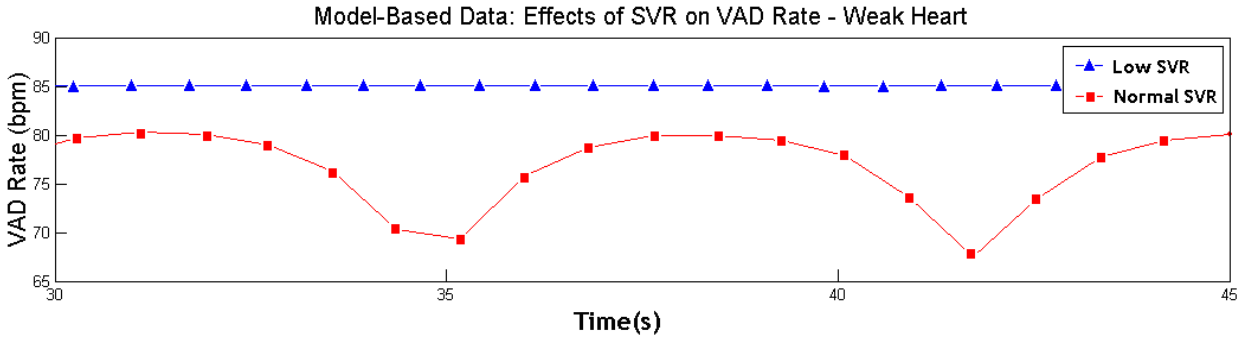

Figure 44: Effects of SVR on VAD-ventricle synchrony.

A monotonic relationship between SVR and synchrony was observed. For a given E_{MAX} and native heart rate, asynchrony can be attained at a certain SVR and this asynchrony can be abolished by lowering SVR. Increasing SVR has little effect on end-ejection VAD volume because within physiologic limits, VAD contraction is powerful enough to eject all of VAD volume during a single contraction. In contrast, increasing SVR reduces left ventricular filling pressure and consequently, reduces the rate of VAD filling and VAD rate in the fill-to-empty mode.

4.3.4 Left Ventricular Diastolic Stiffness

The slope of the passive pressure-volume relationship (E_P) was also varied to examine the effects of a stiff or flaccid left ventricle. Three different values of E_P were investigated: flaccid LV (0.02 mmHg/ml), normal LV (0.06 mmHg/ml), and stiff LV (0.18 mmHg/ml).

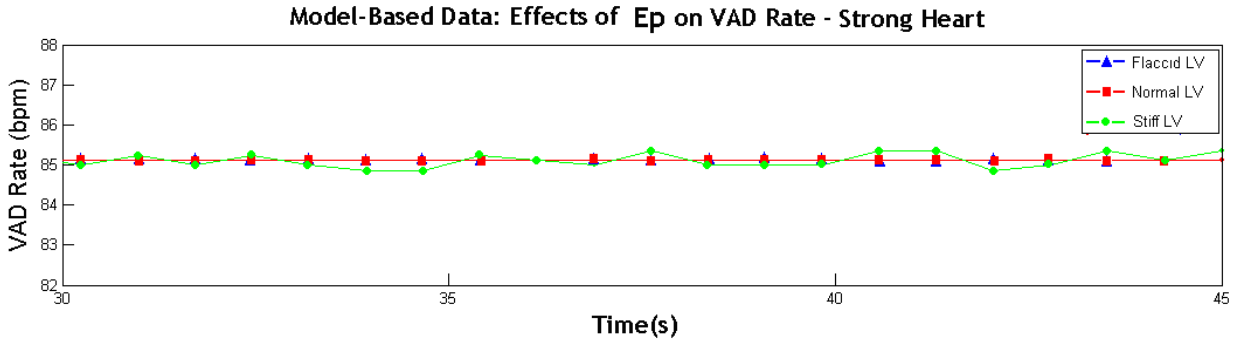

Figure 45: Effects of Ep on VAD-ventricle synchrony (strong heart)

Figure 45 illustrates that variations in E_P, within the range of 0.02 to 0.18, do not significantly affect the VAD-ventricle synchronous behavior. All three examples are shown to be in synchrony with the native heart rate of 85 bpm. As expected, increasing E_P caused LV end-diastolic volume to be reduced (Figure 46), but these effects do not have any impact on VAD filling rate.

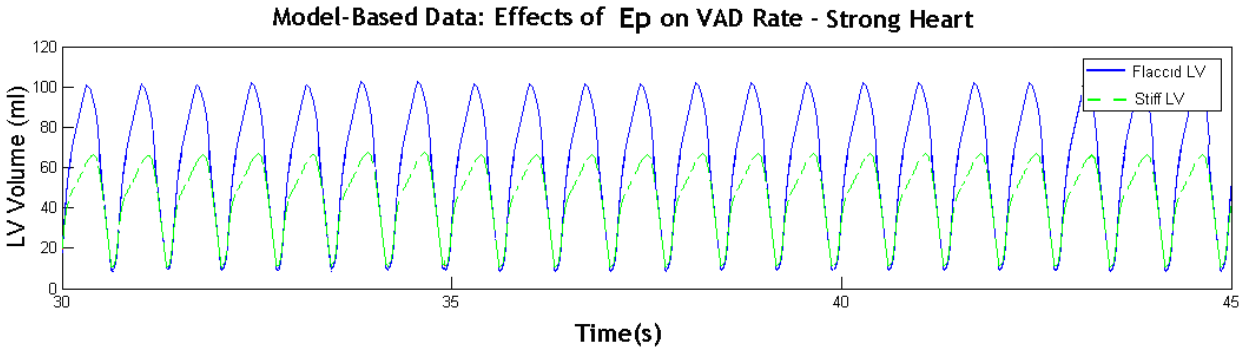

Figure 46: Effects of Ep on LV Volume (strong heart). For clarity volume data for the normal Ep value (0.06 mmHg/ml) are not shown.

Effects of variations in E_P in the case of a weak heart are shown in Figure 47. In contrast to the strong heart (Figure 45), asynchronous behavior exists in this example. However, changes in E_P, once again, do not affect this behavior in that asynchronous behavior is observed for all E_P values.

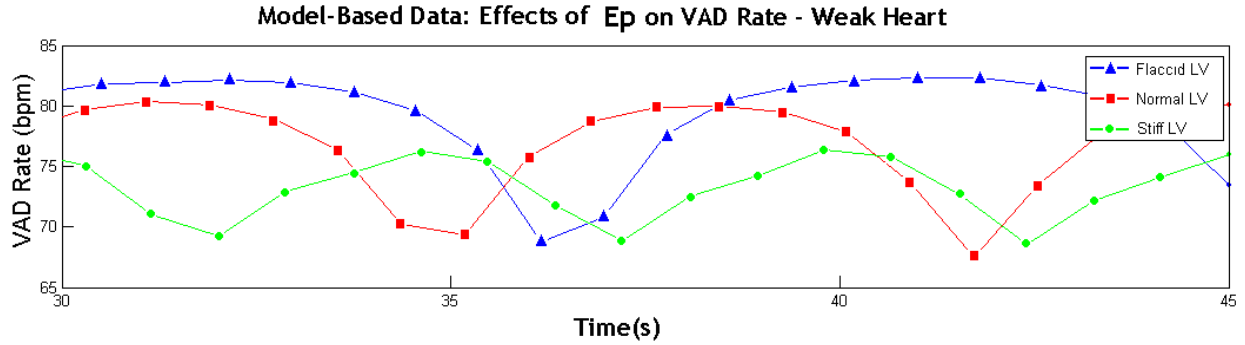

Figure 47: Effects of Ep on VAD-ventricle synchrony (strong heart)

In the weak heart case, end-diastolic volumes were again lower when E_P was increased (data not shown). From these results we can conclude that unlike LV E_{MAX}, native heart rate, and SVR, E_P does not significantly affect VAD-ventricle synchrony.

4.4 MODEL BASED ANALYSIS SUMMARY

Model-based results were qualitatively compared to clinical data obtained from a patient with Thoratec® VAD. Similarities were visible in both LV chamber area and peripheral pressure signals. The VAD rates were also similar (model: 71 bpm, clinical data: 66 bpm). The periodic dampening of LV chamber area was observed to coincide with VAD-ventricle co-pulsations in both the model and clinical results. To quantitatively investigate the occurrence of co-pulsating beats (analysis of synchrony) of the VAD and ventricle, an investigation of the model behavior with respect to key cardiovascular parameters was performed. The results of the model behavior investigation revealed that the likelihood of VAD-ventricle synchrony is determined by a complex interaction of contractility, cardiovascular parameter (such as SVR), and native heart rate. A graphical summary of these interactions is given in Figure 48.

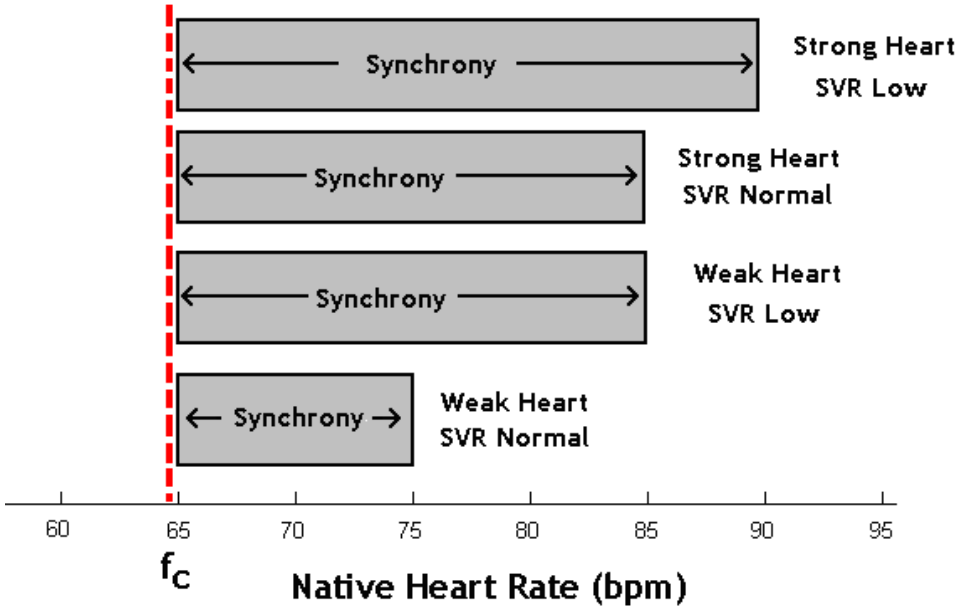

Figure 48: Graphical summary of the influences on VAD-ventricle synchrony.

The vertical broken line indicates the characteristic frequency (f_C). This point represents the minimal native heart rate below which VAD-ventricle synchrony will not exist. Our model-based analysis indicates that f_C is essentially independent of cardiovascular parameters and thus, an intrinsic property of the VAD. There is a also a maximum native heart rate above which VAD-ventricle synchrony will not exist; as shown by the tip of the synchrony bars (shaded areas). Unlike f_C, the maximum native heart rate for synchronous behavior is governed by cardiovascular parameters (E_{MAX} and SVR). To achieve synchrony, the native heart rate must be within the range determined by f_C, E_{MAX} and SVR. Asynchrony ensues with native heart rate outside this range, resulting in beats with co-pulsations and increased ventricular loading.

5.0 RECOMMENDATIONS

While the similarities between simulation and clinical data are promising, there is room for improvement. It is possible that clinical phenomena could be better captured with greater complexity of the circulation model. Improved detail of peripheral pressure would allow for better comparison of model results with the peripheral pressure measurements made clinically (e.g., fingertip pressure). Also, a model of a four-chamber heart will allow for the investigation of left and right heart failure and the role of atrial contractions.

Results from model behavior analysis have demonstrated that contractility, heart rate, and systemic vascular resistance are each independent determinants of synchrony between the VAD and ventricle. However, in the human body, contractility, heart rate, and SVR are controlled by the central nervous system (CNS). Baroreflex is a feedback system of the CNS which adjusts heart rate and SVR in order to regulate systemic blood pressure. Mathematical models of baroreflex control are available, and implementing this process into our current VAD-CVS model may provide further insights into VAD-ventricle interactions.

The clinical utility of our model-based analysis of the VAD-CVS system needs to be examined. It is possible that changes in the degree of synchrony over time can provide information about the ventricular recovery process. Heart failure is most commonly characterized by a decrease in contractility (E_{MAX}) and increase in SVR. The results of model-based analysis indicate that VAD-ventricle synchrony is highly responsive to the reversal of these characteristics of heart failure. Because SVR is readily measured by non-invasive

techniques, it is then conceivable that changes in E_{MAX} could be extracted from analysis of the temporal variations observed in synchrony. However, longitudinal clinical data and further analysis would be required to address these issues.

APPENDIX A

MATLAB CODE

```
%VADSIM.M
% THIS CODE IS THE PRIMARY CODE FOR WHICH TO RUN THE
% CARDIOVASCULAR SIMULATOR

% CLEAR THE WORKSPACE
%clear all

%DEFINE ALL MODEL PARAMETERS AS GLOBAL SO THAT THEY MAY BE USED
IN RUNKUT4.M TO FIND SOLUTIONS
global Dm Rm Da Ra Rc Ls Cs Rs Cr Rp Lp0 Lp1 Rv Di Do i Ev
global Li Lo Ri Ro0 Ro1 Ro2

%Cardiovascular System Model ADOBPTED FROM Breitenstein;

%SET INTIAL VALUES OF CERTAIN PARAMETER WHICH ARE DISPLAYED ON
THE FIRST SCREEN
HR=75;          % HR-Heart rate(bpm)[normal-75;weak-120]
Rs=0.83;          % Rs-system resistance;(0.83-normal,weak; 1.4-
severly   weak   without   pump;   0.83-severly   weak   with
pump)(mmHg.sec/mL)
V_total=370;        %  total  blood  volume;  (280-normal)(mL)  +
Vvad(1)+Vao(1)
Cs=1.33;        % Systemic Complinace (ml/mmHg)
t_eject  =  300;    %  Ejection  time  for  VAD  in  fill-to-empty
operation
end_t=6;        % end of simulation time

Ptf = -35;      % Filling pressure (vacuum) for Thoratec (mmHg)
Pte = 220;      % Ejection pressure for Thoratec (mmHg)
open = 1;

colors = ['b','r','g','c','m','k','y'];
shapes(1,1:length(colors)) = colors;
```

```
shapes(2:3,1:length(colors)) = '-';

zoomswitch=0;
ind=0;
Hf_fig = figure('Name',sprintf('Cardiovascular Simulator'));
set(gcf,'Menubar',menubar);

%fullscreen(Hf_fig);

Ha_ax1=axes;
set(Ha_ax1,'position',[.08 .78 .9 .2],...
    'FontSize',8,...
    'Box','on',...
    'XTickLabelMode','manual','XTickMode','auto',...
    'XTickLabel',[])

Ha_ax2=axes;
set(Ha_ax2,'position',[.08 .53 .9 .2],...
    'FontSize',8,...
    'Box','on',...
    'XTickLabelMode','manual','XTickMode','auto',...
    'XTickLabel',[])

Ha_ax3=axes;
set(Ha_ax3,'position',[.08 .28 .9 .2],...
   'FontSize',8,...
   'Box','on')

HRstr = num2str(HR);
Tstr  = num2str(end_t);
Emax0 = 3;
Rsstr = num2str(Rs);
Cs_str = num2str(Cs);
EtMax_str = num2str(Emax0);
Ptfstr = num2str(Ptf);
Ptestr = num2str(Pte);
t_ejectstr = num2str(t_eject);

istr = 1;
r  = .08;
up = .20;
w  = .05;
h  = .03;
Qo = 0;

Hc_HRedit                                                    =
uicontrol(Hf_fig,'Style','Edit','String',HRstr,'units','normalize
d','Position',[r+0.1 up-.04 w h]);
Hc_HRtext = uicontrol(Hf_fig,'Style','Pushbutton','String','Heart
Rate','Fontweight','Bold','units','normalized',...
    'Fontsize',10,'Position',[r up-.04 w+.03 h],...
    'Callback','HR_help  =  helpdlg(''HR-Heart  rate(bpm)[normal-
75;weak-120]'','''Heart Rate'');');
```

```
Hc_Tedit                                                        =
uicontrol(Hf_fig,'Style','Edit','String',Tstr,'units','normalized
','Position',[r+0.1 up-.08 w h]);
Hc_Ttext                                                        =
uicontrol(Hf_fig,'Style','Pushbutton','String','Time','Fontweight
','Bold','units','normalized',...
    'Fontsize',10,'Position',[r up-.08 w+.03 h],...
    'Callback','T_help    =    helpdlg(''Time    of    Simulation
(seconds)'',''Simulation Time'');');

Hc_Rsedit                                                       =
uicontrol(Hf_fig,'Style','Edit','String',Rsstr,'units','normalize
d','Position',[r+0.3 up w h]);
Hc_Rstext                                                       =
uicontrol(Hf_fig,'Style','Pushbutton','String','SVR','Fontweight'
,'Bold','units','normalized',...
    'Fontsize',10,'Position',[r+.2 up w+.03 h],...
    'Callback','Rs_help  =  helpdlg(''Rs-system  resistance;(0.83-
normal,weak;  1.4-severly  weak  without  pump;  0.83-severly  weak
with pump)(mmHg.sec/mL)'',''Systemic Resistance'');');

Hc_Vtedit                                                       =
uicontrol(Hf_fig,'Style','Edit','String',Cs_str,'units','normaliz
ed','Position',[r+0.3 up-.035 w h]);
Hc_Vttext                                                       =
uicontrol(Hf_fig,'Style','Pushbutton','String','Cs','Fontweight',
'Bold','units','normalized',...
    'Fontsize',10,'Position',[r+.2 up-.035 w+.03 h],...
    'Callback','Rs_help    =    helpdlg(''Compliance;    (1.33-
normal)(mmHg/ml)'',''Systemic Compliance'');');

Hc_Etedit                                                       =
uicontrol(Hf_fig,'Style','Edit','String',EtMax_str,'units','norma
lized','Position',[r+0.3 up-.07 w h]);
Hc_Ettext  =  uicontrol(Hf_fig,'Style','Pushbutton','String','E(t)
max','Fontweight','Bold','units','normalized',...
    'Fontsize',10,'Position',[r+.2 up-.07 w+.03 h],...
    'Callback','Rs_help   =   helpdlg(''Maximum   Elastance;   (3-
normal)(mmHg/ml)'',''Elastance'');');

Hc_Ejectedit                                                    =
uicontrol(Hf_fig,'Style','Edit','String',t_ejectstr,'units','norm
alized','Position',[r+0.5 up-.06 w h],'Visible','on');
Hc_Ejecttext                                                    =
uicontrol(Hf_fig,'Style','Pushbutton','String','Eject
Time','Fontweight','Bold','units','normalized',...
    'Fontsize',10,'Position',[r+.4          up-.06          w+.03
h],'Visible','on',...
    'Callback','Pi_help   =   helpdlg(''Thoratec   Ejecting   Time
(sec)'',''Thoratec Eject Time'');');

Hc_Ptfedit                                                      =
uicontrol(Hf_fig,'Style','Edit','String',Ptfstr,'units','normaliz
ed','Position',[r+0.5 up-.12 w h],'Visible','on');
```

```
Hc_Ptftext = uicontrol(Hf_fig,'Style','Pushbutton','String','Fill
Pres.','Fontweight','Bold','units','normalized',...
    'Fontsize',10,'Position',[r+.4          up-.12          w+.03
h],'Visible','on',...
    'Callback','Pi_help  =  helpdlg(''Thoratec  Vacuum  Setting
(mmHg)'',''Thoratec Vacuum'');');

Hc_Pteedit                                                      =
uicontrol(Hf_fig,'Style','Edit','String',Ptestr,'units','normaliz
ed','Position',[r+0.5 up-.18 w h],'Visible','on');
Hc_Ptetext                                                      =
uicontrol(Hf_fig,'Style','Pushbutton','String','Eject
Pres.','Fontweight','Bold','units','normalized',...
    'Fontsize',10,'Position',[r+.4          up-.18          w+.03
h],'Visible','on',...
    'Callback','Pi_help  =  helpdlg(''Thoratec  Ejection  Setting
(mmHg)'',''Thoratec Ejection'');');

Hc_zoom                                                         =
uicontrol(Hf_fig,'Style','Pushbutton','String','Zoom','Fontweight
','Bold','units','normalized',...
    'Fontsize',10,'Position',[r+.4 up w+.03 h],...
    'Callback','zoomfunc');

Hc_PumpMenu                                                     =
uicontrol(Hf_fig,'Style','popupmenu','String','Pneumatic|Electric
/Pulsatile|Axial|Centrifugal Pump',...
    'units','normalized','Position',[r         up-0.0         3*w
h],'Callback','popupselect');

Hc_PumpOn = uicontrol(Hf_fig,'Style','radiobutton','String','Pump
On','Backgroundcolor',get(Hf_fig,'color'),...
    'units','normalized','Position',[r         up-0.13        3*w
h],'value',1,'Fontsize',12,'Callback','set(Hc_PumpOn,''value'',1)
;set(Hc_PumpOff,''value'',0)');

Hc_PumpOff                                                      =
uicontrol(Hf_fig,'Style','radiobutton','String','Pump
Off','Backgroundcolor',get(Hf_fig,'color'),...
    'units','normalized','Position',[r         up-0.17        3*w
h],'Fontsize',12,'Callback','set(Hc_PumpOn,''value'',1);set(Hc_Pu
mpOff,''value'',1);set(Hc_PumpOn,''value'',0)');

Hc_VADsim  =  uicontrol(Hf_fig,'Style','pushbutton','String','Run
Simulation',...
    'units','normalized','Position',[r+.8       up-0.12       2*w
2*h],'CallBack','runsim');

Hc_PlotOver                                                     =
uicontrol(Hf_fig,'Style','radiobutton','String','Overlay
Plot','Value',1,...
    'units','normalized','Position',[r+.8        up-0.0        2*w
2*h],'Backgroundcolor',get(Hf_fig,'color'),...
    'CallBack','set(Hc_PlotNew,''value'',0);');
```

```
Hc_PlotNew = uicontrol(Hf_fig,'Style','radiobutton','String','New
Plot',...
    'units','normalized','Position',[r+.8       up-0.04       2*w
2*h],'Backgroundcolor',get(Hf_fig,'color'),...
    'CallBack','set(Hc_PlotOver,''value'',0);');

Hc_PlotPv = uicontrol(Hf_fig,'Style','radiobutton',...
    'units','normalized','Position',[r-.06       up+0.04       w
h],'Backgroundcolor',get(Hf_fig,'color'),...
    'value',1,'String','Pv');

Hc_iedit                                                        =
uicontrol(Hf_fig,'Style','Edit','units','normalized',...
    'Backgroundcolor',get(Hf_fig,'color'),'Position',[r+0.65 up w
h]);
Hc_index                                                        =
uicontrol(Hf_fig,'Style','text','String','Index','units','normali
zed','Fontweight','Bold',...
    'Backgroundcolor',get(Hf_fig,'color'),'Position',[r+0.6   up-
.002 w h]);
Hc_Da                                                           =
uicontrol(Hf_fig,'Style','text','String','Da','units','normalized
','Fontweight','Bold',...
    'Backgroundcolor',get(Hf_fig,'color'),'Position',[r+0.6   up-
.042 w h]);
Hc_Dm                                                           =
uicontrol(Hf_fig,'Style','text','String','Dm','units','normalized
','Fontweight','Bold',...
    'Backgroundcolor',get(Hf_fig,'color'),'Position',[r+0.6   up-
.082 w h]);
Hc_Di                                                           =
uicontrol(Hf_fig,'Style','text','String','Di','units','normalized
','Fontweight','Bold',...
    'Backgroundcolor',get(Hf_fig,'color'),'Position',[r+0.6   up-
.122 w h],'Visible','on');
Hc_Do                                                           =
uicontrol(Hf_fig,'Style','text','String','Do','units','normalized
','Fontweight','Bold',...
    'Backgroundcolor',get(Hf_fig,'color'),'Position',[r+0.6   up-
.162 w h],'Visible','on');
Hc_Dastatus                                                     =
uicontrol(Hf_fig,'Style','Edit','units','normalized','Position',[
r+0.65 up-.04 w h]);
Hc_Dmstatus                                                     =
uicontrol(Hf_fig,'Style','Edit','units','normalized','Position',[
r+0.65 up-.08 w h]);
Hc_Distatus                                                     =
uicontrol(Hf_fig,'Style','Edit','units','normalized','Position',[
r+0.65 up-.12 w h],'Visible','on');
Hc_Dostatus                                                     =
uicontrol(Hf_fig,'Style','Edit','units','normalized','Position',[
r+0.65 up-.16 w h],'Visible','on');
```

```
Hc_meanQstr    =   uicontrol(Hf_fig,'Style','text','String','mean
Qo','units','normalized','fontsize',12,...
    'Backgroundcolor',get(Hf_fig,'color'),'Position',[r+0.2   up-
.16 w*2 h]);

Hc_meanPstr    =   uicontrol(Hf_fig,'Style','text','String','mean
Ps','units','normalized','fontsize',12,...
    'Backgroundcolor',get(Hf_fig,'color'),'Position',[r+0.2   up-
.12 w*2 h]);

Hc_meanQ                                                        =
uicontrol(Hf_fig,'Style','text','String','N/A','units','normalize
d','fontsize',12,...
    'Backgroundcolor',get(Hf_fig,'color'),'Position',[r+0.3   up-
.16 w*2 h]);

Hc_meanP                                                        =
uicontrol(Hf_fig,'Style','text','String','N/A','units','normalize
d','fontsize',12,...
  'Backgroundcolor',get(Hf_fig,'color'),'Position',[r+0.3  up-.12
w*2 h]);
```

```
  %  RUMSIM.M EXECUTED BY CLICKING THE RUN SIMULATION BUTTON
  %  ON THE MAIN SCREEN

  %SAVE PREVIOUS RUN FOR COMPARISON IF DESIRED
  if length(Qo) > 10
      Qo_last = Qo;
      Qi_last = Qi;
      Qa_last = Qa;
      Pt_last = Pt;
      Pexternal_last = Pexternal;
      Pp_last = Pp;
      Pv_last = Pv;
      Vlv_last = Vlv;
      Pa_last = Pa;
      Pr_last = Pr;
      Vvad_last = Vvad;
      Pao_last = Pao;
  end
  % CLEAR WORKSPACE IN CASE THE PREVIOIUS SIMULATION RUN WAS
LONGER THAN THE CURRENT RUN
  clear A B x Vd te Pp Qi Qo Ps Pt Vvad Px Pexternal Pv Pa Pao Qa
Pr Pex Vlv Din Dout Daorta Dmitral xx xxdot Vao Vp
  zoomswitch=1;
  zoomfunc
  set(Hf_fig,'WindowButtonDownFcn','Bdown','WindowButtonUpFcn','B
up');
  %COLLECT PARAMETER VALUES AS DEFINED FROM THE USER ON THE MAIN
SCREEN
  HR       = str2num(get(Hc_HRedit,'string'));
  end_t    = str2num(get(Hc_Tedit,'string'));
  Rs       = str2num(get(Hc_Rsedit,'string'));
  Cs       = str2num(get(Hc_Vtedit,'string'));
  Emax0    = str2num(get(Hc_Etedit,'string'));
  Pte      = str2num(get(Hc_Pteedit,'string'));
  Ptf      = str2num(get(Hc_Ptfedit,'string'));
  t_eject  = str2num(get(Hc_Ejectedit,'string'));
  pump     = get(Hc_PumpMenu,'value')-1;

  %BUILD TIME ARRAY FOR SIMULATION
  %Simulation Time--T;
  start_t=0;
  step=0.001;
  t_eject_n = round(0.001*t_eject/step);
  t_eject_nc = t_eject_n;

  %Thoratec Parameters
  %1 mmHg = 1.35951 gmf/cm^2
  %g = 980 cm/s^2; 1 mmHg = 1359.5 gm/cm*s^2
  %1 gm/cm*ml = 1359.5 mmHg*sec^2/ml

  eta_blood  = 0.0007501;       %mmHg.sec/ml or 3 cP
  eta_H2O    = 0.000250;        %mmHg.sec/ml or 1 cP
  Tmax_vol = 110;               %ml
  Vd_vad   = 107;               %ml
```

```
  %Human Values for Cannula
  Tcannula_length_out = 32;     %cm
  Tcannula_length_in  = 24;     %cm

  %LVAD cannula diameter = 1.8 cm
  Tcannula_area   = (0.9^2)*pi; %cm^2
  rho_blood = 1;                %gm/ml

  %GEOMETRY VALUES FOR Rp AND Lp
  Thoratec_length=10;           %cm
  Thoratec_area=5;              %cm


  %INITIAL VALUES OF INLET AND OUTLET RESISTANCE FOR THORATEC
CANNULA
  Ri = .15
  Ro = .05

  %EXPRESSION OF FINDING INDUCTANCE VALUES IN THE MODEL
  Li                                                          =
(9/4)*(rho_blood*Tcannula_length_in)/(1359.5*Tcannula_area);
%Rideout text
  Lo   =  (rho_blood*Tcannula_length_out)/(1359.5*Tcannula_area);
%Rideout text
  Lp = (9/4)*(rho_blood*Thoratec_length)/(1359.5*Thoratec_area);
  Li = Li*1.75
  Lo = Lo


  Rp =.05;    % Resistor in the VAD (mmHg*s/ml)
  Cp = 2.0;   % ml/mmHg as estimated from PV experiments
  Rd = .01;   % Resistance of Drive line air;
  Cd = 4;     % Complinace of Drive line air;

  %cardiovascular   system   model   parameters   (taken   from
BREITENSTEIN);
  Rm = 0.005;         % Rm-mitral valve open;(mmHg.sec/mL)
  Ra = 0.001+.005;    % Ra-aortic valve open;(mmHg.sec/mL)
  Rc     =     0.0398-.005;              %     Rc-characteristic
resistance;(mmHg.sec/mL)
  Ls=5e-4;                          %  Ls-inertance  of  blood  in
aorta;(mmHg.sec^2/mL)
  %Cs=1.33;           % Cs-system compliance;(mL/mmHg)
  Cao = .2;           % Aortic Complinace (ml/mmHg)
  Cr=4.4;             %Cr-pulmonary compliance;(mL/mmHg)
  Vd=5;               % isovolume;

  %generate LV elastance for given Emax0,Ed0,and HR;
  %Left Venticular function parameters
  clear Ev

  Ep = 0.06;  %simplified linear passive pressue relationship
  Vo = 15;    %x-intercept of linear EDPVR
  dV = Vo-Vd;
```

```
%Uses the already created Time scale
    T=start_t:step:end_t;
    n=length(T);
    Ea=EofT(T,HR,Emax0,step);

%Initialize variable for the first iteration of the simulation

Pt(1)=0;
Px(1)=0;
Vvad(1)=107;
Pex=0;
Pi=8;
Pe=8;
Pd=0;

bladder_comp(1) = Cp;
Pp(1)=(Vvad(1)-Vd_vad)/Cp;
Ps(1)=80;
Qi(1)=0; Qo(1)=0;
V_sum(1)=Cs*Ps(1)+Vvad(1);
Vs(1)=Cs*Ps(1);
Di=0;Do=0;
Pexternal(1)=Pd(1);
Qs(1)=0;
Qv(1)=0;
Qe(i)=(Ps(1)-Pe)/Rs;
mode = 1;
T=start_t:step:end_t;
n=length(T);

%RUN THE DESIRED SET OF DIFFERENTIAL EQUATIONS
% THORATEC_CARDIO_FINAL RUNS THE VAD/CVS COUPLED MODEL
% THORATEC3A RUNS THE IN-VITRO EXPERIMENTAL SETUP

thoratec_cardio_final

% FOLLOWING CODE IS USED TO PLOT THE RESULTS
% OF THE DIFFERENTIAL EQUATIONS RUN IN THE
% ABOVE STEP

if get(Hc_PlotOver,'value')
    ind=ind+1;
    if ind == 8;ind=1;end
    set(Ha_ax1,'NextPlot','Add');
    set(Ha_ax2,'NextPlot','Add');
    set(Ha_ax3,'NextPlot','Add');
else
    ind=1;
    set(Ha_ax1,'NextPlot','Replace');
    set(Ha_ax2,'NextPlot','Replace');
    set(Ha_ax3,'NextPlot','Replace');
```

```
end

axes(Ha_ax1)
plot(T,Qi,'b')
hold on
plot(T,Qo,'r')
plot(T,Qa,'g')
hold off
title('FLOW')
xlabel('flow')
legend('Q_I_N','Q_O_U_T','Q_A_O_R_T_A')
axes(Ha_ax2)
plot(T,Pt)
hold on
plot(T,Ps,'r')
plot(T,Pao,'r')
plot(T,Pv,'g')
%plot(T,Ea(1:length(Pv)),'g--')
hold off
title('PRESSURE')
legend('Pt','Pao','Plv')
if strcmp(simu,'novacor')|strcmp(simu,'thoratec')
    hold on
    plot(T(te),eject(te),'r.')
    hold off
end
xlabel('Thoratec Chamber Pressure')

axes(Ha_ax3)
%plot(T,Pao,colors(ind))
plot(T,Vvad)
hold on
plot(T,Vlv,'r')
plot(T,Pexternal,'g')
legend('Vvad','Vlv','Pex')
xlabel('Volume')
hold on
%hold off
```

```
  % EofT.M
  % CODE IS USED TO CREATE THE TIME-VARYING ELASTANCE FUNCTION
  % E(T)

  function Ev=EofT(T,HR,Emax,step)

  %CREATE  A  MATRIX  OF  E(T)  VALUES  FOR  THE  LENGTH  OF  THE
SIMULATION
  % T = SIMULATION TIME
  % HR = HEART RATE (BPM)
  % EMAX = MAXIMUM ELASTANCE OF THE LV
  % STEP = STEP SIZE OF SIMULATION


  En=[];
  Tc=60/HR;                    %Find cycle time for one beat
  tmax = 0.2 + 0.1555*Tc;      %Find time of systole from cycle
time
  points = Tc/step;            %Calculate number of samples in one
cycle
  r  =  ceil(length(T)/points);  %Find  number  of  cycles  needed,
rounding to upper integer

  for j = 1:r+1
      for i = 1:points
          tn(i) = i*(step/tmax);
          t1 = (tn(i)/0.7)^1.9;
          t2 = 1 + t1;
          t3 = 1 + (tn(i)/1.173474)^21.9;
          Ecyc(i) = 1.553174*(t1/t2)*(1/t3);
      end
      En(length(En)+1:length(En)+points) = Ecyc;
      %clear Ecyc
  end

  En=En(1:length(T));

  %Plv = E(t)[Vlv-Vd] + m[Vlv-Vd]  Active + Passive
  % Passive Pressure has been simplified to a linear relationship
  % because the Ax+B method of solving does not allow non-linear
  % E(t) function to be used.

  % From simulation slope of EDPVR assuming linear
  m = .06;

  Ev=En*Emax;
  tsamp = tn*tmax;
```

```
%RUNKUT4.M   4TH ORDER RUNGE-KUTTA METHOD

function x=runkut4(h,A,x,B,u)
% RUNGE KUTTA 4TH ORDER METHOD FOR NUMERICAL
% SOLUTION TO LINEAR FIRST ORDER DIFF EQ'S

xdot = A*x+B*u;
kx1  = h*xdot;
x1   = x+0.5*kx1;

xdot = A*x1+B*u;
kx2  = h*xdot;
x1   = x+0.5*kx2;

xdot = A*x1+B*u;
kx3  = h*xdot;
x1   = x+kx3;

xdot = A*x1+B*u;
kx4  = h*xdot;

x    = x+(kx1+2*kx2+2*kx3+kx4)/6;
```

```
  % THORATEC_CARDIO_FINAL.M
  % FINDS A NUMERICAL SOLUTION FOR 8 STATE EQUATIONS FOR THE
  % THORATEC/CVS MODEL

  % Series Inductor Resistor Capacitor model with Di/Do in state
equations for leaky valves.
  clear cycle_start cycle_end ej

  %IF THORATEC IS ON, USE LEAKY VALVES
  if get(Hc_PumpOn,'Value')
      open = 1;
      leakin  = 0.08
      leakout = 0.03
  % IF THORATEC IS OFF, CLOSED VALVES = 0
  else
      cycle_start = 1;
      cycle_end   = 100;
      open = 0;
      leakin = 0;
      leakout = 0;
  end

  %State equation dX/dt=A(t)*X(t)+B(t)*Vd;
  %Initialize the coefficient matrix
  A=zeros(8);
  %Initialize Variables
  Qi(1)=0; Qa(1)=0; Qo(1)=0; Qv(1) = 0;
  Pr(1)=5; Pa(1)=90;Pao(1)=Pa(1);
  Vr(1)=Cr*Pr(1); Vp(1)=Cs*Pa(1);Vao(1)=Cao*Pao(1);
  Vlv(1)=V_total-Vvad(1)-Vr(1)-Vp(1)-Vao(1);Vvad(1)=50;
  V_sum(1)=Vlv(1)+Vr(1)+Vp(1)+Vao(1)+Vvad(1);
  Pv(1)=(Vlv(1)-Vd)*(Ea(1)+Ep)-Ep*dV;

  %Initialize the x-matrix (state variables)
  x=zeros(8,1);
  x=[Qi(1) Qo(1) Vvad(1) Pao(1) Qa(1) Vlv(1) Pa(1) Pr(1) ]';
  xdot=[0 0 0 0 0 0 0 0];

  Vlv(1)=V_total-Vvad(1)-Vr(1)-Vp(1);
  j=1;
  j2=1;

  % Delay logic implemented so that valves stay open for 100 ms
  % to allow flow to get above zero.  Necessary for the current
  % valve modeling logic

  delay_in = -100;
  delay_out = -100;
  Ri0 = Ri;
  k=1;
  % Begin Simulations. n = number of iterations to be performed
  for i=1:n-1

      % Optional code used if an occlusion run is desired
```

```
      %%%%%% Occlusion Run %%%%%%
      %     if     i>(end_t*500)     Rs     =     0.83+((0.25*(i-
end_t*500))/1000);end
      % Rsys(i) = Rs;
      %determine the valve status

      %VALVE LOGIC - FOR 2 LV VALVES, M = MITRAL, A = AORTIC
      if Pr(i)>=Pv(i)
          Dm=1;
      else
          Dm=0;
      end

      if Pv(i) >= Pao(i)
          Da=1;
      else
          Da=0;
      end

      %THORATEC VALVE LOGIC - I = INLET, O = OUTLET

      if Di == leakin         %IF VALVE IS CLOSE
          if  Pv(i)  >=  Pt(i)    % &  IF  ventricle  presure  >  VAD
pressure
              Di=open;        % Open inlet valve
              delay_in = i;    % Start delay, so flow can reach
positive
          end
      else
          if x(1) <= 0 & i > delay_in + 100
              Di=leakin;         % Close  valve  if  flow  <  0,  and
delay is over
          end
      end

      %Idendical Logic used for outlet valve
      if Do == leakout
          if Pt(i) >= Pao(i)
              Do=open;
              delay_out = i;
          end
      else
          if x(2) <= 0 & i > delay_out + 100
              Do=leakout;
          end
      end

      % Determine the VAD drive pressure status (mode) and aplied
value (Pd)
      % Three Driver Controls Possible
      ejectmode='fill2empty';
      bpm=70;
      per_sys = t_eject/((1000*60)/bpm);
      switch ejectmode
```

```
% FILL-TO-EMPTY, Eject once VAD volume reaches Tmax_vol
% Duration of ejection = t_eject-n
case 'fill2empty'
    if mode == 0
        if x(3) >= Tmax_vol
            if exist('cycle_end');
                cycle_start = cycle_end;
            end
            cycle_end = i;
            mode = 1;
            ej(k) = i;
            k=k+1;
            Pd = Pte;
            t_eject_nc = i+t_eject_n;
        else
            Pd = Ptf;
        end
    else
        if i == t_eject_nc
            mode = 0;
            Pd = Ptf;
        else
            Pd = Pte;
        end
    end
%Fixed ejection rate, set by variable 'bpm'
case 'fixed'
    if j >= (1000*60)/bpm;
        if i+j < n
            cycle_start=i;
            cycle_end  =i+j;
        end
        j=1;
        mode = 1;
        Pd = Pte;
    elseif j > per_sys*(1000*60)/bpm;
        mode = 0;
        Pd = Ptf;
    end
% Pulse ejection rate, singe beat
case 'pulse'
    if i < 2000
        mode=0;
        Pd=0;
    elseif i >=2000 & i<4000
        mode=0;
        Pd=250;
    elseif i >=4000
        mode = 0;
        Pd   = 0;
    end
end
j=j+1;
% DETERMINE VALUE OF VAD BLADDER COMPLIANCE
```

```
      % BASED ON VAD VOLUME OF THE PREVIOUS ITERATION

      if x(3)> 112
          Cp = 1/44.40;
          Vd_vad = 111.148;
      elseif x(3) > 107
          Cp = 1/7.57;
          Vd_vad = 107;
      elseif x(3) > 32 - 0 %- 21.4/cslope
          Cp = 1/.20;
          Vd_vad = 107;
      elseif x(3) > 22-0
          Cp = 1/4.07;
          Vd_vad = 35.69-0;
      else
          Cp = 1/17.63;
          Vd_vad = 25.16-0;
      end

      % Calulate the External Bladder Pressure from the Drive
Pressure (Pd)
      % Pexdot = (1/RC)Pdriver - (1/RC)Pex
      A2 = [-1/(Rd*Cd)];
      B2 = -A2;
      Pex=runkut4(step,A2,Pex,B2,[Pd]);
      xdot2=A2*Pex+B2*[Pd];
      Pex2 = Pex+xdot(3)*.15;

      Ri = Ri0 + exp(-.25*x(6));              % EXPRESSION FOR
VENTRICLE COLLAPSE MODEL
      Ro = 0.00015*abs(Qo(i)) + 0.05;      % EXPRESSION FOR FLOW
DEPENDENT OUTLET RESISTOR

      %%%%%%%%%%%%%%%%%%%%%%%%%%%%%%%%

      % SIMPLIFY STATE SPACE MODEL BY TAKING PARAMETERS INTO LESS
COMPLEX FORM
      xo  = (Do*Lp)/(Lp+Lo);
      xi  = (Di*Lp)/(Lp+Li);
      zi  =  Di/(Lp+Li);
      zo  =  Do/(Lp+Lo);
      ri  = (Di*Rp)/(Lp+Li);
      ro  = (Do*Rp)/(Lp+Lo);
      rri = (Do*Rp+Ri)/(Do*Lp+Li);
      rro = (Di*Rp+Ro)/(Di*Lp+Lo);

      % CREATE COEFFICIENT MATRIX A
      %             Qi          Qo            Vvad            Pao
Qa         Vlv              Pa       Pr
      A(1,:)=[ xi*ro-rri      ri-xi*rro    (xi*zo-zi)/Cp    -xi*zo
0     zi*(Ea(i)+Ep)          0        0         ]/(1-xi*xo);
      A(2,:)=[ ro-xo*rri      xo*ri-rro    (zo-xo*zi)/Cp      -zo
0    xo*zi*(Ea(i)+Ep)        0        0         ]/(1-xi*xo);
```

```
      A(3,:)=[       1            -1              0              0
0          0                  0         0         ];
      A(4,:)=[       0            1               0           -Da/Ra
-1   (Da/Ra)*(Ea(i)+Ep)       0         0         ]/Cao;
      A(5,:)=[       0            0               0              1
-Rc          0                -1        0         ]/Ls;
      A(6,:)=[      -1            0               0            Da/Ra
0 -[Dm/Rm+Da/Ra]*(Ea(i)+Ep)  0       Dm/Rm       ];
      A(7,:)=[       0            0               0              0
1          0                -1/Rs     1/Rs        ]/Cs;
      A(8,:)=[       0            0               0              0
0   (Dm/Rm)*(Ea(i)+Ep)      1/Rs   -(1/Rs+Dm/Rm) ]/Cr;

      %CREATE CONSTANT MATIX B
      %[Vd_vad;Pex;Vd;Ep]
      B(1:2,1) = -A(1:2,3);
      B(1:2,2) =  A(1:2,3)*Cp;
      B(1:8,3) = -A(1:8,6);
      B(1:8,4) = -A(1:8,6)*(Ep*dV)/(Ea(i)+Ep);

      %integration   of   dX/dt   using   Runge-Kutta   4th   order
intergration method;
      x=runkut4(step,A,x,B,[Vd_vad;Pex2;Vd;1]);

      %calculate current derivatives

      xdot=A*x+B*[Vd_vad;Pex2;Vd;1];

      %store data in the simulation variables;
      %v(i)=val;
      Qi(i+1)   = x(1);                                          %
Thoratec Inflow;
      Qo(i+1)   = x(2);                                          %
Thoratec Outflow;
      Vvad(i+1) = x(3);
      Pao(i+1)  = x(4);
      Qa(i+1)   = x(5);
      Vlv(i+1)  = x(6);
      Pa(i+1)   = x(7);
      Pr(i+1)   = x(8);

      Pv(i+1) = (x(6)-Vd)*(Ea(i+1)+Ep)-Ep*dV;
      Pp(i+1) = (x(3)-Vd_vad)/Cp;                                %
Thoratec Pump Presure - due to bladder compliance only;
      Px(i+1) = Pp(i+1)+Pex2;                                    %
Thoratec Bladder Chamber Pressure - total;
      Pt(i+1) = Px(i)+Rp*(Qi(i)-Qo(i))+Lp*(xdot(1)-xdot(2));
      Qv(i+1) = Da*(Pv(i+1)-Pao(i+1))/Ra;
      Pdrive(i+1) = Pex;                                         %
Thoratec Pump Driver Pressure(mmHg);
      Pexternal(i+1)=Pex2;
      Vp(i+1) = Cs*x(7);                                         %
Volume in peripheral systemic capacitor;
```

```
      Vr(i+1) = Cr*x(8);                                                  %
Volume in atrial capacitor;
      Vao(i+1)= Cao*x(4);
      V_sum(i+1) = x(6)+Vr(i+1)+Vp(i+1)+Vao(i+1)+x(3);   % Total
CV volume
      bladder_comp(i+1) = Cp;
      if mode == 0
          te(i)=0;
      else
          te(i)=i;
      end
      te=nonzeros(te)';
      %Qs(i+1)=Cs*xdot(4);

      eject(i)   = mode;
      Din(i)     = Di;
      Dout(i)    = Do;
      Daorta(i)  = Da;
      Dmitral(i) = Dm;

      Amat{i}=A;
      Bmat{i}=B;
      Qao(i) = xdot(4)*Cao;
      Qv(i)  = Da*(Pv(i)-Pao(i))/Ra;
      xx(:,i)=x;
      xxdot(:,i)=xdot;
      Aobalance(i)   =   Qo(i)+Da*(Pv(i)-Pao(i))/Ra   -   Qa(i)   -
Cao*xdot(4);
  end

  set(Hc_meanQ,'string',num2str(mean(Qo(cycle_start:cycle_end))))
;
  set(Hc_meanP,'string',num2str(mean(Pao(cycle_start:cycle_end)))
);

  %DETERMINE MEAN VALUES OF THE LAST COMPLETE BEAT RUN

  rate_n   = 60/[(cycle_end-cycle_start)*step];
  max_Ps   = max(Pao(cycle_start:cycle_end));
  mean_Ps  = mean(Pao(cycle_start:cycle_end));
  min_Ps   = min(Pao(cycle_start:cycle_end));

  max_Pv   = max(Pv(cycle_start:cycle_end));
  mean_Pv  = mean(Pv(cycle_start:cycle_end));
  min_Pv   = min(Pv(cycle_start:cycle_end));

  max_Qo   = max(Qo(cycle_start:cycle_end));
  mean_Qo  = mean(Qo(cycle_start:cycle_end));
  min_Qo   = min(Qo(cycle_start:cycle_end));
  max_Qi   = max(Qi(cycle_start:cycle_end));
  mean_Qi  = mean(Qi(cycle_start:cycle_end));
  min_Qi   = min(Qi(cycle_start:cycle_end));
  max_Pt   = max(Pt(cycle_start:cycle_end));
  mean_Pt  = mean(Pt(cycle_start:cycle_end));
```

```
min_Pt   = min(Pt(cycle_start:cycle_end));

max_Pex   = max(Pexternal(cycle_start:cycle_end));
mean_Pex  = mean(Pexternal(cycle_start:cycle_end));
min_Pex   = min(Pexternal(cycle_start:cycle_end));

max_Vlv   = max(Vlv(cycle_start:cycle_end));
min_Vlv   = min(Vlv(cycle_start:cycle_end));
SVlv      = max_Vlv-min_Vlv;

max_V   = max(Vvad(cycle_start:cycle_end));
min_V   = min(Vvad(cycle_start:cycle_end));
SV      = max_V-min_V;

%DISPLAY MEAN VALUES
disp('')
disp('RESULTS')
disp(' ')
disp(sprintf('Cycle: %g,%g',[T(cycle_start) T(cycle_end)]))
disp(sprintf('Rate:  %g',rate_n))
disp(' ')
disp(sprintf('Max  Ps:  %g',max_Ps))
disp(sprintf('Mean Ps:  %g',mean_Ps))
disp(sprintf('Min  Ps:  %g',min_Ps))
disp(' ')
disp(sprintf('Max  Pv:  %g',max_Pv))
disp(sprintf('Mean Pv:  %g',mean_Pv))
disp(sprintf('Min  Pv:  %g',min_Pv))
disp(' ')
disp(sprintf('Max  Qo:  %g',max_Qo))
disp(sprintf('Mean Qo:  %g',mean_Qo))
disp(sprintf('Min  Qo:  %g',min_Qo))
disp(' ')
disp(sprintf('Max  Qi:  %g',max_Qi))
disp(sprintf('Mean Qi:  %g',mean_Qi))
disp(sprintf('Min  Qi:  %g',min_Qi))
disp(' ')
disp(sprintf('Max  Pt:  %g',max_Pt))
disp(sprintf('Mean Pt:  %g',mean_Pt))
disp(sprintf('Min  Pt:  %g',min_Pt))
disp(' ')
disp(sprintf('Max  Pex:  %g',max_Pex))
disp(sprintf('Mean Pex:  %g',mean_Pex))
disp(sprintf('Min  Pex:  %g',min_Pex))
disp(' ')
disp(sprintf('Max  Vlv:  %g',max_Vlv))
disp(sprintf('Min Vlv:  %g',min_Vlv))
disp(sprintf('Stroke Vlv:  %g',SVlv))
disp(' ')
disp(sprintf('Max  Vol:  %g',max_V))
disp(sprintf('Min Vol:  %g',min_V))
disp(sprintf('Stroke Vol:  %g',SV))
disp(' ')
disp(' ')
```

```
 % THORATEC3A.M
  % SOLVE THE DIFF EQ'S FOR THE IN-VITRO EXPERIMENTS
  %Ri and Ro
  %Cd value
  %leakin and leakout
  %PV curve moved lower half left
  %
  %
  %

  % Series Inductor Resistor Capacitor model with Di/Do in state
equations for leaky valves.
  clear cycle_start cycle_end
  %State equation dX/dt=A(t)*X(t)+B(t)*Vd;
  simu='thoratec';
  A=zeros(4);
  leakin  = 0.08
  leakout = 0.03
  x=zeros(7,1);
  x=[Qi(1) Qo(1) Vvad(1) Ps(1)]';
  xdot=[0 0 0 0];

  j=1;
  j2=1;
  delay_in = -100;
  delay_out = -100;

  for i=1:n-1
      %determine the valve status
      if Di == leakin
          if Pi >= Pt(i)
              Di=1;
              delay_in = i;
          end
      else
          if x(1) <= 0 & i > delay_in + 100
              Di=leakin;
          end
      end

      if Do == leakout
          if Pt(i) >= Ps(i)
              Do=1;
              delay_out = i;
          end
      else
          if x(2) <= 0 & i > delay_out + 100
              Do=leakout;
          end
      end

      % FILL TO EMPTY
```

```
      % Determine the VAD drive pressure status (mode) and aplied
value (Pd)
      ejectmode='fill2empty';
      bpm=60;
      per_sys = t_eject/((1000*60)/bpm);
      switch ejectmode
      case 'fromfile'
      case 'fill2empty'
          if mode == 0
              if x(3) >= Tmax_vol
                  if exist('cycle_end');
                      cycle_start = cycle_end;
                  end
                  cycle_end = i;
                  mode = 1;
                  Pd = Pte;
                  Rd=.01;
                  Cd=4;
                  t_eject_nc = i+t_eject_n;
              else
                  Pd = Ptf;
                  Rd=.01;
                  Cd=4;
              end
          else
              if i == t_eject_nc
                  mode = 0;
                  Pd = Ptf;
                  Rd=.01;
                  Cd=4;
              else
                  Pd = Pte;
                  Rd=.01;
                  Cd=4;
              end
          end
      case 'fixed'
          if j >= (1000*60)/bpm;
              if i+j < n
                  cycle_start=i;
                  cycle_end  =i+j;
              end
              j=1;
              mode = 1;
              Pd = Pte;
              Rd=.01;
              Cd=3;
          elseif j > per_sys*(1000*60)/bpm;
              mode = 0;
              Pd = Ptf;
              Rd=.01;
              Cd=1;
          end
      case 'pulse'
```

```
        if i < 2000
            mode=0;
            Pd=0;
        elseif i >=2000 & i<4000
            mode=0;
            Pd=250;
        elseif i >=4000
            mode = 0;
            Pd   = 0;
        end
    end
    j=j+1;
    nx=0;
     if x(3)> 112-2
         Cp = 1/44.40;
         Vd_vad = 111.148-2;
     elseif x(3) > 107-2
         Cp = 1/7.57;
         Vd_vad = 107-2;
     elseif x(3) > 32
         Cp = 1/.20;
         Vd_vad = 107-2;
     elseif x(3) > 22
         Cp = 1/4.07;
         Vd_vad = 35.69;

     else
         Cp = 1/17.63;
         Vd_vad = 25.16;
      end

    % Calulate the External Bladder Pressure from the Drive
Pressure (Pd)
    % Pexdot = (1/RC)Pdriver - (1/RC)Pex
    A2 = [-1/(Rd*Cd)];
    B2 = -A2;
    Pex=runkut4(step,A2,Pex,B2,[Pd]);
    xdot2=A2*Pex+B2*[Pd];
    Pex2 = Pex+xdot(3)*.15;

    Ro = 0.00015*abs(Qo(i)) + 0.05;
    %   Ri = 0.00025*abs(Qi(i)) + 0.06;
    %   else
    %   Ri = [2*Qi(i)^2 + 200*Qi(i) + 37100]/1000000;
    %   Ro = [2*Qo(i)^2 + 200*Qo(i) + 37100]/1000000;
    % Rout(i) = Ro;
    % Rin(i) = Ri;
    %   end
    %   Rout(i)=Ro;
    %    Rp = abs([6e-7*(Qi(i)-Qo(i)).^2 + 1e-5*(Qi(i)-Qo(i)) +
0.005]);
    %   Rpump(i) = Rp;
    %   Lp = Lpf*(100/Vvad(i));
    %   Pex=Pd(j2);
```

```
      %   j2=j2+1;
      %   if j2 > length(Pd);j2=1;end
      %%%%%%%%%%%%%%%%%%%%%%%%%%%%%%%%%%%%

      xo=(Do*Lp)/(Lp+Lo);
      xi=(Di*Lp)/(Lp+Li);
      zi=Di/(Lp+Li);
      zo=Do/(Lp+Lo);
      ri = (Di*Rp)/(Lp+Li);
      ro = (Do*Rp)/(Lp+Lo);
      rri = (Do*Rp+Ri)/(Do*Lp+Li);
      rro = (Di*Rp+Ro)/(Di*Lp+Lo);


      A(1,:)=[[xi*ro-rri]  [ri-xi*rro]  (xi*zo-zi)/Cp  -xi*zo]/(1-
xi*xo);
      A(2,:)=[ro-xo*rri xo*ri-rro (zo-xo*zi)/Cp -zo]/(1-xi*xo);
      A(3,:)=[1 -1 0 0];
      A(4,:)=[0 1 0 -1/Rs]/Cs;

      %[Vd_vad;Pex;Pi;Pe]
      B(1:4,1) = -A(1:4,3);
      B(1,2) = A(1,3)*Cp;
      B(1,3) = zi;
      B(2,2) = A(2,3)*Cp;
      B(2,3) = xo*zi;
      B(4,4) = 1/(Cs*Rs);


      %integration   of   dX/dt   using   Runge-Kutta   4th   order
intergration method;
      x=runkut4(step,A,x,B,[Vd_vad;Pex2;Pi;Pe]);

      eject(i) = mode;
      Din(i) = Di;
      Dout(i) = Do;


      %calculate current derivatives
      xdot=A*x+B*[Vd_vad;Pex2;Pi;Pe];

      %store data in the simulation variables;
      %v(i)=val;
      Qi(i+1) = x(1);                                          %
Thoratec Inflow;
      Qo(i+1) = x(2);                                          %
Thoratec Outflow;
      Vvad(i+1) = x(3);                                        %
Volume in VAD
      Pp(i+1) = (x(3)-Vd_vad)/Cp;                              %
Thoratec Pump Presure - due to bladder compliance only;
      Ps(i+1) = x(4);                                          %
Systemic Pressure
```

```
      Px(i+1) = Pp(i+1)+Pex2;                                          %
Thoratec Bladder Chamber Pressure - total;
      Pt(i+1) = Px(i)+Rp*(Qi(i)-Qo(i))+Lp*(xdot(1)-xdot(2));
      dQidt(i)= xdot(1);
      dQodt(i)= xdot(2);
      %Pdrive(i+1) = Pd;                                               %
Thoratec Pump Driver Pressure(mmHg);
      Pexternal(i+1)=Pex2;

      Vs(i+1) = Cs*x(4);
      V_sum(i+1) =Cs*Ps(i+1)+x(3);                                     %
Total CV volume
      bladder_comp(i+1) = Cp;
      if mode == 0
          te(i)=0;
      else
          te(i)=i;
      end
      te=nonzeros(te)';
      Qs(i+1)=Cs*xdot(4);
      Qv(i+1)=xdot(3);
      Qe(i+1)=(Ps(i)-Pe)/Rs;
      Amat{i}=A;
      Bmat{i}=B;
      %Pex_new(i)=Pex+xdot(3)*.1;
  end

  set(Hc_meanQ,'string',num2str(mean(Qo(cycle_start:cycle_end))))
;
  set(Hc_meanP,'string',num2str(mean(Ps(cycle_start:cycle_end))))
;

  rate_n   = 60/[(cycle_end-cycle_start)*step];
  max_Ps   = max(Ps(cycle_start:cycle_end));
  mean_Ps  = mean(Ps(cycle_start:cycle_end));
  min_Ps   = min(Ps(cycle_start:cycle_end));

  max_Qo   = max(Qo(cycle_start:cycle_end));
  mean_Qo  = mean(Qo(cycle_start:cycle_end));
  min_Qo   = min(Qo(cycle_start:cycle_end));

  max_Qi   = max(Qi(cycle_start:cycle_end));
  mean_Qi  = mean(Qi(cycle_start:cycle_end));
  min_Qi   = min(Qi(cycle_start:cycle_end));

  max_Pt   = max(Pt(cycle_start:cycle_end));
  mean_Pt  = mean(Pt(cycle_start:cycle_end));
  min_Pt   = min(Pt(cycle_start:cycle_end));

  max_Pp   = max(Pp(cycle_start:cycle_end));
  mean_Pp  = mean(Pp(cycle_start:cycle_end));
  min_Pp   = min(Pp(cycle_start:cycle_end));

  max_Pex   = max(Pexternal(cycle_start:cycle_end));
```

```
mean_Pex  = mean(Pexternal(cycle_start:cycle_end));
min_Pex   = min(Pexternal(cycle_start:cycle_end));

max_V   = max(Vvad(cycle_start:cycle_end));
min_V   = min(Vvad(cycle_start:cycle_end));
SV      = max_V-min_V;

disp('')
disp('RESULTS')
disp(' ')
disp(sprintf('Cycle: %g,%g',[T(cycle_start) T(cycle_end)]))
disp(sprintf('Rate:  %g',rate_n))
disp(' ')
disp(sprintf('Max  Ps:  %g',max_Ps))
disp(sprintf('Mean Ps:  %g',mean_Ps))
disp(sprintf('Min  Ps:  %g',min_Ps))
disp(' ')
disp(sprintf('Max  Qo:  %g',max_Qo))
disp(sprintf('Mean Qo:  %g',mean_Qo))
disp(sprintf('Min  Qo:  %g',min_Qo))
disp(' ')
disp(sprintf('Max  Qi:  %g',max_Qi))
disp(sprintf('Mean Qi:  %g',mean_Qi))
disp(sprintf('Min  Qi:  %g',min_Qi))
disp(' ')
disp(sprintf('Max  Pt:  %g',max_Pt))
disp(sprintf('Mean Pt:  %g',mean_Pt))
disp(sprintf('Min  Pt:  %g',min_Pt))
disp(' ')
disp(sprintf('Max  Pp:  %g',max_Pp))
disp(sprintf('Mean Pp:  %g',mean_Pp))
disp(sprintf('Min  Pp:  %g',min_Pp))
disp(' ')
disp(sprintf('Max  Pex:  %g',max_Pex))
disp(sprintf('Mean Pex:  %g',mean_Pex))
disp(sprintf('Min  Pex:  %g',min_Pex))
disp(' ')
disp(sprintf('Max  Vol:  %g',max_V))
disp(sprintf('Min Vol:  %g',min_V))
disp(sprintf('Stroke Vol:  %g',SV))
disp(' ')
disp(' ')
```

APPENDIX B

DIFFERENTIAL EQUATIONS

Thoratec Model – CVS

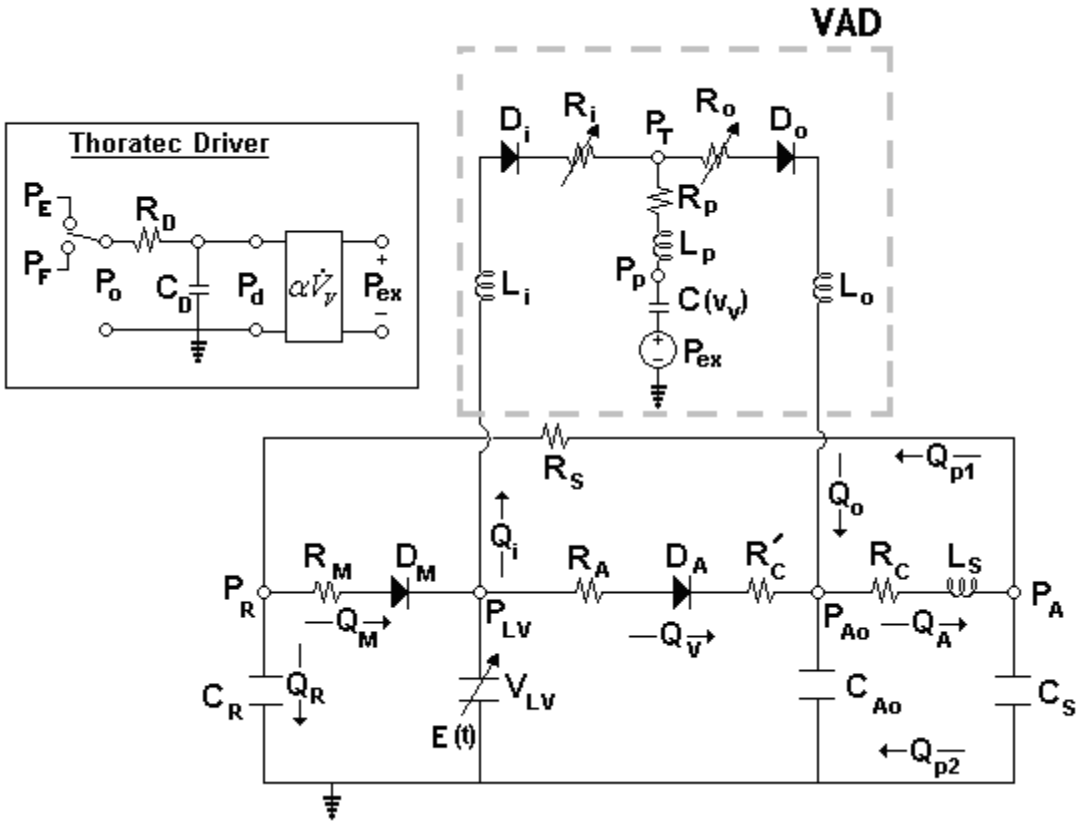

Figure 49: VAD-CVS electric analog diagram

Table 6: Definition of Parameters

$\mathbf{P_o}$	pressure prescribed by the Thoratec driver
$\mathbf{P_d}$	pressure developed in the Thoratec driver
$\mathbf{P_{ex}}$	pressure exerted on the Thoratec bladder
$\mathbf{P_T}$	pressure in the Thoratec bladder (pneumatic + passive)
$\mathbf{P_P}$	passive pressure created in the Thoratec bladder
$\mathbf{R_i}$	resistance of the Thoratec inlet valve (dependent on V_{LV})
$\mathbf{R_o}$	resistance of the Thoratec outlet valve (dependent on Q_O)
$\mathbf{L_i}$	inertance of the Thoratec inlet cannula
$\mathbf{L_P}$	inertance of the Thoratec chamber volume
$\mathbf{L_o}$	inertance of the Thoratec outlet cannula
$\mathbf{R_A}$	resistance of the aortic valve; includes R'c
$\mathbf{R_C}$	characteristic resistance of the systemic system
$\mathbf{R_P}$	resistance of the Thoratec chamber
$\mathbf{R_D}$	resistance of the Thoratec drive line (air)
$\mathbf{C_P}$	compliance of the Thoratec bladder
$\mathbf{C_{Ao}}$	compliance of the aorta
$\mathbf{C_s}$	compliance of the systemic system
$\mathbf{C_R}$	compliance of the atria
$\mathbf{C_D}$	compliance of the Thoratec drive line (air)
$\mathbf{Q_i}$	Thoratec inlet flow
$\mathbf{Q_o}$	Thoratec outlet flow
$\mathbf{D_i}$	Thoratec inlet valve
$\mathbf{D_o}$	Thoratec outlet valve

Table 7: System State Variables

V_{lv}	Volume of Left Ventricle
Q_A	Flow in the Aorta
P_A	Arterial Pressure
Pr	Atrial Pressure
Q_i	Thoratec Inlet Flow
Q_o	Thoratec Outlet Flow
V_V	Volume of the VAD

Beginning with the Thoratec driver, to find the external drive pressure on the pump chamber

$$\boxed{\dot{P}_d = \left(\frac{1}{C_D R_D} P_o - \frac{1}{C_D R_D} P_d \right)} \qquad \text{(A-1)}$$

The pressure source P_o is a square wave generated by the Thoratec driver. P_o is initially a filling pressure near or below 0.0 mmHg. Once the volume of the VAD reaches a volume of 104 ml, P_o steps to an ejection pressure, usually between 200-250 mmHg. The ejection pressure will remain constant for a period of time equal to the VAD ejection time, set by the user. P_o will then return at its filling pressure until the volume of the VAD again reaches 104 ml.

The actual pressure exerted on the VAD bladder (P_{EX}) is given by the following relationship:

$$\boxed{P_{ex} = \alpha \dot{V}_V} \qquad \text{(A-2)}$$

The total pressure in the Thoratec chamber is the sum of the external pressure (P_{EX}) and the pressure due to the pump chamber compliance (P_P). P_P is found from the pressure-volume relationship found from fitting experimental data. The pressure-volume relationship used in this model is:

$$\boxed{P_P = \frac{1}{C(V_V)}\left[V_V - V_{D\text{-}VAD}\right]} \tag{A-3}$$

where V_V, the VAD volume, is a state variable and $V_{D\text{-}VAD}$ is dead or relaxed the VAD.

The Pressure in the left ventricle is found by summing the active pressure resulting from myocardial activation and the passive pressure resulting from ventricle filling. The expression for active pressure is:

$$\boxed{P_{Act} = E_A(t)\left[V_{LV} - V_D\right]} \tag{A-4}$$

Where E_A is the active elastance, found from the normalized curve, and V_D is the unstressed volume or x-intercept of the ESPVR. Passive pressure can be found by estimating the EDPVR by a linear relationship.

$$\boxed{P_{pas} = E_P(t)\left[V_{LV} - V_O\right]} \tag{A-5}$$

Adding the P_{Act} and P_{Pas} yields:

$$\boxed{P_{LV}=E(t)\left[V_{LV}-V_O\right]-E_p(t)*\Delta V} \tag{A-6}$$

where $E(t) = E_A(t) + E_p(t)$ and $\Delta V = V_O - V_D$.

Solving for the state variable, V_{LV}:

$$\dot{V}_{LV}=\frac{D_M}{R_M}\left[P_R-P_{LV}\right]-Q_i-\frac{D_A}{R_A}\left[P_{LV}-P_{Ao}\right]$$

$$\dot{V}_{LV}=\frac{D_M}{R_M}P_R-Q_i-\left[\frac{D_A}{R_A}+\frac{D_M}{R_M}\right]P_{LV}+\frac{D_A}{R_A}P_{Ao}$$

P_{LV} is not a state variable, and must be substituted for V_{LV}.

$$\boxed{\dot{V}_{LV}=\frac{D_M}{R_M}P_R-Q_i-\left[\frac{D_A}{R_A}+\frac{D_M}{R_M}\right]E(t)\left[V_{LV}-V_D\right]+\frac{D_A}{R_A}P_{Ao}} \tag{A-7}$$

Similar calculations can be done on the capacitor nodes C_S, C_{Ao}, and C_R.

$$C_s\dot{P}_A=Q_A-\frac{[P_A-P_R]}{R_S}$$

$$\boxed{\dot{P}_A=\frac{1}{C_s}Q_A-\frac{1}{C_sR_S}P_A+\frac{1}{C_sR_S}P_R} \tag{A-8}$$

$$C_{Ao}\dot{P}_{Ao}=\frac{D_A[P_{LV}-P_{Ao}]}{R_A}+Q_o-Q_A$$

$$\dot{P}_{Ao}=\frac{D_A}{C_{Ao}R_A}P_{LV}-\frac{D_A}{C_{Ao}R_A}P_{Ao}+\frac{1}{C_{Ao}}Q_o-\frac{1}{C_{Ao}}Q_A$$

$$\boxed{\dot{P}_{Ao}=\frac{D_A}{C_{Ao}R_A}E(t)\left[V_{LV}-V_D\right]-\frac{D_A}{C_{Ao}R_A}P_{Ao}+\frac{1}{C_{Ao}}Q_o-\frac{1}{C_{Ao}}Q_A} \quad \text{(A-9)}$$

$$C_R\dot{P}_R=D_M\frac{\left[P_R-P_{LV}\right]}{R_M}+\frac{\left[P_A-P_R\right]}{R_S}$$

$$\boxed{\dot{P}_R=\frac{1}{C_RR_S}P_A-\frac{D_M}{C_RR_M}E(t)\left[V_{LV}-V_D\right]+\left[\frac{D_M}{C_RR_M}-\frac{1}{C_RR_S}\right]P_R} \quad \text{(A-10)}$$

Because Q_i and Q_o are both state variables, the change of volume of the VAD bladder is simply:

$$\boxed{\dot{V}_V=Q_i-Q_o} \quad \text{(A-11)}$$

The change in flow across the inductor L_S is easily defined with state variables.

$$P_{Ao}-P_A=L_S\dot{Q}_A+R_CQ_A$$

$$\boxed{\dot{Q}_A=\frac{1}{L_S}P_{Ao}-\frac{R_C}{L_S}Q_A+-\frac{1}{L_S}P_A} \quad \text{(A-12)}$$

The flow across the inlet (Q_i) and outlet (Qo) inductors becomes more complex because the node P_T is not a state variable. The following expressions relate inlet and outlet flow intermediate variables:

$$L_i\dot{Q}_i = D_iP_{LV} - D_iP_T - R_iQ_i$$

$$L_o\dot{Q}_O = D_oP_T - D_oP_{Ao} - R_oQ_o$$

The variable P_T in terms of state variables, and derivatives of state variables is:

$$\boxed{P_T = P_P + P_{ex} + (Q_i - Q_o)R_P + (\dot{Q}_i - \dot{Q}_o)L_P} \qquad \text{(A-13)}$$

Substituting Equation A-13 into the expression for $\dot{Q}_O$ above yield the following expression:

$$L_i\dot{Q}_i = D_iP_{LV} - D_i\left[P_P + P_{ex} + (Q_i - Q_o)R_P + (\dot{Q}_i - \dot{Q}_o)L_P\right] - R_iQ_i$$

The following algebraic steps were performed to solve in terms of the derivate of Q_i and to remove $\dot{Q}_o$ from the equation.

$$\dot{Q}_i(L_i + D_iL_P) = D_iP_{LV} - D_iP_P - D_iP_{ex} - (D_iR_P + R_i)Q_i + D_iR_PQ_o + D_iL_P\dot{Q}_o$$

$$\dot{Q}_i = \frac{D_iP_{LV} - D_iP_P - D_iP_{ex} - (D_iR_P + R_i)Q_i + D_iR_PQ_o + D_iL_P\dot{Q}_o}{L_i + D_iL_P}$$

$$\frac{\dot{Q}_i}{1-\left(\frac{D_o L_P}{L_P+L_o}\right)\left(\frac{D_i L_P}{L_P+L_i}\right)} =$$
$$\left(\frac{D_i}{L_P+L_i}\right)P_{LV}+\left(\left(\frac{D_i L_P}{L_P+L_i}\right)\left(\frac{D_o}{L_P+L_o}\right)-\frac{D_i}{L_P+L_i}\right)(P_P+\alpha\dot{V}_V P_d)$$
$$-\left(\frac{D_o}{L_P+L_o}\right)\left(\frac{D_i L_P}{L_P+L_i}\right)P_{Ao}+\left(\left(\frac{D_i L_P}{L_P+L_i}\right)\frac{D_o R_P}{L_P+L_o}-\left(\frac{D_o R_P+R_i}{D_o L_P+L_i}\right)\right)Q_i \qquad \text{(A-14)}$$
$$-\left(\left(\frac{D_i L_P}{L_P+L_i}\right)\left(\frac{D_i R_P+R_o}{D_i L_P+L_o}\right)-\left(\frac{D_i R_P}{L_P+L_i}\right)\right)Q_o$$

The same steps to find Q_i where implemented to solve for Q_o.

$$L_o\dot{Q}_O = D_o\left[P_P+P_{ex}+(Q_i-Q_o)R_P+(\dot{Q}_i-\dot{Q}_o)L_P\right]-D_oP_{Ao}-R_oQ_o$$

$$\dot{Q}_o(L_o+D_oL_P) = D_oP_P+D_oP_{ex}+D_oR_PQ_i-(D_oR_P+R_o)Q_o+D_oL_P\dot{Q}_i-D_oP_{Ao}$$

$$\dot{Q}_o = \frac{D_oP_P+D_oP_{ex}+D_oR_PQ_i-(D_oR_P+R_o)Q_o+D_oL_P\dot{Q}_i-D_oP_{Ao}}{L_o+D_oL_P}$$

$$\frac{\dot{Q}_o}{1-\left(\frac{D_o L_P}{L_P+L_o}\right)\left(\frac{D_i L_P}{L_P+L_i}\right)} =$$

$$\left(\frac{D_o L_P}{L_P+L_o}\right)\left(\frac{D_i}{L_P+L_i}\right)P_{LV}+\left(\frac{D_o}{L_P+L_o}-\left(\frac{D_o L_P}{L_P+L_o}\right)\left(\frac{D_i}{L_P+L_i}\right)\right)(P_P+\alpha\dot{V}_V P_d)$$

$$-\left(\frac{D_o}{L_P+L_o}\right)P_{Ao}+\left(\frac{D_o R_P}{L_P+L_o}-\left(\frac{D_o L_P}{L_P+L_o}\right)\left(\frac{D_o R_P+R_i}{D_o L_P+L_i}\right)\right)Q_i \qquad \text{(A-15)}$$

$$+\left(\left(\frac{D_o L_P}{L_P+L_o}\right)\left(\frac{D_i R_P}{L_P+L_i}\right)-\left(\frac{D_i R_P+R_o}{D_i L_P+L_o}\right)\right)Q_o$$

APPENDIX C

THORATEC INLET VALVE RESISTOR CHARACTERIZATION

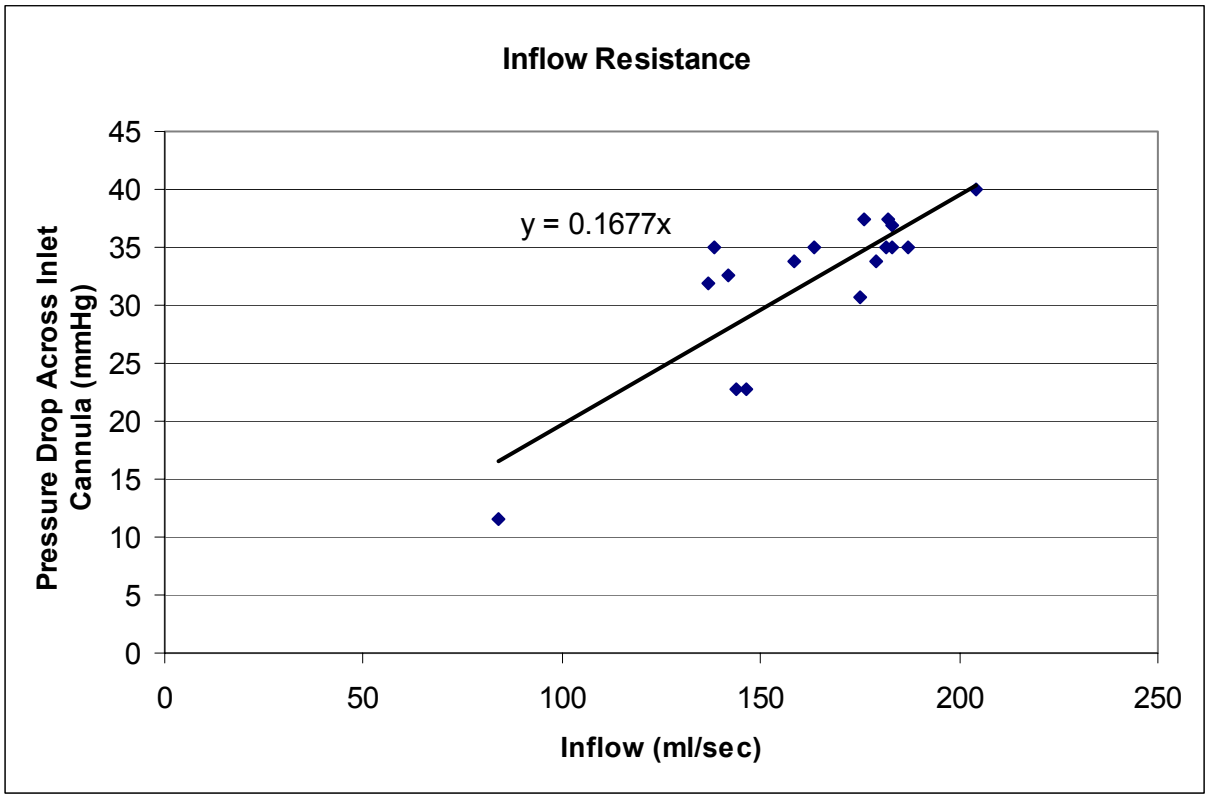

APPENDIX D

MOCK CIRCULATORY SYSTEM RESISTOR CHARACTERIZATION

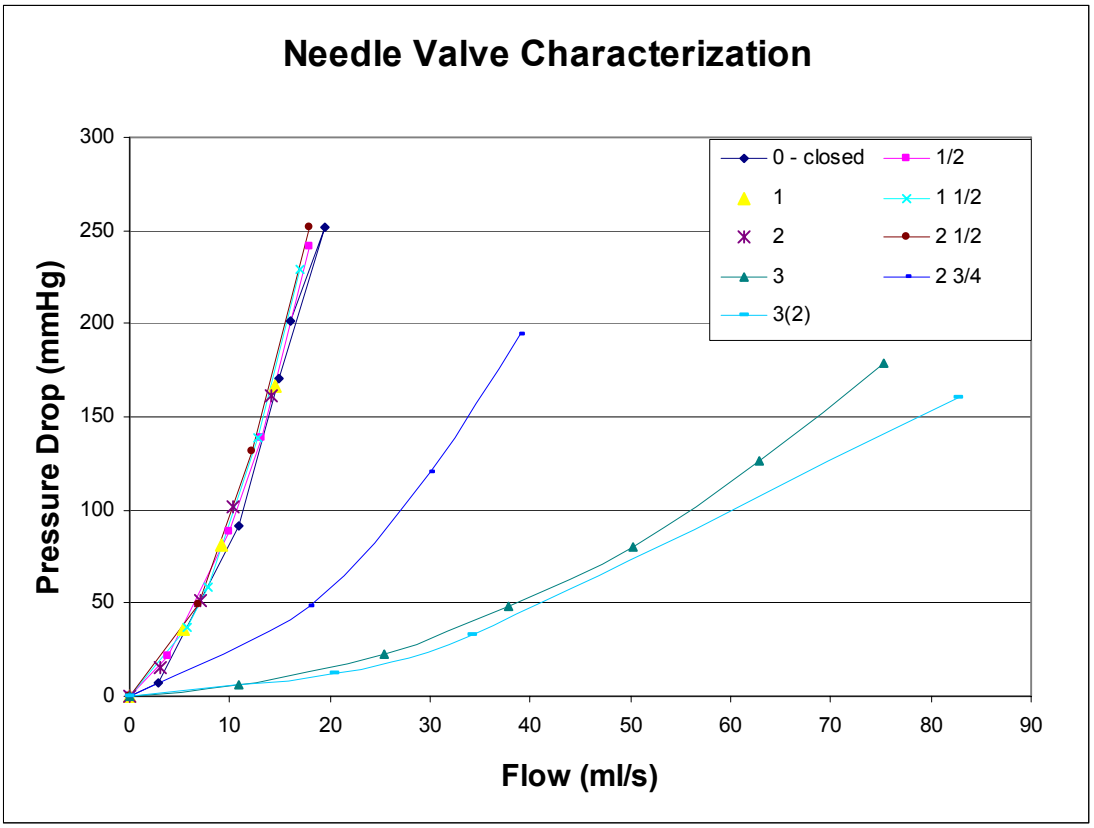

Figure 50: Pressure-flow characterization of Deltol needle valve (Deltol Fluid Products, Bellwood, Ill.) Data series labels represent number of turns the handle is from the closed position.

BIBLIOGRAPHY

1. Entwistle, J.W., 3rd, *Long-term mechanical ventricular assistance toward myocardial recovery.* Cardiol Clin, 2003. **21**(1): p. 75-82.

2. Frazier, O.H., et al., *Improved left ventricular function after chronic left ventricular unloading.* Ann Thorac Surg, 1996. **62**(3): p. 675-81; discussion 681-2.

3. Gorcsan, J., 3rd, et al., *Non-invasive assessment of myocardial recovery on chronic left ventricular assist device: results associated with successful device removal.* J Heart Lung Transplant, 2003. **22**(12): p. 1304-13.

4. Hetzer, R., et al., *Cardiac recovery in dilated cardiomyopathy by unloading with a left ventricular assist device.* Ann Thorac Surg, 1999. **68**(2): p. 742-9.

5. Levin, H.R., et al., *Reversal of chronic ventricular dilation in patients with end-stage cardiomyopathy by prolonged mechanical unloading.* Circulation, 1995. **91**(11): p. 2717-20.

6. McBride, L.R., et al., *Clinical experience with 111 thoratec ventricular assist devices.* Ann Thorac Surg, 1999. **67**(5): p. 1233-8; discussion 1238-9.

7. Muller, J., et al., *Weaning from mechanical cardiac support in patients with idiopathic dilated cardiomyopathy.* Circulation, 1997. **96**(2): p. 542-9.

8. Nakatani, T., et al., *Long-term circulatory support to promote recovery from profound heart failure.* Asaio J, 1995. **41**(3): p. M526-30.

9. Young, J.B., *Healing the heart with ventricular assist device therapy: Mechanisms of cardiac recovery.* Annals of Thoracic Surgery, 2001. **71**(3): p. S210-S219.

10. Mancini, D.M., et al., *Low incidence of myocardial recovery after left ventricular assist device implantation in patients with chronic heart failure.* Circulation, 1998. **98**(22): p. 2383-9.

11. Frazier, O.H., *Prologue: ventricular assist devices and total artificial hearts. A historical perspective.* Cardiol Clin, 2003. **21**(1): p. 1-13.

12. A.H.A., *Heart Disease and Stroke Statistics*. 2003, American Heart Association: Dallas.

13. Vasan, R.S. and D. Levy, *Defining diastolic heart failure: a call for standardized diagnostic criteria.* Circulation, 2000. **101**(17): p. 2118-21.

14. Cohn, J.N., *The management of chronic heart failure.* N Engl J Med, 1996. **335**(7): p. 490-8.

15. Catanese, K.A., et al., *Outpatient left ventricular assist device support: a destination rather than a bridge.* Ann Thorac Surg, 1996. **62**(3): p. 646-52; discussion 653.

16. Dipla, K., et al., *Myocyte recovery after mechanical circulatory support in humans with end-stage heart failure.* Circulation, 1998. **97**(23): p. 2316-22.

17. Heerdt, P.M., et al., *Chronic unloading by left ventricular assist device reverses contractile dysfunction and alters gene expression in end-stage heart failure.* Circulation, 2000. **102**(22): p. 2713-9.

18. Oz, M.C., et al., *Bridge experience with long-term implantable left ventricular assist devices. Are they an alternative to transplantation?* Circulation, 1997. **95**(7): p. 1844-52.

19. Slater, J.P., et al., *Low thromboembolic risk without anticoagulation using advanced-design left ventricular assist devices.* Ann Thorac Surg, 1996. **62**(5): p. 1321-7; discussion 1328.

20. Mancini, D., et al., *Comparison of exercise performance in patients with chronic severe heart failure versus left ventricular assist devices.* Circulation, 1998. **98**(12): p. 1178-83.

21. Emergy RW, J.L., *Directions in cardiac assistance.* J Cardiol Surg, 1991. **6**: p. 400-414.

22. Kinoshita, M., et al., *Cardiac disuse atrophy during LVAD pumping.* ASAIO Trans, 1988. **34**(3): p. 208-12.

23. Maybaum, S., et al., *Partial loading of the left ventricle during mechanical assist device support is associated with improved myocardial function, blood flow and metabolism and increased exercise capacity.* J Heart Lung Transplant, 2002. **21**(4): p. 446-54.

24. Maybaum, S., et al., *Assessment of synchrony relationships between the native left ventricle and the HeartMate left ventricular assist device.* J Heart Lung Transplant, 2002. **21**(5): p. 509-15.

25. Sagawa, K., *Cardiac contraction and the pressure-volume relationship*. 1988, New York: Oxford University Press. xv, 480.

26. Klabunde, R.E., *Cardiovascular Physiology Concepts.* www.oucom.ohiou.edu/CVPhysiology, 1999-2002. **2004**(23, June).

27. Suga, H., Sagawa, K, *Instantaneous pressure-volume relationship and their ratio in the excised, supported canine left ventricle.* Circulation, 1974. **35**: p. 117-126.

28. Vasan, R.S., et al., *Left ventricular dilatation and the risk of congestive heart failure in people without myocardial infarction.* N Engl J Med, 1997. **336**(19): p. 1350-5.

29. Douglas, P.S., et al., *Left ventricular shape, afterload and survival in idiopathic dilated cardiomyopathy.* J Am Coll Cardiol, 1989. **13**(2): p. 311-5.

30. Cohn, J.N., *Structural basis for heart failure. Ventricular remodeling and its pharmacological inhibition.* Circulation, 1995. **91**(10): p. 2504-7.

31. Linzbach, A.J., *Heart failure from the point of view of quantitative anatomy.* Am J Cardiol, 1960. **5**: p. 370-82.

32. Luke Burns, C.C., *Should [beta]-Blockers be Used for the Treatment of Pediatric Patients with Chronic Heart Failure?* Pediatric Drugs, 2002. **4**(12): p. 771-778.

33. Goldstein, D.J. and M. Oz, *Cardiac assist devices*. 1999, Armonk, NY: Futura Pub. Co. xix, 444.

34. Barnard, C.N., *The operation. A human cardiac transplant: an interim report of a successful operation performed at Groote Schuur Hospital, Cape Town.* S Afr Med J, 1967. **41**(48): p. 1271-4.

35. Crawford, M.H., *Ventricular assist devices and the artificial heart.* Cardiol Clin, 2003. **21**(13): p. Foreword.

36. DeVries, W.C., et al., *Clinical use of the total artificial heart.* N Engl J Med, 1984. **310**(5): p. 273-8.

37. Norman, J.C., et al., *Total support of the circulation of a patient with post-cardiotomy stone-heart syndrome by a partial artificial heart (ALVAD) for 5 days followed by heart and kidney transplantation.* Lancet, 1978. **1**(8074): p. 1125-7.

38. Phurrough, S., MD, MPA, *Coverage Decision Memorandum for Ventricular Assist Devices as Destination Therapy*. 2003, Center for Medicare and Medicaide Services.

39. Rose, E.A., *Long-term use of a left ventricular assist device for end-stage heart failure.* N Engl J Med, 2001. **345**(20): p. 1435-1443.

40. Sink, J.D., et al., *Response of hypertrophied myocardium to ischemia: correlation with biochemical and physiological parameters.* J Thorac Cardiovasc Surg, 1981. **81**(6): p. 865-72.

41. Nagueh, S.F., et al., *Decreased expression of tumor necrosis factor-alpha and regression of hypertrophy after nonsurgical septal reduction therapy for patients with hypertrophic obstructive cardiomyopathy.* Circulation, 2001. **103**(14): p. 1844-50.

42. Farrar, D.J., et al., *Long-term follow-up of Thoratec ventricular assist device bridge-to-recovery patients successfully removed from support after recovery of ventricular function.* J Heart Lung Transplant, 2002. **21**(5): p. 516-21.

43. Frazier, O.H. and T.J. Myers, *Left ventricular assist system as a bridge to myocardial recovery.* Annals of Thoracic Surgery, 1999. **68**(2): p. 734-741.

44. Mancini, D.M., et al., *Value of peak exercise oxygen consumption for optimal timing of cardiac transplantation in ambulatory patients with heart failure.* Circulation, 1991. **83**(3): p. 778-86.

45. PixelMEDIA, I., *Thoratec VAD system.* www.thoratec.com, 2004.

46. Arai, H., et al., *Optimal control algorithm for pneumatic ventricular assist devices: its application to automatic control and monitoring of ventricular assist devices.* Artif Organs, 1996. **20**(9): p. 1034-41.

47. Gorcsan, J., 3rd, et al., *Assessment of left ventricular performance by on-line pressure-area relations using echocardiographic automated border detection.* J Am Coll Cardiol, 1994. **23**(1): p. 242-52.

48. Rideout, V.C., *Mathematical and computer modeling of physiological systems*. Prentice Hall biophysics and bioengineering series. 1991, Englewood Cliffs, N.J.: Prentice Hall. xv, 261.

49. Noordergraaf, A., *Circulatory System Dynamics*. 1978, New York: Academic Press.

50. Jager, G.N., *Electrical Model of the Human of the Arterial Tree*. 1965, University of Utrecht.

51. Frank, O., *Die Grundform des arteriellen Pulses.* Z. Biol., 1899. **37**: p. 483-526.

52. Westerhof, N., *Analog studies of human systemic arterial hemodynamics*. 1968, University of Pennsylvania: Philadelphia, PA.

53. Toy, S.M., J. Melbin, and A. Noordergraaf, *Reduced models of arterial systems.* IEEE Trans Biomed Eng, 1985. **32**(2): p. 174-6.

54. Avolio, A.P., *Multi-branched model of the human arterial system.* Med Biol Eng Comput, 1980. **18**(6): p. 709-18.

55. Shroff, S.G., et al., *Physiological relevance of T-tube model parameters with emphasis on arterial compliances.* Am J Physiol, 1995. **269**(1 Pt 2): p. H365-74.

56. Sipkema, P. and N. Westerhof, *Effective length of the arterial system.* Ann Biomed Eng, 1975. **3**(3): p. 296-307.

57. O'Rourke, M.F. and M.G. Taylor, *Input impedance of the systemic circulation.* Circ Res, 1967. **20**(4): p. 365-80.

58. O'Rourke, M.F., *Pressure and flow waves in systemic arteries and the anatomical design of the arterial system.* J Appl Physiol, 1967. **23**(2): p. 139-49.

59. McDonald, D.A., *Blood Flow in Arteries*. 1974, London: Arnold.

60. Liu, Z.R., F. Shen, and F.C. Yin, *Impedance of arterial system simulated by viscoelastic t tubes terminated in windkessels.* Am J Physiol, 1989. **256**(4 Pt 2): p. H1087-99.

61. Campbell, K.B., et al., *Time-domain formulation of asymmetric T-tube model of arterial system.* Am J Physiol, 1990. **258**(6 Pt 2): p. H1761-74.

62. Burattini, R. and K.B. Campbell, *Modified asymmetric T-tube model to infer arterial wave reflection at the aortic root.* IEEE Trans Biomed Eng, 1989. **36**(8): p. 805-14.

63. Starling, E.H., *The Linacre Lecture on the Law of the Heart.* 1918, London: Longmans, Green, and Co.

64. Sarnoff, S.J. and E. Berglund, *Ventricular function. I. Starling's law of the heart studied by means of simultaneous right and left ventricular function curves in the dog.* Circulation, 1954. **9**(5): p. 706-18.

65. Guyton, A.C., *Determination of cardiac output by equating venous return curves with cardiac response curves.* Physiol Rev, 1955. **35**(1): p. 123-9.

66. Sagawa, K., *The circulation and its control: Mechanical properties of the cardiovascular system.*, in *Engineering Principles in Physiology*, J.H.V.B.a.D.S. Gann, Editor. 1973, Academic Press: New York. p. 49-71.

67. Sarnoff, S.J., *Myocardial contractility as described by ventricular function curves; observations on Starling's law of the heart.* Physiol Rev, 1955. **35**(1): p. 107-22.

68. Glower, D.D., et al., *Linearity of the Frank-Starling relationship in the intact heart: the concept of preload recruitable stroke work.* Circulation, 1985. **71**(5): p. 994-1009.

69. Westerhof, N. and G. Elzinga, *The relation between end-diastolic volume and source impedance of the left ventricle.* Arch Int Physiol Biochim, 1974. **82**(2): p. 326-9.

70. Campbell, K.B., et al., *Internal capacitance and resistance allow prediction of right ventricle outflow.* Am J Physiol, 1982. **243**(1): p. H99-112.

71. Shroff, S.G., J.S. Janicki, and K.T. Weber, *Left ventricular systolic dynamics in terms of its chamber mechanical properties.* Am J Physiol, 1983. **245**(1): p. H110-24.

72. Suga, H., K. Sagawa, and L. Demer, *Determinants of instantaneous pressure in canine left ventricle. Time and volume specification.* Circ Res, 1980. **46**(2): p. 256-63.

73. Templeton, G.H. and L.R. Nardizzi, *Elastic and viscous stiffness of the canine left ventricle.* J Appl Physiol, 1974. **36**(1): p. 123-7.

74. Shroff, S.G., J.S. Janicki, and K.T. Weber, *Evidence and quantitation of left ventricular systolic resistance.* Am J Physiol, 1985. **249**(2 Pt 2): p. H358-70.

75. Beneken, J., *A Mathematical Approach to Cardiovascular Function*. 1965, University of Utrecht.

76. Dick, D.E., *A Hybrid Computer Study of Major Transients in the Canine Cardiovascular System*. 1968, University of Wisconsin.

77. McLeod, J., *PHYSBE...a Physiological Simulation Benchmark Experiment.* Simulation, 1966. **7**(6): p. 324-329.

78. Woodard, J.C., et al., *Computer model of ventricular interaction during left ventricular circulatory support.* ASAIO Trans, 1989. **35**(3): p. 439-41.

79. Platt, K.L., et al., *Performance optimization of left ventricular assistance. A computer model study.* Asaio J, 1993. **39**(1): p. 29-38.

80. Ferrari, G., et al., *A modular numerical model of the cardiovascular system for studying and training in the field of cardiovascular physiopathology.* J Biomed Eng, 1992. **14**(2): p. 91-107.

81. Ferrari, G., et al., *A computer controlled mock circulatory system for mono- and biventricular assist device testing.* Int J Artif Organs, 1998. **21**(1): p. 26-36.

82. Breitenstein, D.S., *Cardiovascular modeling : The mathematical expression of blood circulation*. 1993. p. xv, 109 leaves.

83. Jin, Z. and J. Qin, *An electric model with time varying resistance for a pneumatic membrane blood pump.* Asaio J, 1993. **39**(1): p. 56-61.

84. Yu, Y.-C., *Minimally invasive estimation of cardiovascular parameters*. 1998. p. xv, 197 leaves.

85. Vandenberghe, S., *Modeling the Interaction between Cardiac Assist Devices and the Left Ventricle*, in *Civil Engineering Department*. 2004, Ghent University. p. 308.

86. Vandenberghe, S., et al., *Unloading effect of a rotary blood pump assessed by mathematical modeling.* Artif Organs, 2003. **27**(12): p. 1094-101.

87. De Lazzari, C., et al., *A desk-top computer model of the circulatory system for heart assistance simulation: effect of an LVAD on energetic relationships inside the left ventricle.* Med Eng Phys, 1994. **16**(2): p. 97-103.

88. Thoratec, *Thoratec VAD clinical operation and patient management*. 2003, Pleasanton, CA.

89. Rosenberg, G., Winfred M. Phillips, Donald L. Landis, *Design and Evaluation of the Pennsylvania State University Mock Circulatory System.* Asaio J, 1981. **4**(2): p. 41-49.

90. Shroff, S., *Left Ventricular Active Pressure Waveform.* Cardiovacular System Modeling (BioE 2515), 2003. **University of Pittsburgh**.

91. Guyton and Hall, *Textbook of Medical Physiology - 10th Edition*. 2000.